



## City Research Online

### City, University of London Institutional Repository

---

**Citation:** Human, Trevor (2014). Landauer's theory of charge and spin transport in magnetic multilayers. (Unpublished Doctoral thesis, City University London)

This is the unspecified version of the paper.

This version of the publication may differ from the final published version.

---

**Permanent repository link:** <https://openaccess.city.ac.uk/id/eprint/3415/>

**Link to published version:**

**Copyright:** City Research Online aims to make research outputs of City, University of London available to a wider audience. Copyright and Moral Rights remain with the author(s) and/or copyright holders. URLs from City Research Online may be freely distributed and linked to.

**Reuse:** Copies of full items can be used for personal research or study, educational, or not-for-profit purposes without prior permission or charge. Provided that the authors, title and full bibliographic details are credited, a hyperlink and/or URL is given for the original metadata page and the content is not changed in any way.

Landauer's theory of charge and spin  
transport in magnetic multilayers.

by

Trevor Human

Doctor of Philosophy in Mathematics

City University

Mathematics Department

March, 2014



# CONTENTS

1. <i>Introduction</i> . . . . .	25
1.1 Spintronics . . . . .	25
1.2 Magnetic multilayers . . . . .	27
1.3 Current-induced switching of magnetization . . . . .	36
1.4 Nonequilibrium Keldysh formalism . . . . .	42
1.5 The parabolic band model . . . . .	48
1.6 Landauer's approach . . . . .	51
2. <i>General Formula and Methodology</i> . . . . .	53
2.1 Spin wave functions . . . . .	53
2.2 General transfer matrix . . . . .	58
2.3 Spin current components . . . . .	60
2.4 Landauer formalism . . . . .	64
3. <i>Tunneling Magnetoresistance in the Trilayer</i> . . . . .	69
3.1 Reduction of the general formalism for collinear configurations . . . . .	69
3.2 Collinear trilayer spin band configuration . . . . .	75
3.3 Potential barrier sandwiched between two potential wells . . . . .	79
3.4 Single potential barrier . . . . .	81
3.5 Potential well adjacent to a potential barrier . . . . .	82

---

3.6	Resonant tunneling in a double barrier . . . . .	84
4.	<i>Spin Current Components in a Five Layer Junction</i> . . . . .	88
4.1	Spin band configuration of a simple five layer junction . . . . .	88
4.2	Spin current components and destructive interference . . . . .	90
4.3	Spin current with exact matching in the two ferromagnets . . .	104
4.4	Spin transport properties and interlayer exchange coupling in the nonmagnetic spacer . . . . .	111
4.5	Angular dependence of spin current in the nonmagnetic leads .	116
4.6	Angular dependence of spin current in the nonmagnetic spacer	125
4.7	Spin current at the interfaces of the polarizing magnet as a function of polarizing magnet width . . . . .	130
5.	<i>Landauer Boundary Conditions</i> . . . . .	137
5.1	Limit of a semi-infinite potential step . . . . .	137
5.2	Five layer junction approximation to the classical trilayer with semi-infinite ferromagnets . . . . .	138
6.	<i>Out-of-plane Spin Current in the Nonmagnetic Spacer</i> . . . . .	144
6.1	Origin of out-of-plane spin current . . . . .	144
6.2	Interface between a semi-infinite magnet and a semi-infinite nonmagnet . . . . .	146
6.3	Electrons with arbitrary spin polarization incident on a mag- net with fixed magnetization . . . . .	152
6.4	Incident and reflected spin currents in a junction with an in- sulating switching magnet . . . . .	160
6.5	Junction with an insulating barrier . . . . .	170

---

7. *Conclusions* . . . . . 176



## LIST OF FIGURES

1.1	Schematic picture of a magnetic multilayer nanostructure. . . . .	27
1.2	Schematic picture of CPP geometry. . . . .	32
1.3	Schematic picture of CIP geometry. . . . .	32
1.4	Resistor model of CIP and CPP GMR. . . . .	33
1.5	Schematic picture of a magnetic layer structure for current-induced switching (magnetic layers are red, nonmagnetic layers are light blue). . . . .	37
1.6	Schematic picture of a junction in which current-induced switching is studied experimentally. . . . .	40
1.7	Resistance vs current hysteresis loop (after Grollier et al. [20]).	41
1.8	Schematic picture of a magnetic layer structure. All currents flow in the direction of the $y$ – axis which is perpendicular to the layers. . . . .	42
1.9	Schematic picture showing the exchange splitting of $\uparrow$ and $\downarrow$ spin electron bands. . . . .	49
1.10	Schematic picture showing the Fermi energy levels of two nonmagnetic metals A and B. . . . .	49
1.11	Band schematic of a magnet sandwiched between two nonmagnets. . . . .	50
1.12	Potential well/barrier representation for each spin band. . . . .	51

---

2.1	Multi-layered system with constant potentials in either spin band and angle of rotated magnetization in each layer. . . . .	57
2.2	Electrons of all energies $\omega$ up to $\mu_L$ ( $\mu_R$ ) and momenta $k_{\parallel}$ parallel to the layers are omitted from the left and right reservoirs.	66
3.1	Schematic picture showing the $\uparrow$ and $\downarrow$ spin potentials of the ferromagnetically aligned trilayer for each spin band. . . . .	77
3.2	Schematic picture showing the $\uparrow$ and $\downarrow$ spin potentials of the antiferromagnetically aligned trilayer for each spin band. . . . .	78
3.3	Potential barrier sandwiched between a left well of width $A$ and a right well of width $B$ . . . . .	79
3.4	Potential barrier sandwiched between left and potential right wells with exact matching providing symmetry. . . . .	80
3.5	Single potential barrier. . . . .	82
3.6	Potential well adjacent to a potential barrier . . . . .	83
3.7	Schematic picture showing the $\uparrow$ and $\downarrow$ spin bands of the ferromagnetically aligned trilayer with matching across the non-magnetic spacer and the left and right leads. . . . .	85
3.8	Two separated potential barriers. . . . .	85
3.9	Two separated potential barriers with exact matching providing symmetry. . . . .	86
3.10	Schematic plot of Eq. 3.21 showing solutions at intersections with constant $\Gamma_0$ . . . . .	87
4.1	Schematic picture of a simple five layer junction. . . . .	88
4.2	Schematic picture showing the $\uparrow$ and $\downarrow$ spin bands of a simple five layer junction. . . . .	90

---

4.3	Five layer junction represented by two potential wells. . . . .	91
4.4	$J_{\parallel}^T$ , the total in-plane spin current component for incident electrons from the left and right (single $k_{\perp}$ ) as a function of $x$ , the position in the junction. . . . .	92
4.5	$J_{\parallel}^L$ , the in-plane spin current component for incident electrons from the left (single $k_{\perp}$ ) as a function of $x$ , the position in the junction. . . . .	93
4.6	$J_{\parallel}^R$ , the in-plane spin current component for incident electrons from the right (single $k_{\perp}$ ) as a function of $x$ , the position in the junction. . . . .	94
4.7	$J_{\parallel}^T$ , the total in-plane spin current component for incident electrons from the left and right (sum over $k_{\parallel}$ ) as a function of $x$ , the position in the junction. . . . .	95
4.8	$J_{\parallel}^L$ , the in-plane spin current component for incident electrons from the left (sum over $k_{\parallel}$ ) as a function of $x$ , the position in the junction. . . . .	96
4.9	$J_{\parallel}^R$ , the in-plane spin current component for incident electrons from the right (sum over $k_{\parallel}$ ) as a function of $x$ , the position in the junction. . . . .	96
4.10	$J_{\perp}^T$ , the total out-of-plane spin current component for incident electrons from the left and right (single $k_{\perp}$ ) as a function of $x$ , the position in the junction. . . . .	97
4.11	$J_{\perp}^T$ , the constant non-zero out-of-plane spin current component for incident electrons from the left and right (single $k_{\perp}$ ) as a function of $x$ , the position in the nonmagnetic spacer. . . . .	98

---

4.12	$J_{\perp}^L$ , the out-of-plane spin current component for incident electrons from the left (single $k_{\perp}$ ) as a function of $x$ , the position in the junction. . . . .	99
4.13	$J_{\perp}^R$ , the out-of-plane spin current component for incident electrons from the right (single $k_{\perp}$ ) as a function of $x$ , the position in the junction. . . . .	99
4.14	$J_{\perp}^T$ , the total out-of-plane spin current component for incident electrons from the left and right (sum over $k_{\parallel}$ ) as a function of $x$ , the position in the junction. . . . .	100
4.15	$J_{\perp}^T$ , the constant non-zero out-of-plane spin current component for incident electrons from the left and right (sum over $k_{\parallel}$ ) as a function of $x$ , the position in the nonmagnetic spacer. . . . .	101
4.16	$J_{\perp}^L$ , the out-of-plane spin current component for incident electrons from the left (sum over $k_{\parallel}$ ) as a function of $x$ , the position in the junction. . . . .	102
4.17	$J_{\perp}^R$ , the out-of-plane spin current component for incident electrons from the right (sum over $k_{\parallel}$ ) as a function of $x$ , the position in the junction. . . . .	102
4.18	$J_{\perp}^L + J_{\perp}^R$ . The sum of the total out-of-plane spin current contributions from the left and right as a function of $x$ , the position in the junction. . . . .	103
4.19	Symmetric five layer junction represented by two matched potential wells. . . . .	104

---

4.20	$J_{\parallel}^T$ , the total in-plane spin current component for incident electrons from the left and right (sum over $k_{\parallel}$ ) as a function of $x$ , the position in the symmetric junction. . . . .	105
4.21	$J_{\parallel}^L$ , the in-plane spin current component for incident electrons from the left (sum over $k_{\parallel}$ ) as a function of $x$ , the position in the symmetric junction. . . . .	106
4.22	$J_{\parallel}^R$ , the in-plane spin current component for incident electrons from the right (sum over $k_{\parallel}$ ) as a function of $x$ , the position in the symmetric junction. . . . .	106
4.23	$J_{\perp}^T$ , the total out-of-plane spin current component for incident electrons from the left and right (sum over $k_{\parallel}$ ) as a function of $x$ , the position in the symmetric junction. . . . .	107
4.24	$J_{\perp}^L$ , the out-of-plane spin current component for incident electrons from the left (sum over $k_{\parallel}$ ) as a function of $x$ , the position in the symmetric junction. . . . .	108
4.25	$J_{\perp}^R$ , the out-of-plane spin current component for incident electrons from the right (sum over $k_{\parallel}$ ) as a function of $x$ , the position in the symmetric junction. . . . .	108
4.26	$J_{\perp}^L$ , the constant non-zero out-of-plane spin current component for incident electrons from the left (sum over $k_{\parallel}$ ) as a function of $x$ , the position in the nonmagnetic spacer of the symmetric junction. . . . .	109

- 
- 4.27  $J_{\perp}^R$ , the constant non-zero out-of-plane spin current component for incident electrons from the right (sum over  $k_{\parallel}$ ) as a function of  $x$ , the position in the nonmagnetic spacer of the symmetric junction. . . . . 110
- 4.28  $J_{\perp}^L + J_{\perp}^R$ . The sum of the total out-of-plane spin current contributions from the left and right as a function of  $x$ , the position in the symmetric junction. . . . . 111
- 4.29  $J_{\parallel}^{L\uparrow}$ ,  $J_{\parallel}^{L\downarrow}$  and  $J_{\parallel}^L$ . The in-plane spin current in the left lead for  $\uparrow$  and  $\downarrow$  spin electrons incident from the left as a function of  $\theta \in [0, \pi]$ . . . . . 117
- 4.30  $J_{\parallel}^{R\uparrow}$ ,  $J_{\parallel}^{R\downarrow}$  and  $J_{\parallel}^R$ . The in-plane spin current in the left lead for  $\uparrow$  and  $\downarrow$  spin electrons incident from the right as a function of  $\theta \in [0, \pi]$ . . . . . 118
- 4.31  $J_{\perp}^{L\uparrow}$ ,  $J_{\perp}^{L\downarrow}$  and  $J_{\perp}^L$ . The out-of-plane spin current components in the left lead for  $\uparrow$  and  $\downarrow$  spin electrons incident from the left as a function of  $\theta \in [0, \pi]$ . . . . . 119
- 4.32  $J_{\perp}^{R\uparrow}$ ,  $J_{\perp}^{R\downarrow}$  and  $J_{\perp}^R$ . The out-of-plane spin current components in the left lead for  $\uparrow$  and  $\downarrow$  electrons incident from the right as a function of  $\theta \in [0, \pi]$ . . . . . 120
- 4.33  $J_{\parallel}^{L\uparrow}$ ,  $J_{\parallel}^{L\downarrow}$  and  $J_{\parallel}^L$ . The in-plane spin current in the right lead for  $\uparrow$  and  $\downarrow$  spin electrons incident from the left as a function of  $\theta \in [0, \pi]$ . . . . . 121
- 4.34  $J_{\parallel}^{R\uparrow}$ ,  $J_{\parallel}^{R\downarrow}$  and  $J_{\parallel}^R$ . The in-plane spin current in the right lead for  $\uparrow$  and  $\downarrow$  spin electrons incident from the right as a function of  $\theta \in [0, \pi]$ . . . . . 122

- 
- 4.35  $J_{\perp}^{L\uparrow}$ ,  $J_{\perp}^{L\downarrow}$  and  $J_{\perp}^L$ . The out-of-plane spin current components in the right lead for  $\uparrow$  and  $\downarrow$  spin electrons incident from the left as a function of  $\theta \in [0, \pi]$ . . . . . 123
- 4.36  $J_{\perp}^{R\uparrow}$ ,  $J_{\perp}^{R\downarrow}$  and  $J_{\perp}^R$ . The out-of-plane spin current components in the right lead for  $\uparrow$  and  $\downarrow$  electrons incident from the right as a function of  $\theta \in [0, \pi]$ . . . . . 124
- 4.37  $J_{\parallel}^{L\uparrow}$ ,  $J_{\parallel}^{L\downarrow}$  and  $J_{\parallel}^L$ . The in-plane spin current in the spacer for  $\uparrow$  and  $\downarrow$  spin electrons incident from the left as a function of  $\theta \in [0, \pi]$ . . . . . 126
- 4.38  $J_{\parallel}^{R\uparrow}$ ,  $J_{\parallel}^{R\downarrow}$  and  $J_{\parallel}^R$ . The in-plane spin current in the spacer for  $\uparrow$  and  $\downarrow$  spin electrons incident from the right as a function of  $\theta \in [0, \pi]$ . . . . . 127
- 4.39  $J_{\perp}^{L\uparrow}$ ,  $J_{\perp}^{L\downarrow}$  and  $J_{\perp}^L$ . The out-of-plane spin current components in the spacer for  $\uparrow$  and  $\downarrow$  spin electrons incident from the left as a function of  $\theta \in [0, \pi]$ . . . . . 128
- 4.40  $J_{\perp}^{R\uparrow}$ ,  $J_{\perp}^{R\downarrow}$  and  $J_{\perp}^R$ . The out-of-plane spin current components in the spacer for  $\uparrow$  and  $\downarrow$  electrons incident from the right as a function of  $\theta \in [0, \pi]$ . . . . . 129
- 4.41 Schematic picture of a simple five layer junction with  $\uparrow$  and  $\downarrow$  spin electrons incident from the left and right semi-infinite leads. . . . . 131
- 4.42 Five layer junction represented by two matched potential wells. 131

---

4.43	$J_{\parallel}^T$ , the total in-plane spin current component for incident electrons from the left and right (sum over $k_{\parallel}$ ), calculated in the left lead as a function of the width $\omega a$ of the polarizing magnet. . . . .	132
4.44	$J_{\parallel}^T$ , the total in-plane spin current component for incident electrons from the left and right (sum over $k_{\parallel}$ ), calculated throughout the polarizing magnet of fixed width $\omega_n a$ . . . . .	133
4.45	$J_{\perp}^T$ , the total out-of-plane spin current component for incident electrons from the left and right (sum over $k_{\parallel}$ ), calculated in the left lead as a function of the width $\omega a$ of the polarizing magnet. . . . .	134
4.46	$J_{\perp}^T$ , the total out-of-plane spin current component for incident electrons from the left and right (sum over $k_{\parallel}$ ), calculated throughout the polarizing magnet of fixed width $\omega_n a$ . . . . .	135
5.1	Schematic picture of a single semi-infinite potential step. . . . .	137
5.2	Schematic picture of a single finite potential step in the limit $a \rightarrow \infty$ . . . . .	138
5.3	Schematic picture of the classical theoretical trilayer junction (two semi-infinite magnets separated by a nonmagnetic spacer). . . . .	139
5.4	Classical trilayer represented by two semi-infinite potential wells with exact matching in both spin bands. . . . .	139
5.5	Schematic picture of two semi-infinite magnets separated by a nonmagnetic spacer with left and right leads. . . . .	140

---

5.6	Five layer approximation to the classical trilayer represented by two large potential wells with exact matching in both spin bands. . . . .	140
5.7	The total in-plane spin current ( $J_{\parallel}^T$ ) as a function of $x$ , the position spanning the interfaces of the spacer in the classical trilayer junction (3 Layer) as well as the comparative results for the five layer approximation (5 Layer). . . . .	142
5.8	The total out-of-plane spin current ( $J_{\perp}^T$ ) as a function of $x$ , the position spanning the interfaces of the spacer in the classical trilayer junction (3 Layer) as well as the comparative results for the five layer approximation (5 Layer). . . . .	143
6.1	Magnetic nanostructure showing the magnetizations of the polarizing and switching magnets and the resulting in- and out-of-plane spin current components in the nonmagnetic spacer. .	144
6.2	Schematic picture of a single interface between a semi-infinite magnet and a semi-infinite nonmagnet. . . . .	146
6.3	Schematic picture of a single interface between a semi-infinite magnet and a semi-infinite nonmagnet with arbitrary spin polarization. . . . .	152
6.4	Schematic picture of a simple five layer junction with $\uparrow$ and $\downarrow$ spin electrons incident from the left and right semi-infinite leads. . . . .	162
6.5	Five layer junction represented by two matched potential barriers. . . . .	162

- 
- 6.6  $J_{\parallel}^T$  and  $J_{\perp}^T$ . The total in- and out-of-plane spin current components (sum over  $k_{\parallel}$ ), calculated in the spacer as a function of the width of the switching magnet,  $p \in [p_0, p_n]$ . . . . . 163
- 6.7  $J_{\parallel}^{inc}$ ,  $J_{\parallel}^{ref}$  and  $J_{\parallel}^T$ . The total in-plane spin current (sum over  $k_{\parallel}$ ) separated into the contributions due to the incident and reflected electrons within the spacer, calculated in the spacer as a function of the width of the switching magnet,  $p \in [p_0, p_n]$ . 166
- 6.8  $J_{\perp}^{inc}$ ,  $J_{\perp}^{ref}$  and  $J_{\perp}^T$ . The total out-of-plane spin current (sum over  $k_{\parallel}$ ) separated into the contributions due to the incident and reflected electrons within the spacer, calculated in the spacer as a function of the width of the switching magnet,  $p \in [p_0, p_n]$ . . . . . 168
- 6.9 Schematic picture of a six layer junction with  $\uparrow$  and  $\downarrow$  spin electrons incident from the left and right semi-infinite leads. . . 170
- 6.10 Six layer junction represented by two matched potential barriers (magnets) followed by a third potential barrier (insulator). 171
- 6.11 Keldysh spin (charge) current as a function of the width of the insulating barrier (taken from [28]). . . . . 172
- 6.12  $J_{\parallel}^T$ ,  $J_{\perp}^T$  and  $J_c$ . The total in- and out-of-plane spin current components (sum over  $k_{\parallel}$ ), calculated in the spacer as a function of the width of the insulating layer,  $s \in [s_0, s_n]$ , along with the corresponding results for the charge current. . . . . 173

- 
- 6.13  $J_{\parallel}^{inc}$ ,  $J_{\parallel}^{ref}$  and  $J_{\parallel}^T$ . The total in-plane spin current (sum over  $k_{\parallel}$ ) separated into the contributions due to the incident and reflected electrons within the spacer, calculated in the spacer as a function of the width of the insulating layer,  $s \in [s_0, s_n]$ . . 174
- 6.14  $J_{\perp}^{inc}$ ,  $J_{\perp}^{ref}$  and  $J_{\perp}^T$ . The total out-of-plane spin current (sum over  $k_{\parallel}$ ) separated into the contributions due to the incident and reflected electrons within the spacer, calculated in the spacer as a function of the width of the insulating layer,  $s \in [s_0, s_n]$ . . . . . 175



## ACKNOWLEDGEMENTS

First and foremost, I would like to thank my supervisor, Professor George Mathon, not only for his knowledge, advice and support but for the inspiration he instilled in me as an undergraduate student, the belief he showed when taking me under his wing and the experience I have gained through our time together. George invited my wife and I into his home, was a welcome guest at our wedding and introduced me to his friend and colleague, Professor Peter Grünberg, soon after he was named a Nobel Prize laureate for the discovery of Giant Magnetoresistance. He has been a great mentor and friend.

I would also like to thank all of the staff in the Mathematics department at City University for their involvement in my journey and for the opportunity they afforded me to participate in this research degree. They have all shown great patience and understanding along the way.

I thank Dr Andrey Umerski and Dr Alessandro De Martino for reading my thesis and for their valued input.

I thank my parents and siblings for their endless support, especially my sister Chantel for being the catalyst in my voyage into the world of mathematics and for supporting me throughout, and my beautiful wife Jacqueline,

for all of her love, support and understanding.

Finally, I would like to dedicate this thesis to my darling little girl, Lola, whose elated arrival during the write up stages provided a much needed lift in focus and motivation.

## ABSTRACT

The nonequilibrium Keldysh formalism has been used to study the spin transport effects found in magnetic multi-layered nanostructures. We formulate a new methodology based on Landauer and show it to be in very good qualitative agreement with Keldysh. However, our theory provides more information regarding the physics of these effects because it allows us to calculate the contributions of individual electrons incident from either side of a junction as well as the contributions within a single layer that are incident on and reflected from an adjacent interface.

Chapter 1 provides a consolidated introduction to spintronics in magnetic multilayer nanostructures (the key focus of this thesis) including phenomena such as giant magnetoresistance (GMR), tunneling magnetoresistance (TMR) and current induced switching of magnetization. We then describe how to calculate the local charge and spin current in the direction perpendicular to the layers of an arbitrary magnetic layer structure using the nonequilibrium Keldysh formalism before introducing our Landauer approach to investigating the transport of charge and spin current in these magnetic multilayers using the simplest parabolic band model for electrons in each layer.

---

In Chapter 2 we formulate our approach by defining the general solution to the wave equation for a given layer in a system in terms of the angle by which the spin polarization is rotated in-plane in that layer and the generalized wave vectors for each electron spin band. We determine a general transfer matrix that enables us to solve explicitly the coefficients of the wave functions in each layer of any general multi-layered system before defining an expression for the in-plane and out-of-plane spin current components in terms of these wave functions before detailing our Landauer formalism to calculating the local spin current in a realistic system consisting of ferromagnets with a finite exchange splitting and appropriate boundary conditions.

We apply our formulated approach in Chapter 3 to a set of collinear spin problems whereby the two magnetic layers in our general multilayer junction (consisting of two ferromagnets separated by a non-magnetic spacer layer) have their rotated magnetizations either ferromagnetically or antiferromagnetically aligned (parallel/anti-parallel to the net magnetization). Our analytical results provide the necessary conditions for optimising tunneling magnetoresistance (TMR) and show how a ‘switching’ effect can be used to control it. We achieve this by calculating analytically in the ferromagnetic configuration the necessary conditions to support a 100% transmission success rate in one spin channel whilst making it very difficult for transmission to occur in the other spin channel. However, we show conclusively that re-aligning the magnetization to the antiferromagnetic configuration under the same conditions will make it very difficult for transmission to occur in either spin channel.

In Chapter 4 we investigate the spin current in a general five layer junction and show that a zero out-of-plane spin current in the nonmagnetic spacer exists only when perfect symmetry is introduced because the contribution from the left cancels exactly the contribution from the right. We identify a number of properties within the nonmagnetic layers and observe the effect of varying the angle of rotated magnetization and width of the polarizing magnet on the spin current components in the nonmagnetic layers.

In Chapter 5 we define the appropriate boundary conditions for our Landauer approach before investigating analytically the origin of out-of-plane spin current in the nonmagnetic spacer in Chapter 6 by looking specifically at an interface between a semi-infinite magnet and a semi-infinite nonmagnet and obtaining qualitative insight into the out-of-plane spin current found in a non-magnetic spacer sandwiched between two finite ferromagnets. In this final chapter we also calculate numerically the effect of an additional insulating barrier on our classical junction consisting of a nonmagnetic spacer sandwiched between two ferromagnets. We compare our results for the charge and spin current in the nonmagnetic spacer to those obtained previously using the Keldysh formalism before showing for the first time the physical dependence on multiple magnetic interfaces of the out-of-plane spin current in a nonmagnetic spacer and how the out-of-plane spin current in the spacer can be large even when the charge current and the in-plane spin current are both negligibly small.



# 1. INTRODUCTION

## *1.1 Spintronics*

The main topic of this thesis is concerned with spin electronics, or spintronics. Spintronics is a relatively new research area which, unlike conventional electronics, takes into consideration the spin of an electron. Spin is the term used in quantum mechanics and particle physics to identify the intrinsic form of angular momentum carried by individual particles. Spin is thereby a purely quantum mechanical phenomenon with no counterpart in classical mechanics. There are therefore two types of angular momentum in quantum mechanics, orbital angular momentum which is the quantum-mechanical counterpart to the classical notion of angular momentum and spin angular momentum. Orbital angular momentum arises when a particle executes a rotating or twisting trajectory, for example, when an electron orbits a nucleus. The existence of spin angular momentum is inferred from experiments, such as the Stern-Gerlach experiment, in which a beam of particles are passed through an inhomogeneous magnetic field and observed in their deflection to possess an intrinsic angular momentum that only takes certain quantized values and cannot be accounted for by orbital angular momentum alone [1], [2].

---

The existence of an intrinsic spin angular momentum of electrons together with the Coulomb interaction (electrostatic interaction between electrically charged particles) has the consequence that in some materials the Coulomb interaction favours energetically the parallel arrangement of electron spins, which results in a net total spin angular momentum. With it there is the associated net magnetic moment (magnetization). This occurs in magnetic materials such as Iron, Nickel and Cobalt [3]. It follows that the spin state of each individual electron in a magnetic material can be classified as having a spin orientation parallel (up-spin) or anti-parallel (down-spin) to the net magnetization. The spin state of electrons clearly affects the magnetic and electronic properties of that material. However, the electron spin orientation in a macroscopic material changes as the electron travels through the material and, on average, has thus no effect on its transport properties such as resistance. The distance over which the direction of the spin angular momentum is conserved is determined by the spin-dependent scattering and is characterized by the so called spin diffusion length. There are several sources of spin dependent scattering, the most important are magnetic impurities, spin-orbit interaction and scattering from spin waves in a ferromagnet. The spin diffusion length in most materials is of the order of tens or hundreds of nanometers [4]. To exploit the existence of spin in electronics it is, therefore, necessary to grow new materials (nanostructures) whose dimensions (in at least one direction) are smaller than the spin diffusion length. This can be achieved by growing very perfect layer structures in which the thicknesses of the constituent layers are all smaller than the spin diffusion length. If such layer structures contain magnetic layers they are called magnetic multilayers.

A typical magnetic multilayer is shown schematically in Fig. 1.1 whereby a series of magnets (M) and nonmagnets (NM) are connected to left and right leads.

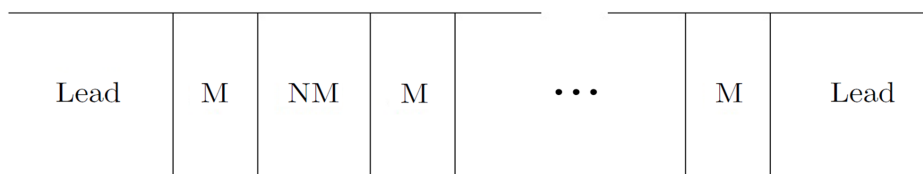


Fig. 1.1: Schematic picture of a magnetic multilayer nanostructure.

## 1.2 Magnetic multilayers

Magnetic multilayers pose great challenges both to experiment and theory. Experimentally, they have to be grown with atomic control over the thicknesses of individual layers and with interfaces between the layers so perfect that, ideally, the momentum of carriers parallel to the layers is conserved. This is now possible for metallic magnetic multilayers which are the subject of this thesis. The restriction to metallic multilayers is for two reasons. Firstly, research into properties of metallic magnetic multilayers is by far the most advanced and the second reason is that currently they are the only systems that can be used in spintronics. Multilayers based on magnetic semiconductors are being studied extensively but, at present, their low Curie temperature prevents their commercial application in spintronics.

Theoretically, magnetic multilayers are also challenging since they are in-

---

herently inhomogeneous systems. However, for perfect epitaxial layers, the inhomogeneity is only in one dimension and we shall see that such quasi-one-dimensional inhomogeneity can be included in theory without any approximations.

The key feature that distinguishes magnetic multilayers from conventional (macroscopic) magnets is the experimentally established fact that the transport of charge is mediated in them by carriers whose spin remains conserved across the whole thickness of the multilayer. In a conventional magnet the spin of an individual charge carrier flips between its up ( $\uparrow$ ) and down ( $\downarrow$ ) spin projections over a characteristic distance  $l_{sf}$  (spin diffusion length) which is of the order of several tens of nanometers. This is much shorter than the dimensions of conventional electronics components. It follows that spin memory is lost in macroscopic samples and, therefore, the spin angular momentum plays no role in transport of charge. This is why for decades spin was ignored by conventional semiconductor electronics. However, when an ultrathin layer structure with a thickness smaller than  $l_{sf}$  is prepared the spin “remembers” its orientation across the whole thickness of the structure, which means that carriers with different spin orientations do not mix and flow independently as if in two separate wires connected in parallel [5]. If the multilayer contains magnetic components, then the two spin channels are inequivalent. This is because the numbers of charge carriers with  $\uparrow$  and  $\downarrow$  spin are unequal in a ferromagnet and, even more importantly,  $\uparrow$  and  $\downarrow$  spin carriers see different potentials at nonmagnet/magnet interfaces and are thus scattered there at different rates.

---

This has interesting and highly exploitable consequences. Because of different scattering rates for  $\uparrow$  and  $\downarrow$  spin carriers at nonmagnet/magnet interfaces the total resistance of a magnetic nanostructure depends on the magnetic configuration of all its magnetic components. This in turn can be altered by an applied magnetic field and, therefore, the resistance of a magnetic nanostructure can be changed by the applied field. The effect is known as the giant magnetoresistance (GMR) since the relative change of the resistance can be very large, of the order of 100%. When two magnetic electrodes are separated by an insulating tunneling barrier a similar effect, called tunneling magnetoresistance (TMR), can occur. The GMR effect was discovered about twenty years ago [6] and a large TMR effect was first observed in 1995 [7]. With the discovery of the GMR effect the era of spintronics had begun. Both GMR and TMR effects have been thoroughly explored over the last ten years and have found many applications. For example, the TMR effect is now used to read information stored on a computer hard disc and TMR reading heads (spin valves) are now fitted to all modern computers. The TMR effect can also be used to store information using a process called magnetic random access memory (MRAM) that is currently being developed. It is now, therefore, well established that by altering the magnetic configuration of a magnetic multilayer we can influence the charge current flowing in it. However, it was recognized only much more recently [8] that, conversely, by passing a strong charge current one can alter the magnetic state of a magnetic multilayer. The structure in which this effect occurs consists of a left lead, a thick left magnetic layer (polarizing magnet), a nonmagnetic metallic spacer

---

layer, a thin second magnet (switching magnet) and a semi-infinite right lead. It was proposed by Slonczewski [8] that the current passing through the left magnetic layer becomes spin polarized and, therefore, the flow of charge from the left magnetic layer to the right magnetic layer is accompanied by a flow of spin. The flow of the spin angular momentum is called spin current. The spin current is conserved in the nonmagnetic parts of the structure but the spin of a carrier entering a ferromagnet can change its orientation provided such a spin flip is compensated for by the corresponding change to the total spin of the magnet so that the total angular momentum of the whole system is conserved. It follows that spin current can be absorbed by the ferromagnet. The rate of change of the total spin, given by the difference between the spin current entering a magnet and that leaving the magnet, is equal to the torque exerted on the magnetic moment of the ferromagnet. If the charge current, and the associated spin current, is strong enough the spin-transfer torque can cause total reversal of the magnetization. This effect is called current-induced switching of magnetization. Quite apart from being fundamentally interesting in its own right, current-induced switching of magnetization has important potential applications since it is envisaged that it could be used to write information in MRAM [9].

Even in the absence of charge current, i.e. when the magnetic multilayer is in equilibrium, there is a flow of spin current between two magnetic layers separated by a nonmagnetic metallic spacer layer provided the magnetic moments of the two magnets are not collinear. This leads to a static torque being exerted by one magnet on the other and the effect is known as oscil-

---

latory exchange coupling [10] between the two magnets since the sign of the torque depends in an oscillatory manner on the thickness of the nonmagnetic spacer. The oscillatory exchange coupling was discovered at the same time as the GMR effect but a close link between this effect and current-induced switching of magnetization was not made until very recently [11].

It can be seen that the four effects which effectively define the new area of spintronics, i.e. GMR, TMR, oscillatory exchange coupling and current-induced switching of magnetization all rely on the length of the magnetic structure in at least one direction being shorter than the spin diffusion length  $l_{sf}$ . Since this is for most metals of the order of several tens of nanometers [6], spintronics can only operate in nanoscale devices.

There is one feature that distinguishes the GMR from TMR, oscillatory exchange coupling and current induced switching of magnetization. The GMR is the only effect that is observed in two qualitatively different geometries. In the first case, the current flows perpendicular to the layers (CPP) geometry as shown in Fig. 1.2.

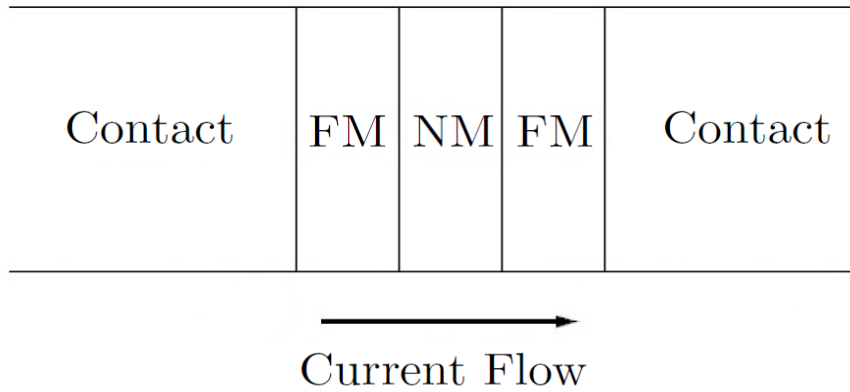


*Fig. 1.2:* Schematic picture of CPP geometry.

The second more usual GMR geometry corresponds to the situation when the current flows in plane of the layers (CIP) as shown in Fig. 1.3.

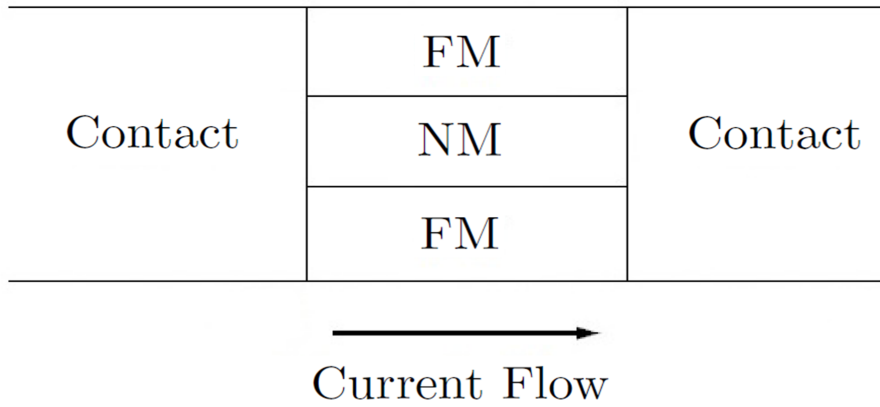


*Fig. 1.3:* Schematic picture of CIP geometry.

Since the lateral dimensions of the layer structure in the direction parallel to the layers are macroscopic (often of the order of centimeters), the CIP GMR always takes place in the diffusive limit (the elastic mean free path is much shorter than the lateral dimensions of the layer structure). That

means that a semi-classical description of the CIP GMR is appropriate. In fact, the CIP GMR effect in a trilayer can be explained qualitatively using a simple resistor model that applies to both CIP and CPP GMR as shown in Fig. 1.4. In the ferromagnetic configuration of the trilayer, carriers with  $\uparrow$  spin are weakly scattered both in the first and second ferromagnets whereas the  $\downarrow$  spin carriers are strongly scattered in both ferromagnetic layers. This can be modelled by two small resistors in the  $\uparrow$  spin channel and by two large resistors in the  $\downarrow$  spin channel in the equivalent resistor network shown in Fig. 1.4a.

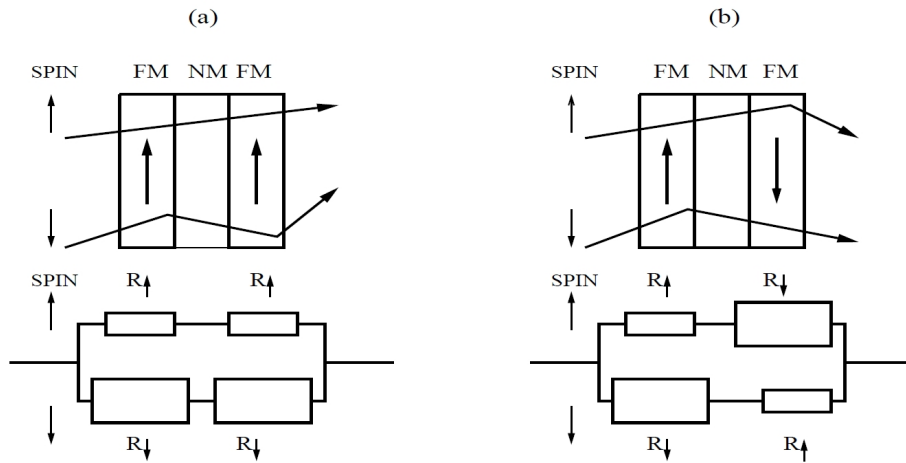


Fig. 1.4: Resistor model of CIP and CPP GMR.

Since the  $\uparrow$  and  $\downarrow$  spin channels are connected in parallel, the total resistance of the trilayer in its ferromagnetic configuration is determined by the low-resistance  $\uparrow$  spin channel which shorts the high-resistance  $\downarrow$  spin channel. It follows that the total resistance of the trilayer in its ferromagnetic configuration is low. On the other hand,  $\downarrow$  spin carriers in the antiferromagnetic configuration are strongly scattered in the first ferromagnetic layer but

---

weakly scattered in the second ferromagnetic layer. The  $\uparrow$  spin carriers are weakly scattered in the first ferromagnetic layer and strongly scattered in the second. This is modelled in Fig. 1.4b by one large and one small resistor in each spin channel. There is no shorting now and the total resistance in the antiferromagnetic configuration is, therefore, much higher than that in the ferromagnetic configuration. This simple physical model of the GMR effect is believed to be qualitatively correct and is supported by more realistic calculations based on the Boltzmann equation [12].

On the other hand, CPP GMR, TMR, oscillatory exchange coupling and current induced switching of magnetization all take place in the CPP geometry. They are thus inherently quantum effects and, consequently, require quantum treatment of the transport of charge and spin current.

Yet another factor that distinguishes the CIP GMR from the rest is the role of impurities. The CIP GMR can only occur in the presence of impurities or in the presence of roughness at the interfaces between magnetic and nonmagnetic layers. The CPP GMR, TMR, oscillatory exchange coupling and current induced switching of magnetization can all operate in perfect samples providing reliable penetration, i.e. in the ballistic limit.

In this thesis we shall not consider impurities. It follows that we can treat theoretically only the CPP geometry in which the effect of impurities can be minimized in well grown experimental samples.

---

There are several theoretical methods that have been developed to calculate the transport of charge in magnetic multilayers. Initially, the standard k-space Kubo formula has been generalised to real space so that it could be applied to spatially inhomogeneous systems [13]. The Kubo formula has the advantage that it can be formulated for a fully realistic electronic structure of each layer in the magnetic multilayer.

Another method that has been used is the Landauer formula which provides a very physical insight into the transport of charge current in spatially inhomogeneous systems [14]. It is relatively easy to formulate the Landauer theory using a simple parabolic band description of the electronic structure of individual layers. However, it is more difficult to generalise this approach to a more realistic band structure since the Landauer formulation relies on the calculation of the electron wave function in each layer. This is relatively straightforward for a parabolic band approximation to the electronic structure but much more difficult for a fully realistic description of the local electronic structure.

The main aim of this thesis is to generalise the Landauer formulation to include the transport of spin in magnetic multilayers. This has not been done within the spin diffusive limit before and we shall see that the Landauer description of the transport of spin provides a very physical insight that cannot be obtained by other methods. Our aim is to provide physical insight into the behaviour of the spin current that flows through a magnetic multilayer. This is important because the spin current vector determines

---

the magnetic torque acting on the switching magnet in a junction in which current-induced switching of magnetization was predicted by Slonczewski [8]. Since our main motivation is to clarify physical processes that govern current-induced switching of magnetization, we shall first review briefly the switching effect itself. Throughout the thesis we shall be frequently comparing our results with those obtained from the Keldysh theory of spin current [15], [16], [17]. We shall, therefore, also briefly describe the Keldysh formulation and discuss how it compares with the Landauer approach we adopt here.

### 1.3 *Current-induced switching of magnetization*

It is now well established that by altering the magnetic configuration of a magnetic multilayer we can influence the charge current flowing in it. It was pointed out by Slonczewski [8] that, conversely, by passing a strong charge current one can alter the magnetic state of a magnetic multilayer. The layer structure in which this effect is expected to occur is shown schematically in Fig. 1.5

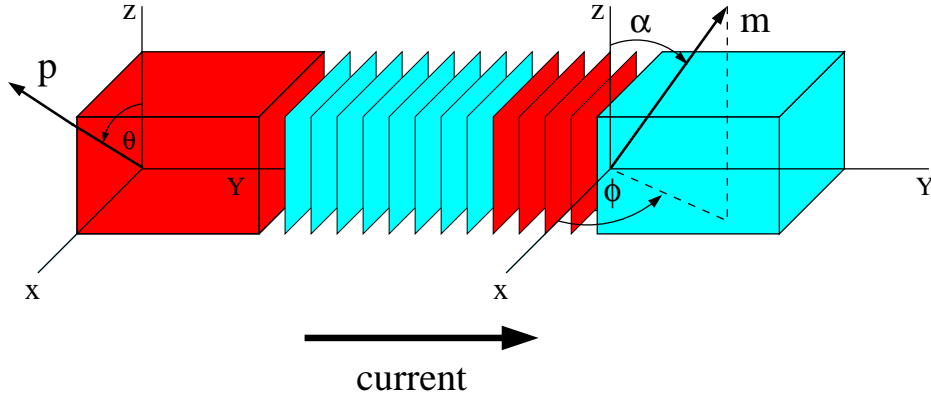


Fig. 1.5: Schematic picture of a magnetic layer structure for current-induced switching (magnetic layers are red, nonmagnetic layers are light blue).

Where  $\mathbf{p}$  and  $\mathbf{m}$  are unit vectors in the direction of the magnetization. The structure consists of a left semi-infinite lead, a thick left magnetic layer (polarizing magnet), a nonmagnetic metallic spacer layer, a thin second magnet (switching magnet) and a right semi-infinite lead. It is assumed that the magnetization of the polarizing magnet is pinned (for example by a strong anisotropy field) in a particular direction  $\theta$ . Slonczewski argued that the left magnet will then spin polarize the current passing through it and the resultant spin current flowing through the spacer can be absorbed by the switching magnet. The rate of change of the total spin, given by the difference between the spin current entering the switching magnet and that leaving the magnet, is equal to the torque exerted on the magnetic moment of the switching magnet. If the charge current, and the associated spin current, is strong enough the spin-transfer torque can cause total reversal of the switching magnet moment. This effect is called current-induced switching of magnetization.

---

On the most elementary level, one can simply assume that the polarizing magnet produces a spin current that gets partially or fully absorbed by the switching magnet and explore the consequences of the resultant torque acting on the magnetization of the switching magnet. This can be done using a phenomenological Landau-Lifshitz equation with an appropriate spin-transfer torque term. To treat correctly the dynamics of current-induced switching of magnetization, it is also necessary to include in the Landau-Lifshitz equation the usual Gilbert damping term [18].

However, the phenomenological approach leaves many questions unanswered. In particular, to understand and optimize the switching effect, we need to know the magnitude and direction of the spin-transfer torque for any specific combination of nonmagnetic and magnetic layer materials. We also require the dependencies of the spin-transfer torque on the thicknesses of both the nonmagnetic and magnetic layers. Finally, to describe correctly the switching effect, we also need to know the detailed dependence of the spin-transfer torque on the angle between the magnetizations of the polarizing and switching magnets. To answer all these questions we need to calculate microscopically the spin current entering and leaving the switching magnet, i.e. the torque acting on it. The most direct microscopic approach is the original calculation of Slonczewski [8] for a simple parabolic band model of a magnetic multilayer. He calculated the spin current (torque) from the one-electron wave functions assuming that the magnetizations of the polarizing and switching magnets are kept at a given fixed angle. This type of calculation corresponds to a scattering experiment. An incoming electron with

---

a given spin orientation (determined by the polarizing magnet) is scattered off an exchange field of the switching magnet which is not parallel to the spin orientation of the incident electron. Calculations based on this idea are designed to tell us how much of the spin angular momentum of the incident electron is absorbed by the switching magnet. The reaction of the switching magnet to the absorbed spin angular momentum is ignored at this stage and is determined separately in a second independent calculation using the phenomenological Landau-Lifshitz equation. In the way originally described by Slonczewski the method was applicable without any approximations only to ferromagnets with a very large exchange splitting of  $\uparrow$  and  $\downarrow$  spin bands. On a more fundamental level, evaluating the spin current directly from one-electron wave functions requires some justification since one also has to link the current obtained from the spin current operator to an applied bias. The extension of Slonczewski's approach to an arbitrary magnetic multilayer and the proper justification of his method using the generalisation of Landauer's formula to the case of spin current will be given in Section 2.4.

It is useful at this stage to discuss briefly the experimental verification of Slonczewski's idea. A typical junction in which current-induced switching is studied experimentally [19] is shown schematically in Fig. 1.6.

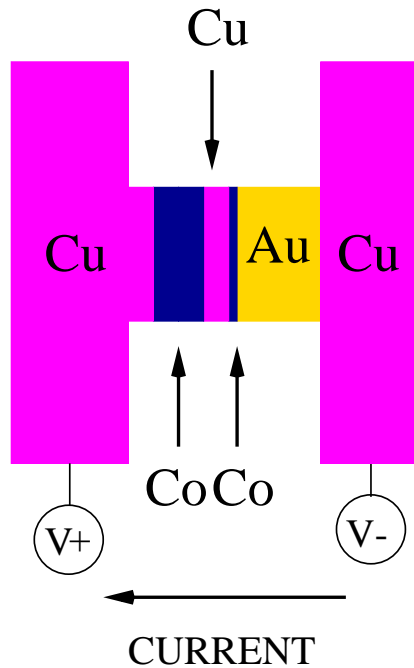


Fig. 1.6: Schematic picture of a junction in which current-induced switching is studied experimentally.

The thickness of the polarizing magnet is 40nm, that of the switching magnet is 2.5nm and the nonmagnetic spacer is 6nm thick. The materials most commonly used for the two magnets and the spacer are Cobalt and Copper, respectively. The junction cross section is approximately oval-shaped and its diameter is only 130nm. A small diameter is necessary so that the torque due to the Oersted field (auxiliary magnetic field) generated by a charge current of  $10^7$  to  $10^8 A/cm^2$ , required for current-induced switching, is much smaller than the spin-transfer torque we are interested in.

We now review briefly the experimental set-up which is used to study current-induced switching. The aim of most experiments is to determine the orientation of the switching magnet moment as a function of the current

(applied bias) in the junction. Discontinuities in such a dependence indicate sudden jumps of the magnetization direction, i.e. current-induced switching. The orientation of the switching magnet moment  $\mathbf{m}$  relative to that of the polarizing magnet  $\mathbf{p}$ , which is fixed, is determined by measuring the resistance of the junction. Because of the GMR effect, the resistance of the junction is higher when the magnetizations of the two magnets are antiparallel than when they are parallel. In other words, what is observed are hysteresis loops of resistance versus current. A typical experimental hysteresis loop of this type [20] is reproduced in Fig. 1.7.

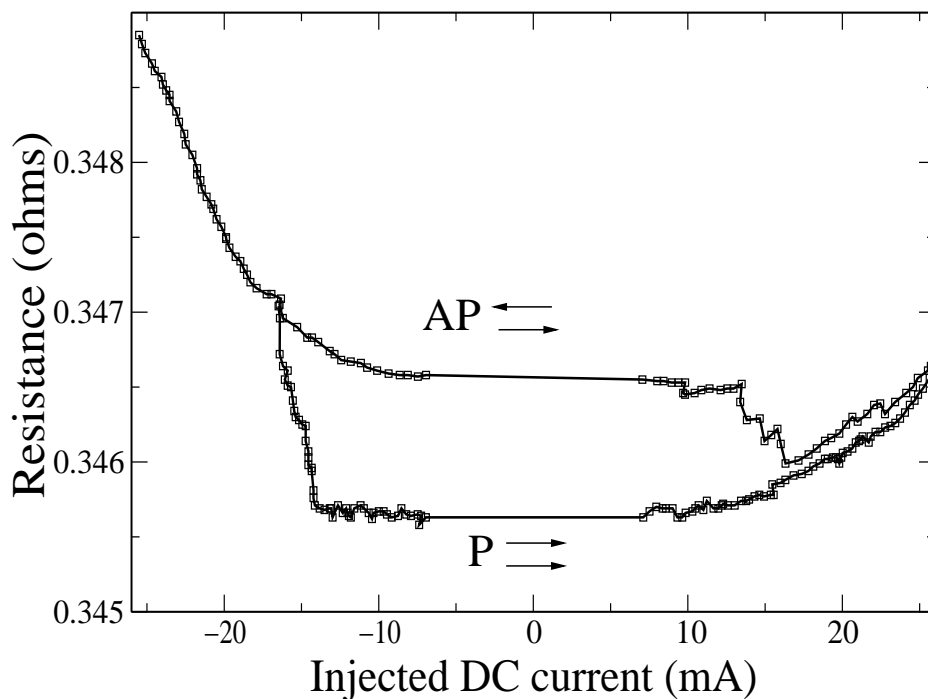


Fig. 1.7: Resistance vs current hysteresis loop (after Grollier et al. [20]).

It can be seen from Fig. 1.7 that, for any given current, the switching magnet moment is stationary (the junction resistance has a well defined

value), i.e. the system is in a steady state. This holds true everywhere on the hysteresis loop except for the two discontinuities where current-induced switching occurs. The experiment thus clearly confirms the current-induced switching of magnetization predicted theoretically by Slonczewski.

### 1.4 Nonequilibrium Keldysh formalism

Following [21] we now describe briefly how to calculate, using the non-equilibrium Keldysh formalism, the local charge and spin currents flowing in the direction perpendicular to the layers of an arbitrary magnetic layer structure. We shall assume that the magnetic layer structure is sandwiched between two reservoirs with a bias  $V_b$  applied between them to produce a spin-polarized current. The structure we consider is shown schematically in Fig. 1.8.

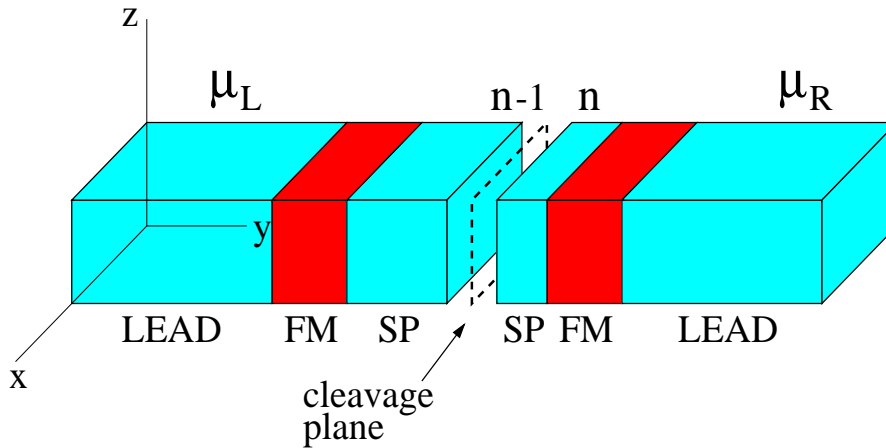


Fig. 1.8: Schematic picture of a magnetic layer structure. All currents flow in the direction of the  $y$  - axis which is perpendicular to the layers.

Typically, the two reservoirs will be semi-infinite nonmagnetic leads and the magnetic structure consists of a left magnet (FM) separated from the right magnet by a nonmagnetic spacer layer (SP). The spacer layer may be either a nonmagnetic metal or an insulator. Although this is the most common situation, an arbitrary finite number of other layers (magnetic or nonmagnetic) can be easily incorporated into the structure. The broken line in Fig. 1.8 represents a cleavage plane separating the system into two independent parts so that charge carriers cannot move between the two surface planes labelled  $n - 1$  and  $n$ . Our ability to cleave the whole system in this way is essential for the implementation of the Keldysh formalism. This cannot be easily done in the continuum model we shall adopt in the formulation of the Landauer approach in Section 2.4. However, the separation of the system into two independent parts is easily done within a discrete tight-binding parameterization of the band structure by simply switching off the matrix of hopping integrals  $t_{n\nu, n-1\mu}$  between atomic orbitals  $\nu, \mu$  localized in planes  $n - 1$  and  $n$ . We shall, therefore, adopt the tight-binding description in this section. Each layer in the structure is therefore described by a tight-binding model, in general multi-orbital with  $s$ ,  $p$ , and  $d$  orbitals whose one-electron parameters are fitted to first-principle bulk band structure. The Hamiltonian is, therefore, of the form

$$H = H_0 + H_{int} + H_{anis} \quad (1.1)$$

where the one-electron hopping term  $H_0$  is given by

$$H_0 = \sum_{\mathbf{k}_{\parallel\sigma}} \sum_{m\mu, n\nu} t_{m\mu, n\nu}(\mathbf{k}_{\parallel}) c_{\mathbf{k}_{\parallel}m\mu\sigma}^\dagger c_{\mathbf{k}_{\parallel}n\nu\sigma} \quad (1.2)$$

where  $c_{\mathbf{k}_{\parallel}m\mu\sigma}^\dagger$  creates an electron in a Bloch state, with in-plane wave vector

$\mathbf{k}_{\parallel}$  and spin  $\sigma$ , formed from a given atomic orbital  $\mu$  in plane  $m$ .  $H_{int}$  is an on-site interaction between electrons in  $d$  orbitals which leads to an exchange splitting of the bands in the ferromagnets and is neglected in the spacer and lead. Finally,  $H_{anis}$  contains effective fields corresponding to uniaxial  $\mathbf{H}_u$  and easy-plane  $\mathbf{H}_p$  anisotropies.

Using the equation of motion for the spin angular momentum operator, it is straightforward to show within the tight-binding description [22] that the operator for spin angular momentum current between planes  $n - 1$  and  $n$  is given by

$$\mathbf{j}_{n-1} = -\frac{i}{2} \sum_{\mathbf{k}_{\parallel}\mu\nu} t(\mathbf{k}_{\parallel})_{n\nu,n-1\mu} (c_{\mathbf{k}_{\parallel}n\nu\uparrow}^{\dagger}, c_{\mathbf{k}_{\parallel}n\nu\downarrow}^{\dagger}) \boldsymbol{\sigma} (c_{\mathbf{k}_{\parallel}n-1\mu\uparrow}, c_{\mathbf{k}_{\parallel}n-1\mu\downarrow})^T + h.c. \quad (1.3)$$

Here,  $\boldsymbol{\sigma} = (\sigma_x, \sigma_y, \sigma_z)$ , where the components are Pauli matrices. Eq. 1.3 yields the charge current operator if  $\frac{1}{2}\boldsymbol{\sigma}$  is replaced by a unit matrix multiplied by the electronic charge  $e/\hbar$ , where  $e$  is the electronic charge (negative). All currents flow in the direction of the  $y$ -axis, perpendicular to the layers, and the components of the vector  $\mathbf{j}$  correspond to transport of  $x$ ,  $y$ , and  $z$  components of spin.

To use the Keldysh formalism [15], [16], [17] to calculate the charge or spin currents flowing between the planes  $n - 1$  and  $n$ , we consider an initial state at time  $\tau = -\infty$  in which the hopping integral  $t_{n\nu,n-1\mu}$  between planes  $n - 1$  and  $n$  is switched off. Then both sides of the system are in equilibrium but with different chemical potentials  $\mu_L$  on the left and  $\mu_R$  on the right, where  $\mu_L - \mu_R = eV_b$ . The interplane hopping is then turned on adiabati-

cally and the system evolves to a steady state. The cleavage plane, across which the hopping is initially switched off, may be taken in either the spacer or in one of the magnets or in one of the leads.

In principle, the Keldysh method is valid for arbitrary bias  $V_b$  but here we restrict ourselves to small bias corresponding to linear response which is valid for metallic multilayers.

Following Keldysh [15], [16], we define a two-time matrix

$$G_{RL}^+(\tau, \tau') = i \langle c_L^\dagger(\tau') c_R(\tau) \rangle \quad (1.4)$$

where  $R \equiv (n, \nu, \sigma')$  and  $L \equiv (n-1, \mu, \sigma)$ , and we suppress the  $\mathbf{k}_\parallel$  label. The thermal average in Eq. 1.4 is calculated for the steady state of the coupled system. The matrix  $G_{RL}^+$  has dimensions  $2m \times 2m$  where  $m$  is the number of orbitals on each atomic site, and is written so that the  $m \times m$  upper diagonal block contains matrix elements between  $\uparrow$  spin orbitals and the  $m \times m$  lower diagonal block relates to  $\downarrow$  spin.  $2m \times 2m$  hopping matrices  $t_{LR}$  and  $t_{RL}$  are written similarly and in this case only the diagonal blocks are nonzero. If we denote  $t_{LR}$  by  $t$ , then  $t_{RL} = t^\dagger$ . We also generalize the definition of  $\boldsymbol{\sigma}$  so that its components are now direct products of the  $2 \times 2$  Pauli matrices  $\sigma_x, \sigma_y, \sigma_z$  and the  $m \times m$  unit matrix. The thermal average of the spin current operator, given by Eq. 1.3, may now be expressed as

$$\langle \mathbf{j}_{n-1} \rangle = \frac{1}{2} \sum_{\mathbf{k}_\parallel} Tr \{ [G_{RL}^+(\tau, \tau) t - G_{LR}^+(\tau, \tau) t^\dagger] \boldsymbol{\sigma} \} \quad (1.5)$$

Introducing the Fourier transform  $G^+(\omega)$  of  $G^+(\tau, \tau')$ , which is a function of

$\tau - \tau'$ , we have

$$\langle \mathbf{j}_{n-1} \rangle = \frac{1}{2} \sum_{\mathbf{k}_{\parallel}} \int \frac{d\omega}{2\pi} \text{Tr} \{ [G_{RL}^+(\omega)t - G_{LR}^+(\omega)t^\dagger] \boldsymbol{\sigma} \} \quad (1.6)$$

Again, the charge current is given by Eq. 1.6 with  $\frac{1}{2}\boldsymbol{\sigma}$  replaced by the unit matrix multiplied by  $e/\hbar$ .

Similarly, the total spin angular momentum on atomic planes on either side of the cleavage plane, in the non-equilibrium state, is given by

$$\langle \mathbf{S}_{n-1} \rangle = -\frac{1}{2} i\hbar \sum_{\mathbf{k}_{\parallel}} \int \frac{d\omega}{2\pi} \text{Tr} \{ G_{LL}^+(\omega) \boldsymbol{\sigma} \} \quad (1.7)$$

$$\langle \mathbf{S}_n \rangle = -\frac{1}{2} i\hbar \sum_{\mathbf{k}_{\parallel}} \int \frac{d\omega}{2\pi} \text{Tr} \{ G_{RR}^+(\omega) \boldsymbol{\sigma} \} \quad (1.8)$$

Following Keldysh [15], [16] we now write

$$G_{AB}^+(\omega) = \frac{1}{2} (F_{AB} + G_{AB}^a - G_{AB}^r) \quad (1.9)$$

where the suffices  $A$  and  $B$  are either  $R$  or  $L$ .  $F_{AB}(\omega)$  is the Fourier transform of

$$F_{AB}(\tau, \tau') = -i \langle [C_A(\tau), C_B^\dagger(\tau')] \rangle \quad (1.10)$$

and  $G^a, G^r$  are the usual advanced and retarded Green functions [23]. Note that in References [16] and [17] the definitions of  $G^a$  and  $G^r$  are interchanged and that in the Green function matrix defined by these authors  $G^+$  and  $G^-$  should be interchanged.

Charge and spin current are related by Eqs. 1.6-1.8 to the quantities  $G^a$ ,  $G^r$ , and  $F_{AB}$ . The latter are calculated for the coupled system by starting with decoupled left and right systems, each in equilibrium, and turning on the hopping between planes  $L$  and  $R$  as a perturbation. Hence, we express  $G^a$ ,  $G^r$ , and  $F_{AB}$  in terms of retarded surface Green functions  $g_L \equiv g_{LL}$ ,  $g_R \equiv g_{RR}$  for the decoupled equilibrium system. It is then straightforward to show [24] that the spin current between planes  $n - 1$  and  $n$  can be written as the sum  $\langle \mathbf{j}_{n-1} \rangle = \langle \mathbf{j}_{n-1} \rangle_1 + \langle \mathbf{j}_{n-1} \rangle_2$ , where the two contributions to the spin current  $\langle \mathbf{j}_n \rangle_1$  and  $\langle \mathbf{j}_n \rangle_2$  are given by

$$\langle \mathbf{j}_{n-1} \rangle_1 = \frac{1}{4\pi} \sum_{\mathbf{k}_{\parallel}} \int d\omega \operatorname{ReTr}\{(B - A)\boldsymbol{\sigma}\}[f(\omega - \mu_L) + f(\omega - \mu_R)] \quad (1.11)$$

$$\begin{aligned} \langle \mathbf{j}_{n-1} \rangle_2 = \frac{1}{2\pi} \sum_{\mathbf{k}_{\parallel}} \int d\omega \operatorname{ReTr}\{[g_L t A B g_R^\dagger t^\dagger - A B \\ + \frac{1}{2}(A + B)]\boldsymbol{\sigma}\}[f(\omega - \mu_L) - f(\omega - \mu_R)] \end{aligned} \quad (1.12)$$

Here,  $A = [1 - g_R t^\dagger g_L t]^{-1}$ ,  $B = [1 - g_R^\dagger t^\dagger g_L^\dagger t]^{-1}$ , and  $f(\omega - \mu)$  is the Fermi function with chemical potential  $\mu$  and  $\mu_L - \mu_R = eV_b$ . In the linear-response case of small bias which we are considering, the Fermi functions in Eq. 1.12 are expanded to first order in  $V_b$ . Hence the energy integral is avoided, being equivalent to multiplying the integrand by  $eV_b$  and evaluating it at the common zero-bias chemical potential  $\mu_0$ . Eq. 1.11 and 1.12 contain all the information about the transport of spin and charge in the direction perpendicular to the layers of an arbitrary magnetic layer structure. The spin current was evaluated from the above equations by Edwards et al [24]. for a

---

single-orbital tight-binding band as well as for a more realistic multi-orbital band structure. However, it is the results for a single-orbital band that are most directly comparable with the results obtained from our generalised Landauer formula we derive in Section 2.4

### 1.5 *The parabolic band model*

In order to investigate the transport of charge current and spin current in these magnetic multilayers, we shall use the simplest parabolic band model for electrons in each layer. In nonmagnetic layers, the potential an electron sees is independent of its spin. On the other hand, in magnetic layers, electron-electron interaction results in a spin-dependant potential which leads to an exchange splitting of electron bands. In other words, the bands of electrons with spin parallel and antiparallel to a spin quantization axis are shifted relative to one another by an energy  $\Delta$  which is called the exchange splitting. It follows that the potentials seen by electrons with spin parallel to the spin quantization axis ( $\uparrow$  spin electrons) and anti-parallel to the quantization axis ( $\downarrow$  spin electrons) satisfy  $V^\uparrow - V^\downarrow = \Delta$ . This is shown schematically in Fig. 1.9.

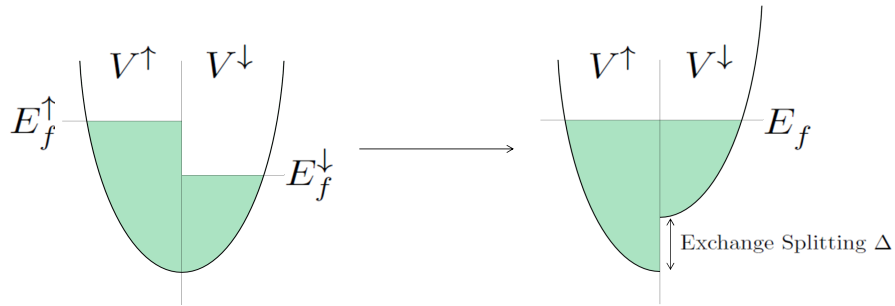


Fig. 1.9: Schematic picture showing the exchange splitting of  $\uparrow$  and  $\downarrow$  spin electron bands.

If we were to take a nonmagnetic metal A with a Fermi level (the highest occupied energy level) a distance  $E_f^A$  from a vacuum (zero energy level) and a nonmagnetic metal B with a Fermi level a distance  $E_f^B$  from zero (Fig. 1.10)

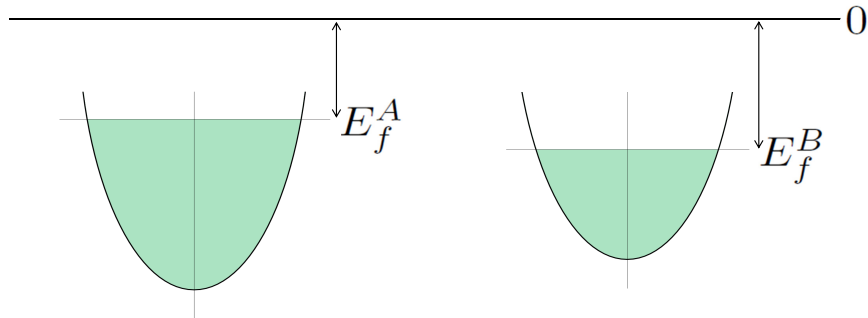


Fig. 1.10: Schematic picture showing the Fermi energy levels of two nonmagnetic metals A and B.

and place them in contact, electrons will initially flow from A to B creating excess negative charge in B. This in turn creates a repulsion Coulomb

potential which lifts the electron energy levels in metal B upwards until the two Fermi energy levels are equal and a state of equilibrium is achieved. This behaviour is in fact true for all layers in a multi-layered system in that each band of electrons will flow throughout the system and achieve a common Fermi energy level. To further illustrate this schematic picture, we will look at a hypothetical multilayer consisting of a magnetic layer sandwiched between two nonmagnets as illustrated in Fig. 1.11.

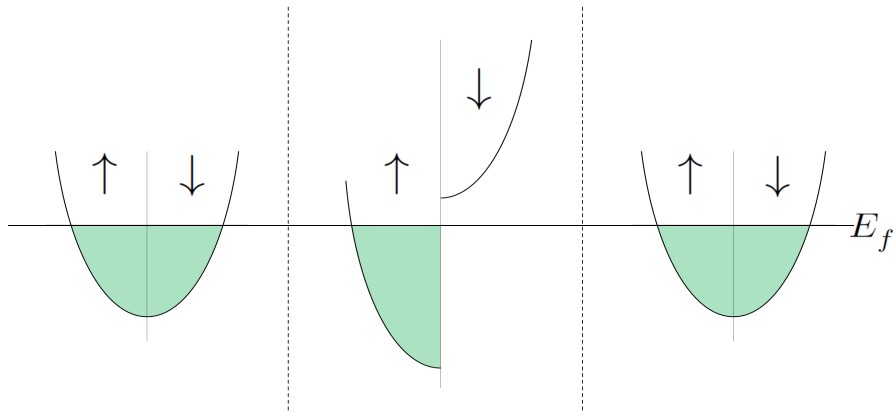


Fig. 1.11: Band schematic of a magnet sandwiched between two nonmagnets.

From this picture, we can now represent this multilayer for each spin band as a potential barrier or potential well. In this instance, an  $\uparrow$  spin incident electron flowing from the left of our system to the right will see a potential well in its path and a  $\downarrow$  spin incident electron will see a potential barrier as illustrated in Fig. 1.12.

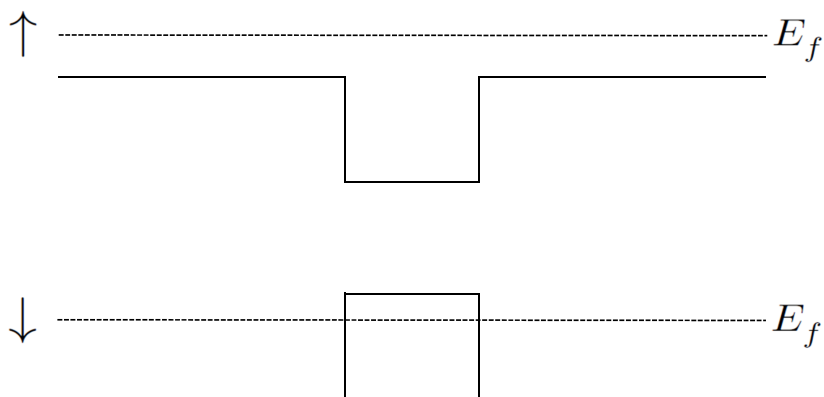


Fig. 1.12: Potential well/barrier representation for each spin band.

### 1.6 Landauer's approach

Landauer's approach to calculating charge and spin transport is useful in the sense that it divides such calculations into four individual scattering problems. We can construct some desired magnetic nanostructure contained between two reservoirs of electrons of all energies and emit a single electron with spin orientation parallel ( $\uparrow$ ) or anti-parallel ( $\downarrow$ ) to the net magnetization. This single electron will propagate through the system from the left reservoir to the right and its influence on the charge current and spin transport effects throughout can be calculated. The total left to right moving effects will therefore be the sum of  $\uparrow$  and  $\downarrow$  spin incident electrons from the left reservoir and similarly, the total right to left moving effects will be given by the sum of  $\uparrow$  and  $\downarrow$  spin incident electrons from the right reservoir. The total effects are then simply given by the difference between left and right. Finally, the sum of all such propagating electrons can be converted into an energy integral to

give a complete physical calculation. The ability to study total spin transport effects more closely by looking at individual contributions will provide greater insight into such effects. We will formulate our Landauer approach in more detail in Section 2.4 by looking at a general system consisting of two Ferromagnets separated by a nonmagnetic spacer layer.

## 2. GENERAL FORMULA AND METHODOLOGY

### 2.1 Spin wave functions

The wave function  $\psi$  for all positions and times is determined by solving Schrödinger's Equation (Eq. 2.1).

$$i\hbar \frac{d\psi}{dt} = \hat{H}\psi \quad (2.1)$$

$$\hat{H} = \frac{-\hbar^2}{2m} \nabla^2 + V(\underline{r}) \quad (2.2)$$

The kinetic and potential energies are transformed into the Hamiltonian,  $\hat{H}$ , which acts upon the wave function to generate the evolution of the wave function in time and space. In our problem, there is a further dimension to account for. The carriers of charge in metals are electrons and quantum mechanics tells us that each electron has an internal angular momentum called spin which can only have two values. These are usually referred to as spin projections “up” ( $\uparrow$ ) or “down” ( $\downarrow$ ). In a magnetic metal such as Iron the numbers of  $\uparrow$  spin and  $\downarrow$  spin electrons are unequal and, since there is an elementary magnetic moment associated with each spin, a net magnetic moment arises. We can account for this phenomenon analytically by allowing the wave function to become two part for  $\uparrow$  and  $\downarrow$  spin

$$\psi(\underline{r}, t) = \begin{pmatrix} \psi^\uparrow \\ \psi^\downarrow \end{pmatrix} \quad (2.3)$$

The Hamiltonian,  $\hat{H}$ , can then be written as a 2x2 matrix operator of the form

$$\hat{H} = T + V \quad (2.4)$$

where

$$T = \frac{-\hbar^2}{2m} \begin{pmatrix} \nabla^2 & 0 \\ 0 & \nabla^2 \end{pmatrix} \quad (2.5)$$

and  $V$  is a 2x2 matrix corresponding to the potential energy of the material in the layer, given by

$$V = \begin{pmatrix} V_{NM} & 0 \\ 0 & V_{NM} \end{pmatrix} + V_X \quad (2.6)$$

Here,  $V_{NM}$  is the nonmagnetic potential of the layer and  $V_X$  is a 2x2 matrix corresponding to the spin potentials in the layer, given by

$$V_X = \frac{\Delta_S}{2} \begin{pmatrix} 1 & 0 \\ 0 & -1 \end{pmatrix} \quad (2.7)$$

$\Delta_S$  is the difference in  $\uparrow$  and  $\downarrow$  spin potentials such that the potentials for the  $\uparrow$  and  $\downarrow$  spin orientations in magnetic layers are shifted by  $\Delta_S = V_S^\uparrow - V_S^\downarrow$  and the potential in nonmagnetic layers are spin independent where  $\Delta_S = 0$ .

We will need to account for magnetic layers in which the spin polarization is rotated in the  $yz$  - plane by an angle  $\theta$  and thus the  $\uparrow$  and  $\downarrow$  spin

potentials will be in the direction parallel/antiparallel to the magnetization respectively, hence, we can take

$$V_{\bar{X}} = \frac{\Delta_S}{2} \begin{pmatrix} \cos \theta & \sin \theta \\ \sin \theta & -\cos \theta \end{pmatrix} \quad (2.8)$$

Therefore, the time-independent Schrödinger equation,  $E\psi = \hat{H}\psi$ , gives

$$T\psi + V_{NM}\psi + V_{\bar{X}}\psi - E\psi = 0 \quad (2.9)$$

We can choose a unitary 2x2 matrix

$$S = \begin{pmatrix} \cos \frac{\theta}{2} & \sin \frac{\theta}{2} \\ -\sin \frac{\theta}{2} & \cos \frac{\theta}{2} \end{pmatrix} \quad (2.10)$$

such that  $V_{\bar{X}} = S^{-1}V_X S$ , and multiply throughout Eq. 2.9 to obtain

$$ST\psi + SV_{NM}\psi + SV_{\bar{X}}\psi - SE\psi = 0 \quad (2.11)$$

Since  $T$ ,  $E$  and  $V_{NM}$  are diagonal, and  $S^{-1}S = I$ , the identity matrix, this is the same as

$$TS\psi + V_{NM}S\psi + SV_{\bar{X}}(S^{-1}S)\psi - ES\psi = 0 \quad (2.12)$$

which can be written as

$$T(S\psi) + V_{NM}(S\psi) + SV_{\bar{X}}S^{-1}(S\psi) - E(S\psi) = 0 \quad (2.13)$$

Here we note that since  $V_{\bar{X}} = S^{-1}V_X S$ , it is also true that  $SV_{\bar{X}}S^{-1} = V_X$  and hence we can write Eq. 2.9 for a new wave function  $\phi = S\psi$  as

$$T\phi + V_{NM}\phi + V_X\phi - E\phi = 0 \quad (2.14)$$

which is equivalent to a system of two independent wave equations given by

$$\frac{-\hbar^2}{2m}\nabla^2\phi^\uparrow + (V_{NM} + \frac{\Delta_S}{2} - E)\phi^\uparrow = 0 \quad (2.15a)$$

$$\frac{-\hbar^2}{2m}\nabla^2\phi^\downarrow + (V_{NM} - \frac{\Delta_S}{2} - E)\phi^\downarrow = 0 \quad (2.15b)$$

The general solution for each can be written as

$$\phi^\uparrow = A^\uparrow e^{k^\uparrow x} + B^\uparrow e^{-k^\uparrow x} \quad (2.16a)$$

$$\phi^\downarrow = A^\downarrow e^{k^\downarrow x} + B^\downarrow e^{-k^\downarrow x} \quad (2.16b)$$

Where  $A^\uparrow, B^\uparrow, A^\downarrow$  and  $B^\downarrow$  are constants and  $k^\uparrow$  and  $k^\downarrow$  are the generalized wave vectors that can be either pure imaginary or real where  $k^{\uparrow 2} = \frac{2m}{\hbar^2}(V_{NM} + \frac{\Delta_S}{2} - E)$  and  $k^{\downarrow 2} = \frac{2m}{\hbar^2}(V_{NM} - \frac{\Delta_S}{2} - E)$ .

Thus, since  $\phi = S\psi$ , the original wave function  $\psi$  is given by  $\psi = S^{-1}\phi$  or

$$\psi = \begin{pmatrix} \psi^\uparrow \\ \psi^\downarrow \end{pmatrix} = \begin{pmatrix} \cos \frac{\theta}{2} & \sin \frac{\theta}{2} \\ -\sin \frac{\theta}{2} & \cos \frac{\theta}{2} \end{pmatrix}^{-1} \begin{pmatrix} \phi^\uparrow \\ \phi^\downarrow \end{pmatrix} \quad (2.17)$$

It should be noted that throughout this thesis we will always consider multi-layered systems with constant potentials in each layer, i.e. the potential in each layer is independent of the position in that layer, as illustrated in Fig. 2.1.

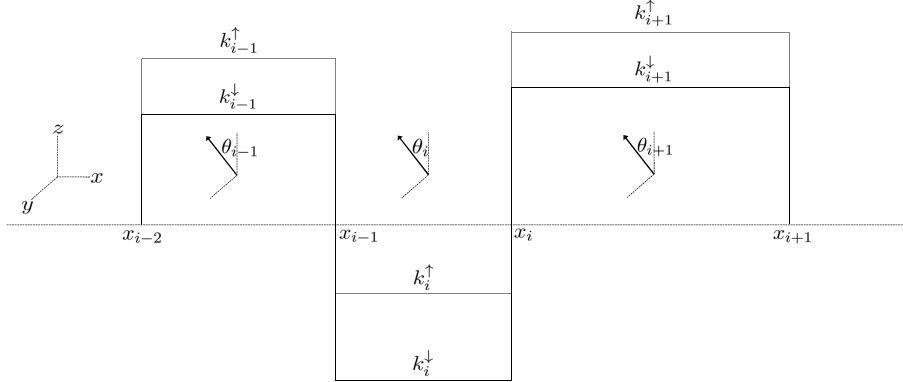


Fig. 2.1: Multi-layered system with constant potentials in either spin band and angle of rotated magnetization in each layer.

Solving for  $\psi$  (Eq. 2.17) and converting to one-dimension given that we are always sending electrons from either side along the  $x$  – axis, we obtain the general solution (Eq. 2.18) to the wave equation for the  $i^{\text{th}}$  layer in a system in terms of  $\theta_i$ , the angle by which the spin polarization is rotated in-plane in that layer, and the generalized wave vectors  $k_i^\uparrow$  and  $k_i^\downarrow$ .

$$\psi_i^\uparrow = (A_i^\uparrow e^{k_i^\uparrow x} + B_i^\uparrow e^{-k_i^\uparrow x}) \cos \frac{\theta_i}{2} - (A_i^\downarrow e^{k_i^\downarrow x} + B_i^\downarrow e^{-k_i^\downarrow x}) \sin \frac{\theta_i}{2} \quad (2.18a)$$

$$\psi_i^\downarrow = (A_i^\uparrow e^{k_i^\uparrow x} + B_i^\uparrow e^{-k_i^\uparrow x}) \sin \frac{\theta_i}{2} + (A_i^\downarrow e^{k_i^\downarrow x} + B_i^\downarrow e^{-k_i^\downarrow x}) \cos \frac{\theta_i}{2} \quad (2.18b)$$

It follows from our multi-layered system that we can separate the variables in Schrödinger's Equation (Eq. 2.1) and introduce two components of the generalized wave vector  $k^{\uparrow,\downarrow} = k_{\parallel}^{\uparrow,\downarrow} + k_{\perp}^{\uparrow,\downarrow}$ , where  $k_{\perp}$  and  $k_{\parallel}$  are the components of the wave vector perpendicular (parallel) to the layers. Assuming that such

separation of variables has been made, we shall always be solving a quasi-one-dimensional problem in which the potential varies only in the direction perpendicular to the layers and can be characterized by  $k_{\perp}$ . Throughout the thesis we shall assume this is the case and when the total spin (charge) currents are required, an integration with respect to  $k_{\parallel}$  needs to be performed so that the total energy for all motion parallel ( $E_{\parallel}$ ) and perpendicular ( $E_{\perp}$ ) to the layers is kept constant and equal to the common Fermi energy  $E_f = E_{\parallel} + E_{\perp}$ . This will be mentioned whenever appropriate.

## 2.2 General transfer matrix

In this section we will derive a general transfer matrix that allows us to solve for the unknown coefficients of the wave functions given by Eq. 2.18 in each layer of a magnetic multilayer nanostructure.

The wave function  $\psi$  and its derivative must be continuous throughout the junction. It is therefore true that  $\psi_{i-1} = \psi_i$  and  $\psi'_{i-1} = \psi'_i$  at  $x = x_i$ . This gives us the following system of equations

$$\begin{pmatrix} \psi_{i-1}^{\uparrow} \\ \psi_{i-1}^{\downarrow} \\ \psi_{i-1}^{\uparrow'} \\ \psi_{i-1}^{\downarrow'} \end{pmatrix}_{x_i} = \begin{pmatrix} \psi_i^{\uparrow} \\ \psi_i^{\downarrow} \\ \psi_i^{\uparrow'} \\ \psi_i^{\downarrow'} \end{pmatrix}_{x_i} \quad (2.19)$$

From this and the general solution (Eq. 2.18) we see that if we define  $\vec{A}_i$  as

the column vector

$$\vec{A}_i = \begin{pmatrix} A_i^\uparrow \\ B_i^\uparrow \\ A_i^\downarrow \\ B_i^\downarrow \end{pmatrix} \quad (2.20)$$

and  $M_i$  as the 4x4 matrix

$$M_i = \begin{pmatrix} e^{k_i^\uparrow x_i} \cos \frac{\theta_i}{2} & e^{-k_i^\uparrow x_i} \cos \frac{\theta_i}{2} & -e^{k_i^\downarrow x_i} \sin \frac{\theta_i}{2} & -e^{-k_i^\downarrow x_i} \sin \frac{\theta_i}{2} \\ e^{k_i^\uparrow x_i} \sin \frac{\theta_i}{2} & e^{-k_i^\uparrow x_i} \sin \frac{\theta_i}{2} & e^{k_i^\downarrow x_i} \cos \frac{\theta_i}{2} & e^{-k_i^\downarrow x_i} \cos \frac{\theta_i}{2} \\ k_i^\uparrow e^{k_i^\uparrow x_i} \cos \frac{\theta_i}{2} & -k_i^\uparrow e^{-k_i^\uparrow x_i} \cos \frac{\theta_i}{2} & -k_i^\downarrow e^{k_i^\downarrow x_i} \sin \frac{\theta_i}{2} & k_i^\downarrow e^{-k_i^\downarrow x_i} \sin \frac{\theta_i}{2} \\ k_i^\uparrow e^{k_i^\uparrow x_i} \sin \frac{\theta_i}{2} & -k_i^\uparrow e^{-k_i^\uparrow x_i} \sin \frac{\theta_i}{2} & k_i^\downarrow e^{k_i^\downarrow x_i} \cos \frac{\theta_i}{2} & -k_i^\downarrow e^{-k_i^\downarrow x_i} \cos \frac{\theta_i}{2} \end{pmatrix} \quad (2.21)$$

We have that  $M_i \vec{A}_i = M_{i-1} \vec{A}_{i-1}$ . Multiplying either side by the inverse matrix  $M_i^{-1}$  gives  $\vec{A}_i = M_i^{-1} M_{i-1} \vec{A}_{i-1}$ . By simplifying  $M_i^{-1} M_{i-1}$ , we can define the transfer matrix across  $x_i$  as  $M_i^T$  such that  $\vec{A}_i = M_i^T \vec{A}_{i-1}$  where

$$M_i^T = \frac{1}{2} \begin{pmatrix} \xi(k_i^\uparrow, k_{i-1}^\uparrow) \cos \frac{\theta_i - \theta_{i-1}}{2} & \xi(k_i^\uparrow, k_{i-1}^\downarrow) \sin \frac{\theta_i - \theta_{i-1}}{2} \\ -\xi(k_i^\downarrow, k_{i-1}^\uparrow) \sin \frac{\theta_i - \theta_{i-1}}{2} & \xi(k_i^\downarrow, k_{i-1}^\downarrow) \cos \frac{\theta_i - \theta_{i-1}}{2} \end{pmatrix} \quad (2.22)$$

and  $\xi(\alpha, \beta)$  is a 2x2 matrix defined for all  $\alpha, \beta$  by

$$\xi(\alpha, \beta) = \begin{pmatrix} e^{-x_i(\alpha-\beta)} \left(1 + \frac{\beta}{\alpha}\right) & e^{-x_i(\alpha+\beta)} \left(1 - \frac{\beta}{\alpha}\right) \\ e^{x_i(\alpha+\beta)} \left(1 - \frac{\beta}{\alpha}\right) & e^{x_i(\alpha-\beta)} \left(1 + \frac{\beta}{\alpha}\right) \end{pmatrix} \quad (2.23)$$

We have now established a tool that allows us to solve explicitly the coefficients of the wave functions at each layer of interest in any general multilayered system. These wave functions hold all the information of the system and can be used to calculate a variety of quantum mechanical attributes and phenomena. We will use this tool throughout the thesis to solve for these wave functions and use them to calculate charge current, tunnelling magnetoresistance (TMR), exchange coupling and the spin transport effects in various magnetic multilayer nanostructures.

### 2.3 Spin current components

Now that we have the wave functions, we can calculate directly the spin current at any point in a magnetic multilayer junction. It is known from the equation of continuity [25] that the ordinary charge current,  $\vec{j}$ , can be obtained once the wave function,  $\psi$ , is known where  $\vec{j}$  is given by the expression

$$\vec{j} = \frac{-i\hbar}{2m} \{(\nabla\psi)\psi^* - (\nabla\psi^*)\psi\} \quad (2.24)$$

We can similarly derive expressions for the  $x$ ,  $y$  and  $z$  components of the spin current. The magnetic multilayers described in this thesis consist of magnetic layers that have their spin angular momentum fixed parallel to a spin quantization axis aligned with the  $z$ -axis. In such layers, the spin precesses about the direction of the magnetization in the magnet and since this is in the  $z$  direction, the  $z$  component of the spin current is clearly conserved and it is only the  $x$  and  $y$  components that precess. We make this choice of

the direction of magnetization parallel to the  $z$  - *axis* so that we need not consider the  $z$  component of the spin current when studying the transport of spin throughout the layers as it is only the magnetic layers with rotated magnetization in which the  $z$  component of the spin current is not conserved. We will therefore formulate expressions for the in-plane spin current (parallel to the layers) and the out-of-plane spin current (perpendicular to the layers) given by the  $x$  and  $y$  components respectively.

From Schrödinger's Equation (Eq. 2.1), the two-part wave function  $\psi$  (Eq. 2.3) and the Pauli matrices [27] or spin operators for each component  $\sigma_x, \sigma_y$  and  $\sigma_z$ , we are able to deduce the following set of equations

$$i\hbar \frac{d\psi}{dt} = \hat{H}\psi, \hat{H} = T + V \quad (2.25)$$

$$\psi = \begin{pmatrix} \psi^\uparrow \\ \psi^\downarrow \end{pmatrix}, T = \frac{-\hbar^2}{2m} \begin{pmatrix} \nabla^2 & 0 \\ 0 & \nabla^2 \end{pmatrix}, V = \begin{pmatrix} V^\uparrow & 0 \\ 0 & V^\downarrow \end{pmatrix} \quad (2.26)$$

$$\sigma_x = \begin{pmatrix} 0 & 1 \\ 1 & 0 \end{pmatrix}, \sigma_y = \begin{pmatrix} 0 & -i \\ i & 0 \end{pmatrix}, \sigma_z = \begin{pmatrix} 1 & 0 \\ 0 & -1 \end{pmatrix} \quad (2.27)$$

In analogy with the derivation of ordinary charge current, we expect that the  $x$  component of spin current,  $J_x$ , satisfies the equation of continuity

$$\frac{d}{dt} [\psi^\dagger \sigma_x \psi] + \nabla \cdot J_x = 0 \quad (2.28)$$

where  $\psi^\dagger$  denotes the transpose of the conjugate of  $\psi$

$$\begin{aligned}
\frac{d}{dt} [\psi^\dagger \sigma_x \psi] &= \frac{d}{dt} \left[ \begin{pmatrix} \psi^{\uparrow*} & \psi^{\downarrow*} \end{pmatrix} \begin{pmatrix} 0 & 1 \\ 1 & 0 \end{pmatrix} \begin{pmatrix} \psi^\uparrow \\ \psi^\downarrow \end{pmatrix} \right] = \frac{d}{dt} [\psi^{\downarrow*} \psi^\uparrow + \psi^{\uparrow*} \psi^\downarrow] \\
&= \frac{d\psi^{\downarrow*}}{dt} \psi^\uparrow + \psi^{\downarrow*} \frac{d\psi^\uparrow}{dt} + \frac{d\psi^{\uparrow*}}{dt} \psi^\downarrow + \psi^{\uparrow*} \frac{d\psi^\downarrow}{dt}
\end{aligned} \tag{2.30}$$

From Schrödinger's Equation we have that

$$\frac{d\psi}{dt} = \frac{i\hbar}{2m} \nabla^2 \psi - \frac{i}{\hbar} V \psi \tag{2.31}$$

Therefore

$$\frac{d\psi^*}{dt} = \frac{-i\hbar}{2m} \nabla^2 \psi^* + \frac{i}{\hbar} V \psi^* \tag{2.32}$$

and so, by substitution

$$\begin{aligned}
\frac{d}{dt} [\psi^\dagger \sigma_x \psi] &= \frac{-i\hbar}{2m} \nabla^2 \psi^{\downarrow*} \psi^\uparrow + \frac{i}{\hbar} V^\downarrow \psi^{\downarrow*} \psi^\uparrow + \frac{i\hbar}{2m} \nabla^2 \psi^\uparrow \psi^{\downarrow*} - \frac{i}{\hbar} V^\uparrow \psi^\uparrow \psi^{\downarrow*} \\
&\quad - \frac{i\hbar}{2m} \nabla^2 \psi^{\uparrow*} \psi^\downarrow + \frac{i}{\hbar} V^\uparrow \psi^{\uparrow*} \psi^\downarrow + \frac{i\hbar}{2m} \nabla^2 \psi^\downarrow \psi^{\uparrow*} - \frac{i}{\hbar} V^\downarrow \psi^\downarrow \psi^{\uparrow*} \\
&= \frac{-i\hbar}{2m} \{ (\nabla^2 \psi^{\downarrow*}) \psi^\uparrow - \psi^{\downarrow*} (\nabla^2 \psi^\uparrow) + (\nabla^2 \psi^{\uparrow*}) \psi^\downarrow - \psi^{\uparrow*} (\nabla^2 \psi^\downarrow) \} \\
&\quad - \frac{i}{\hbar} (V^\uparrow - V^\downarrow) (\psi^\uparrow \psi^{\downarrow*} - \psi^{\uparrow*} \psi^\downarrow) \tag{2.33}
\end{aligned}$$

Here we first look at a nonmagnetic layer whereby  $V^\uparrow = V^\downarrow$ , removing the last term of Eq. 2.33 to give

$$\frac{d}{dt} [\psi^\dagger \sigma_x \psi] = \frac{-i\hbar}{2m} \{ (\nabla^2 \psi^{\downarrow*}) \psi^\uparrow - \psi^{\downarrow*} (\nabla^2 \psi^\uparrow) + (\nabla^2 \psi^{\uparrow*}) \psi^\downarrow - \psi^{\uparrow*} (\nabla^2 \psi^\downarrow) \} \tag{2.34}$$

Therefore, the equation of continuity is satisfied when the  $x$  component of the spin current is given by

$$J_x = \frac{i\hbar}{2m} \{ (\nabla \psi^{\downarrow*}) \psi^\uparrow - \psi^{\downarrow*} (\nabla \psi^\uparrow) + (\nabla \psi^{\uparrow*}) \psi^\downarrow - \psi^{\uparrow*} (\nabla \psi^\downarrow) \} \tag{2.35}$$

This remains true in a magnetic layer, however, the equation of continuity will include a further term involving the difference in  $\uparrow$  and  $\downarrow$  spin potentials. This can be expected since the spin current is not conserved in the same way as ordinary charge current. We are only interested however in  $J_x$  and so we simply call this term  $C_x$  in our equation of continuity such that

$$\frac{d}{dt} [\psi^\dagger \sigma_x \psi] + \nabla \cdot J_x = C_x \tag{2.36}$$

Similarly, it can be shown for the y component that

$$\frac{d}{dt} [\psi^\dagger \sigma_y \psi] + \nabla \cdot J_y = C_y \quad (2.37)$$

where

$$J_y = \frac{\hbar}{2m} \{ -(\nabla \psi^{\downarrow*}) \psi^\uparrow + \psi^{\downarrow*} (\nabla \psi^\uparrow) + (\nabla \psi^{\uparrow*}) \psi^\downarrow - \psi^{\uparrow*} (\nabla \psi^\downarrow) \} \quad (2.38)$$

We now note that by letting  $(\nabla \psi^{\downarrow*}) \psi^\uparrow = a$  and  $\psi^{\downarrow*} (\nabla \psi^\uparrow) = b$  we have that

$$J_x = \frac{i\hbar}{2m} \{ (a - a^*) - (b - b^*) \} = \frac{\hbar}{m} \Im \{ b - a \} \quad (2.39)$$

$$J_y = \frac{-\hbar}{2m} \{ (a + a^*) - (b + b^*) \} = \frac{\hbar}{m} \Re \{ b - a \} \quad (2.40)$$

where  $\Im, \Re$  denote the imaginary and real parts respectively. Substituting back for  $a$  and  $b$ , we can define  $J$  (Eq. 2.41a) such that the in-plane (parallel) and out-of-plane (perpendicular) spin current components,  $J_{\parallel}$  and  $J_{\perp}$ , can be obtained from the imaginary and real parts of  $J$  respectively (Eq. 2.41b)

$$J = \frac{\hbar}{m} \{ (\nabla \psi^\uparrow) \psi^{\downarrow*} - (\nabla \psi^{\downarrow*}) \psi^\uparrow \} \quad (2.41a)$$

$$J_{\parallel} = \Im \{ J \} \text{ and } J_{\perp} = \Re \{ J \} \quad (2.41b)$$

## 2.4 Landauer formalism

In order to calculate the local spin current in a realistic system consisting of ferromagnets with a finite exchange splitting, it is necessary to specify

appropriate boundary conditions in the left and right leads such that we can correctly match the wave functions across all interfaces. This was done previously by Landauer [5] in a similar problem involving charge current. He showed that the conductance of a system sandwiched between two reservoirs is given by its total quantum mechanical transmission coefficient,  $T$ . Since the charge current is conserved throughout the system, the total transmission coefficient therefore provides us with all the information there is about the transport of charge. Similarly, if we are only interested in the spin current due to a single interface between a nonmagnet and a magnet, the concept of conductance remains valid and can be easily generalized to include spin dependant scattering from the local exchange potential. However, since spin current is not conserved, we need to calculate it locally within the structure. To determine the local spin current without any approximations, the Landauer method needs to be applied to the whole magnetic layer structure as was done previously by Camley [26]. We will use this approach by looking at our general system consisting of two ferromagnets separated by a nonmagnetic spacer layer. The left magnet (polarizing magnet) has its magnetization rotated by angle  $\theta$  in the  $yz$ -plane and the right magnet (switching magnet) has its magnetization fixed parallel to the spin quantization axis ( $z$ -axis). The magnets are then connected to left and right reservoirs by nonmagnetic leads. An infinitesimal bias  $V_b$  is applied between the left and right reservoirs so that their electron distributions are characterised by two Fermi functions  $f(\omega - \mu_L)$  and  $f(\omega - \mu_R)$  with  $\mu_L - \mu_R = eV_b$ . Since we assume that  $V_b$  is infinitesimal, the one-electron states of the system can be calculated from the Schrödinger Equation (Eq. 2.1) neglecting the effect of  $V_b$ . We classify

the electron spin projections as  $\uparrow$  or  $\downarrow$ , parallel or antiparallel respectively to the global spin quantization axis ( $z$  - axis).

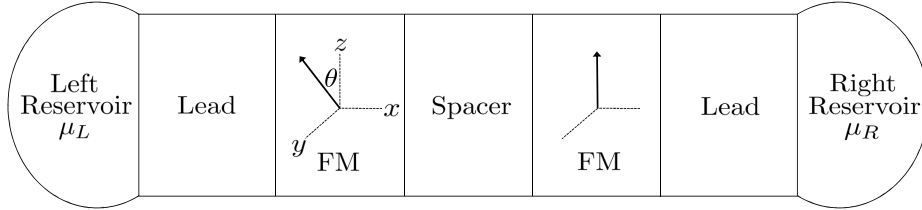


Fig. 2.2: Electrons of all energies  $\omega$  up to  $\mu_L$  ( $\mu_R$ ) and momenta  $k_{\parallel}$  parallel to the layers are omitted from the left and right reservoirs.

Electrons of either spin orientation ( $\uparrow, \downarrow$ ) are incident on the system both from the left and right reservoirs. In order to determine the spin current from Eq. 2.41, we therefore need to solve four independent one-electron scattering problems. The first problem corresponds to an  $\uparrow$  spin electron incident from the left which is partially reflected both to the  $\uparrow$  spin and  $\downarrow$  spin channels in the left lead and partially transmitted to the  $\uparrow$  spin and  $\downarrow$  spin channels in the right lead. Similarly, a  $\downarrow$  spin electron incident from the left reservoir is reflected and transmitted to both  $\uparrow$  spin and  $\downarrow$  spin channels in the left and right leads respectively. Finally, both  $\uparrow$  spin and  $\downarrow$  spin electrons incident from the right reservoir are similarly reflected and transmitted to both spin channels in the right and left leads respectively.

If  $J_i^L(\sigma, \omega, k_{\parallel})$  is the in- or out-of-plane spin current component ( $i = \parallel, \perp$ ) due to an electron of spin  $\sigma$  incident from the left reservoir with an energy

$\omega$  and parallel wave vector  $k_{\parallel}$ , and  $J_i^R(\sigma, \omega, k_{\parallel})$  is the corresponding contribution due to an electron incident from the right reservoir, we can write the total spin current in any part of the structure by summing over the contributions from all the electrons incident on the entire system as

$$J_i^{tot} = \sum_{k_{\parallel}} \int d\omega \{ f(\omega - \mu_L) [J_i^L(\uparrow, \omega, k_{\parallel}) + J_i^L(\downarrow, \omega, k_{\parallel})] + f(\omega - \mu_R) [J_i^R(\uparrow, \omega, k_{\parallel}) + J_i^R(\downarrow, \omega, k_{\parallel})] \} \quad (2.42)$$

where  $J_i^{L(R)} = j_i^{L(R)}(dk_{\perp}/d\omega)$  was used to convert the sum over  $k_{\perp}$  into an energy integral where  $\omega = \frac{\hbar^2}{2m}(k_{\parallel}^2 + k_{\perp}^2)$ . Using the identities Eq. 2.43 and Eq. 2.44

$$f_R = (1/2)[f_R + f_L] + (1/2)[f_R - f_L] \quad (2.43)$$

$$f_L = (1/2)[f_R + f_L] - (1/2)[f_R - f_L] \quad (2.44)$$

where  $f_L$  and  $f_R$  denote the Fermi functions in the left and right reservoirs, we can finally write the total spin current as Eq. 2.45

$$J_i^{tot} = \sum_{k_{\parallel}, \sigma} \int d\omega \{ [J_i^L(\sigma, \omega, k_{\parallel}) + J_i^R(\sigma, \omega, k_{\parallel})](f_L + f_R) + [J_i^L(\sigma, \omega, k_{\parallel}) - J_i^R(\sigma, \omega, k_{\parallel})](f_L - f_R) \} \quad (2.45)$$

---

This form of the Landauer (Eq. 2.45) is immediately useful for discussing some general properties of the spin current. In the absence of bias, only the terms proportional to the sum of the Fermi functions remain. It can be shown that  $J_{\parallel}^{tot} = 0$  both in the spacer and in the leads. We also have  $J_{\perp}^{tot} = 0$  in the leads but  $J_{\perp}^{tot} \neq 0$  in the spacer. The term  $J_{\perp}^{tot}$  in the spacer determines the oscillatory exchange coupling between the two ferromagnets. This thesis is primarily concerned with that part of the spin current which couples to  $f_L - f_R$  and hence vanishes in the absence of bias. We call this the transport spin current  $J^T$  and we will later evaluate the transport spin current from Eq. 2.45 throughout various magnetic multilayer junctions for the simple parabolic band model using the transfer matrix method to determine the electron wave functions in each layer of interest.

### 3. TUNNELING MAGNETORESISTANCE IN THE TRILAYER

#### 3.1 *Reduction of the general formalism for collinear configurations*

We will first look at a set of collinear spin problems whereby the two magnetic layers in our general multilayer junction (Fig. 2.2) have their rotated magnetizations either ferromagnetically or anti-ferromagnetically aligned (parallel/anti-parallel to the net magnetization). The general formalisms for systems consisting of layers with rotated spin angular momentum can be easily reduced to these collinear spin problems simply by setting the angle of rotated magnetization  $\theta = 0$  in all layers that are ferromagnetically aligned and  $\theta = \pi$  in those that are anti-ferromagnetically aligned. We will then proceed to find analytical conditions for optimising tunneling magnetoresistance (TMR) in given systems and to show how a ‘switching’ effect can be used to control it.

Hence, the general wave functions (Eq. 2.18) for the  $i^{th}$  layer are reduced

to

$$\psi_i^\uparrow = -A_i^\downarrow e^{k_i^\downarrow x} - B_i^\downarrow e^{-k_i^\downarrow x} \quad (3.1a)$$

$$\psi_i^\downarrow = A_i^\uparrow e^{k_i^\uparrow x} + B_i^\uparrow e^{-k_i^\uparrow x} \quad (3.1b)$$

if parallel ( $\theta_i = 0$ ) and

$$\psi_i^\uparrow = -A_i^\uparrow e^{k_i^\uparrow x} - B_i^\uparrow e^{-k_i^\uparrow x} \quad (3.2a)$$

$$\psi_i^\downarrow = -A_i^\downarrow e^{k_i^\downarrow x} - B_i^\downarrow e^{-k_i^\downarrow x} \quad (3.2b)$$

if anti-parallel ( $\theta_i = \pi$ ).

The general transfer matrix (Eq. 2.22) for an interface between two layers that are both aligned parallel to the spin quantization axis ( $z$ -axis) such that  $\frac{1}{2}(\theta_i - \theta_{i-1}) = 0$  reduces to

$$M_i^T = \frac{1}{2} \begin{pmatrix} \xi(k_i^\uparrow, k_{i-1}^\uparrow) & 0 \\ 0 & \xi(k_i^\downarrow, k_{i-1}^\downarrow) \end{pmatrix} \quad (3.3)$$

Similarly, in the anti-ferromagnetic configuration, the general transfer matrix for an interface between a layer aligned parallel to the spin quantization axis and a ferromagnet with magnetization rotated by  $\pi$  such that  $\frac{1}{2}(\theta_i - \theta_{i-1}) = \pm \frac{\pi}{2}$  reduces to

$$M_i^T = \frac{1}{2} \begin{pmatrix} 0 & \pm\xi(k_i^\uparrow, k_{i-1}^\downarrow) \\ \mp\xi(k_i^\downarrow, k_{i-1}^\uparrow) & 0 \end{pmatrix} \quad (3.4)$$

The transfer matrix for the ferromagnetically aligned system whereby  $\frac{1}{2}(\theta_i - \theta_{i-1}) = 0$  shows that in this instance, the original 4x4 transfer matrix (Eq. 2.22) is made up of two identical 2x2 matrix systems in terms of  $\uparrow$  and  $\downarrow$  spin potentials and so we need only solve a general 2x2 system of the form

$$\vec{A}_i = M_i^T \vec{A}_{i-1} \quad (3.5)$$

where

$$\psi_i = A_i e^{k_i x} + B_i e^{-k_i x} \quad (3.6)$$

$$\vec{A}_i = \begin{pmatrix} A_i \\ B_i \end{pmatrix} \quad (3.7)$$

$$M_i^T = \begin{pmatrix} e^{-x_i(k_i - k_{i-1})} \left(1 + \frac{k_{i-1}}{k_i}\right) & e^{-x_i(k_i + k_{i-1})} \left(1 - \frac{k_{i-1}}{k_i}\right) \\ e^{x_i(k_i + k_{i-1})} \left(1 - \frac{k_{i-1}}{k_i}\right) & e^{x_i(k_i - k_{i-1})} \left(1 + \frac{k_{i-1}}{k_i}\right) \end{pmatrix} \quad (3.8)$$

We can use this form of the transfer matrix (Eq. 3.8) to solve for the wave functions in each layer of a general magnetic multilayer junction consisting of  $n$  layers. The solution on the far left (semi-infinite lead) is of the form  $\psi_0 = A_0 e^{k_0 x} + B_0 e^{-k_0 x}$  where  $A_0 e^{k_0 x}$  corresponds to the incident wave and  $B_0 e^{-k_0 x}$ , the reflected wave. Thus, we have that  $A_0 = 1$  and  $B_0 = R$ , the reflection coefficient. Similarly, in the right semi-infinite lead, we have that  $A_n = T$ , the amplitude of the transmission coefficient, and  $B_n = 0$ , assuming there are no incident electrons from the right of the junction.

We can use this form of the transfer matrix (Eq. 3.8) to solve for the wave functions in each layer of a general magnetic multilayer junction consisting of  $n$  layers. The solution on the far left (semi-infinite lead) is of the form  $\psi_0 = A_0 e^{k_0 x} + B_0 e^{-k_0 x}$  where  $A_0 e^{k_0 x}$  corresponds to the incident wave and  $B_0 e^{-k_0 x}$ , the reflected wave. Thus, we have that  $A_0 = 1$  and  $B_0 = R$ , the reflection coefficient. Similarly, in the right semi-infinite lead, we have that  $A_n = T$ , the amplitude of the transmission coefficient, and  $B_n = 0$ , assuming there are no incident electrons from the right of the junction.

We can use this form of the transfer matrix (Eq. 3.8) to solve for the wave functions in each layer of a general magnetic multilayer junction consisting of  $n$  layers. The solution on the far left (semi-infinite lead) is of the form  $\psi_0 = A_0 e^{k_0 x} + B_0 e^{-k_0 x}$  where  $A_0 e^{k_0 x}$  corresponds to the incident wave and  $B_0 e^{-k_0 x}$ , the reflected wave. Thus, we have that  $A_0 = 1$  and  $B_0 = R$ , the reflection coefficient. Similarly, in the right semi-infinite lead, we have that  $A_n = T$ , the amplitude of the transmission coefficient, and  $B_n = 0$ , assuming there are no incident electrons from the right of the junction.

We can use this form of the transfer matrix (Eq. 3.8) to solve for the wave

functions in each layer of a general magnetic multilayer junction consisting of  $n$  layers. The solution on the far left (semi-infinite lead) is of the form  $\psi_0 = A_0 e^{k_0 x} + B_0 e^{-k_0 x}$  where  $A_0 e^{k_0 x}$  corresponds to the incident wave and  $B_0 e^{-k_0 x}$ , the reflected wave. Thus, we have that  $A_0 = 1$  and  $B_0 = R$ , the reflection coefficient. Similarly, in the right semi-infinite lead, we have that  $A_n = T$ , the amplitude of the transmission coefficient, and  $B_n = 0$ , assuming there are no incident electrons from the right of the junction.

Substituting for  $\vec{A}_i$ ,  $M_i^T$  and  $\vec{A}_{i-1}$  in Eq. 3.5, we have

$$\begin{aligned} \begin{pmatrix} T \\ 0 \end{pmatrix} &= \begin{pmatrix} A_n \\ B_n \end{pmatrix} = M_n^T \begin{pmatrix} A_{n-1} \\ B_{n-1} \end{pmatrix} = M_n^T M_{n-1}^T \begin{pmatrix} A_{n-2} \\ B_{n-2} \end{pmatrix} \\ &= M_n^T M_{n-1}^T \dots M_1^T \begin{pmatrix} A_0 \\ B_0 \end{pmatrix} = M_n^T M_{n-1}^T \dots M_1^T \begin{pmatrix} 1 \\ R \end{pmatrix} \end{aligned} \quad (3.9)$$

Therefore, by defining  $M^{Total}$  as the total transfer matrix across the entire system from left to right, we have

$$\begin{pmatrix} T \\ 0 \end{pmatrix} = M^{Total} \begin{pmatrix} 1 \\ R \end{pmatrix} \quad (3.10)$$

where

$$M^{Total} = M_n^T M_{n-1}^T \dots M_1^T \quad (3.11)$$

Eq. 3.10 gives us two equations with two unknowns and so we can solve explicitly for the transmission and reflection coefficients,  $T$  and  $R$  respectively. By letting  $m_{ij}$  denote the element of  $M^{Total}$  in the  $i^{th}$  row and  $j^{th}$  column, we have

$$R = \frac{-m_{21}}{m_{22}} \quad (3.12)$$

$$T = m_{11} + m_{12}R \quad (3.13)$$

The transmission and reflection coefficients provide a great deal of insight into the physical properties and quantum effects found in these collinearly arranged magnetic multilayer junctions. As such, we are seeking conditions that imply good tunneling magnetoresistance (TMR). That is to say, conditions which assist the total transmission of a propagating particle from left to right in our system. This can be sufficiently formulated from the modulus square of the transmission coefficient,  $|T|^2 = 1$ . Similarly, total transmission implies zero reflection and so, we can initially check the conditions satisfying  $R = 0$ . From the expressions for  $R$  and  $T$  (Eq. 3.12 and Eq. 3.13), we see that since these coefficients are complex, we will need to satisfy the following three conditions

$$\Re\{m_{21}\} = 0 \quad (3.14)$$

$$\Im\{m_{21}\} = 0 \quad (3.15)$$

$$\Re\{m_{22}\} \neq 0 \text{ or } \Im\{m_{22}\} \neq 0 \quad (3.16)$$

Eq. 3.14, Eq. 3.15 and Eq. 3.16 impose that both the real ( $\Re$ ) and imaginary ( $\Im$ ) parts of the numerator  $m_{21}$  of  $R$  (Eq. 3.12) are exactly zero under the same conditions, whilst ensuring that this does not imply that the denominator  $m_{22}$  of  $R$  is also zero. The latter restriction is sufficiently upheld if either the real and/or imaginary parts of  $m_{22}$  are non-zero. We will use these conditions throughout the remainder of this chapter to investigate analytically the optimum conditions for supporting such tunneling effects in various scattering problems resulting from the trilayer junction.

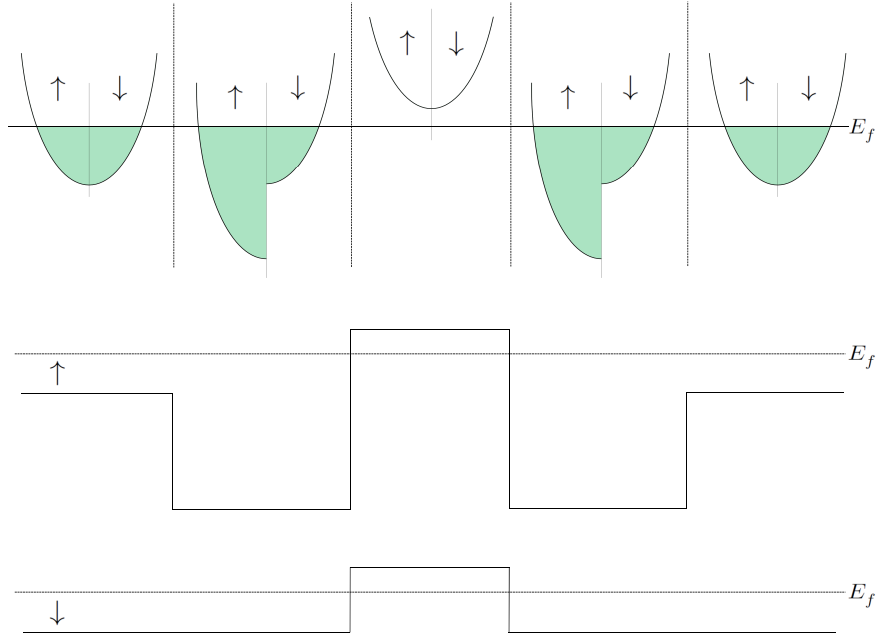
### 3.2 Collinear trilayer spin band configuration

We now have all the tools we need to jump straight in to a much studied tunneling problem, the trilayer. The trilayer is a magnetic multilayer nanostructure consisting of a nonmagnetic spacer layer sandwiched between two magnets. The two magnets are either ferromagnetically (parallel) or antiferromagnetically (anti-parallel) aligned. The ferromagnetic configuration has been shown experimentally to produce good transmission (resonant

---

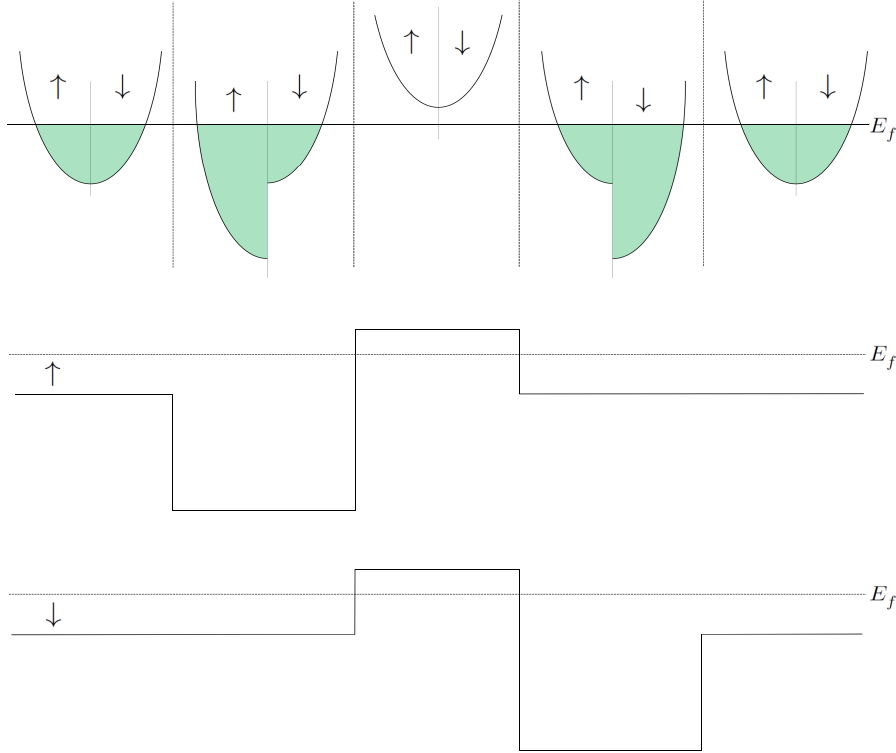
tunneling) versus the antiferromagnetic configuration which produces poor transmission. This forms the basis of tunneling magnetoresistance (TMR). Electrons under the right conditions can propagate through the system until a ‘switching’ effect is enforced causing the anti-parallel configuration to occur and hence reducing the tunneling effect. We will now explore the trilayer and seek analytically the right conditions for TMR.

Fig. 3.1 shows the  $\uparrow$  and  $\downarrow$  spin band schematic for the ferromagnetically aligned trilayer contained between left and right leads. Below this band schematic is a potential well/barrier representation for both the  $\uparrow$  and  $\downarrow$  spin bands. From this we can see that an  $\uparrow$  spin electron moving across the system from left to right will encounter a potential barrier sandwiched between two potential wells, whereas a  $\downarrow$  spin electron will simply encounter a single potential barrier.



*Fig. 3.1:* Schematic picture showing the  $\uparrow$  and  $\downarrow$  spin potentials of the ferromagnetically aligned trilayer for each spin band.

Similarly, Fig. 3.2 shows the band schematic for the antiferromagnetic configuration whereby the switching magnet on the right has had its spin angular momentum reversed to an anti-parallel configuration. Here we see that an  $\uparrow$  spin electron moving across the system from left to right will encounter a potential well followed by a potential barrier, whereas a  $\downarrow$  spin electron will now have a potential well proceeding the barrier in its path.



*Fig. 3.2:* Schematic picture showing the  $\uparrow$  and  $\downarrow$  spin potentials of the antiferromagnetically aligned trilayer for each spin band.

In both of these collinear configurations (Fig. 3.1) and (Fig. 3.2), the  $\uparrow$  and  $\downarrow$  spin bands are matched in the left and right semi-infinite leads. Furthermore we see from the potential well/barrier representations in each that we have four individual scattering problems to investigate analytically using the conditions derived in Sec. 3.1 for optimising the probability of resonant tunnelling of individual electrons propagating from left to right.

### 3.3 Potential barrier sandwiched between two potential wells

The first tunneling problem is for the  $\uparrow$  spin incident electron in the ferromagnetic configuration of a trilayer junction (Fig. 3.1) consisting of a potential barrier sandwiched between two potential wells. We first look at an asymmetric configuration with no matching of the potentials in the left and right wells. This can be easily achieved by using different widths for each well as illustrated in Fig. 3.3.

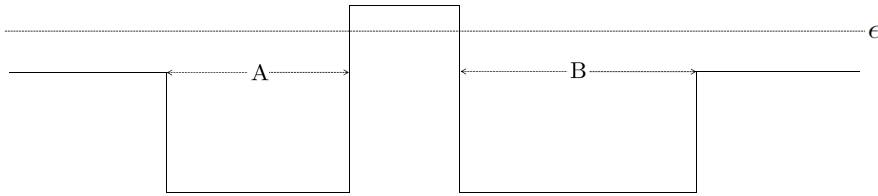


Fig. 3.3: Potential barrier sandwiched between a left well of width  $A$  and a right well of width  $B$ .

Studying this general trilayer problem and solving for the total transfer matrix (Eq. 3.11) for a single incident electron travelling with energy  $\epsilon$  from the left, we can determine the necessary conditions for zero reflection in terms of the transfer matrix elements. In doing so, we see that the first condition (Eq. 3.14) reduces to  $\sinh(A - B) = 0$ , showing that it is necessary for the wells to be of equal width and so we define the system as symmetric as illustrated in Fig. 3.4.

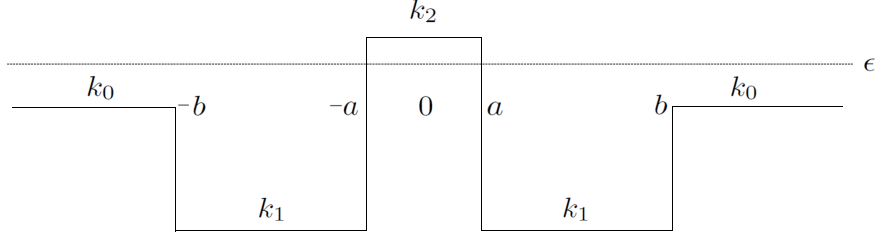


Fig. 3.4: Potential barrier sandwiched between left and potential right wells with exact matching providing symmetry.

Here, the first condition (Eq. 3.14) is immediately satisfied. The second condition (Eq. 3.15) shows that it is possible to impose zero reflection and hence total transmission for the ferromagnetically aligned symmetric trilayer junction by means of satisfying Eq. 3.17

$$\sin[2(b-a)|k_1| + \Gamma] = \Delta \quad (3.17)$$

where  $\Delta$  is given by

$$\Delta = \frac{(|k_1^2| + |k_0^2|)(|k_1^2| + k_2^2) \tanh 2ak_2}{(|k_1^2| - |k_0^2|) \sqrt{(|k_1^2| - k_2^2)^2 \tanh^2 2ak_2 + 4|k_1^2|k_2^2}} \quad (3.18)$$

and  $\Gamma$  is given by

$$\tan \Gamma = \frac{1}{2} \left( \frac{|k_1|}{k_2} - \frac{k_2}{|k_1|} \right) \tanh 2ak_2 \quad (3.19)$$

Finally, we will also need to ensure that we satisfy the third condition (Eq. 3.16) which reduces to Eq. 3.20

$$\tanh 2ak_2 \neq \frac{2k_2^2(|k_1^2| - |k_0^2|)}{2|k_0^2|k_2^2 + |k_1^4| + k_2^4} \quad (3.20)$$

From this see that we can indeed achieve full transmission of an  $\uparrow$  spin electron in the ferromagnetically aligned trilayer if the conditions given by Eq. 3.17 and Eq. 3.20 are met. These conditions seem surprisingly easy to satisfy since Eq. 3.18 shows  $\Delta$  to be a constant, however, we do need to ensure that  $|\Delta| \leq 1$  since  $|\sin[2(b-a)|k_1| + \Gamma]|$  can never exceed one. This makes a lot of sense since  $2a$  is the width of the barrier. Therefore, for a very narrow barrier, the factor  $\tanh 2ak_2$  will be very small and these conditions will be easily satisfied. Conversely, for a wide barrier, it would be impossible to satisfy.

### 3.4 Single potential barrier

The next tunneling problem is for the  $\downarrow$  spin incident electron in the ferromagnetic configuration of a trilayer junction (Fig. 3.1) consisting of a single potential barrier as illustrated in Fig. 3.5

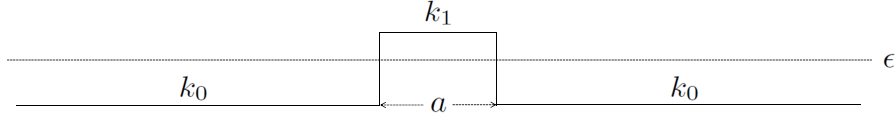


Fig. 3.5: Single potential barrier.

Calculating the total transfer matrix (Eq. 3.11) in this instance for a single electron travelling with energy  $\epsilon$  from the left and solving for zero reflection by the potential barrier, we see from the first condition (Eq. 3.14) that  $ak_1 = 0$ . This can only be satisfied by having a barrier of width  $a = 0$  and so this proves that full transmission is impossible. We can note however that for a very thin barrier, the reflection coefficient will tend to zero and hence the rate of transmission will improve and approach one.

### 3.5 Potential well adjacent to a potential barrier

The third tunneling problem is for the  $\uparrow$  spin incident electron in the anti-ferromagnetic configuration of a trilayer junction (Fig. 3.1) consisting of a potential well adjacent to a potential barrier. In this instance the potential well precedes the barrier as illustrated in Fig. 3.6

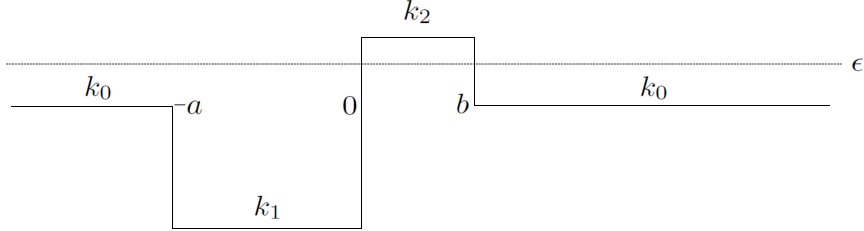


Fig. 3.6: Potential well adjacent to a potential barrier

Calculating the total transfer matrix (Eq. 3.11) for a single electron travelling with energy  $\epsilon$  from the left and solving for zero reflection in the left semi-infinite lead as before, we see from the first condition (Eq. 3.14) that  $ak_1 = in\pi$ . This can be easily satisfied for all propagating waves in the left polarizing magnet (potential well) of the form  $k_1 = \frac{in\pi}{a}$ . However, the second condition (Eq. 3.15) can only be satisfied if  $bk_2 = 0$ . Similarly to the single barrier problem, this proves conclusively that we can never achieve exactly zero reflection, and hence total transmission, since we cannot have a system whereby  $bk_2 = 0$ . We can note however that by fitting an integer number of wavelengths across the well, the reflection coefficient becomes proportional to the width of the barrier  $b$  and so for a very thin barrier, we can come very close to total transmission, however, we can never achieve exactly one.

This is exactly true for the fourth tunneling problem for the  $\downarrow$  spin incident electron in the antiferromagnetic configuration of a trilayer junction (Fig. 3.2) consisting of a potential barrier that precedes an adjacent potential well. We can fit an integer number of wavelengths across the right switching magnet however we can only approach full transmission as the width of the

barrier approaches zero.

Therefore, in conclusion for the collinear trilayer contained between left and right leads, we have shown that in the ferromagnetic configuration, we can indeed transmit  $\uparrow$  spin electrons with a 100% success rate by developing a symmetric trilayer junction with exact matching in the  $\uparrow$  spin band of the left polarizing and right switching magnets and by fitting an integer number of wavelengths across these magnetic layers. If we then introduce a wide enough nonmagnetic spacer layer (potential barrier) sandwiched between the left and right ferromagnets, we can still allow for this 100% success rate in the  $\uparrow$  spin channel whilst making it very difficult for transmission to occur in the  $\downarrow$  spin channel. Additionally once the magnetization of the right switching magnet has been realigned to the antiferromagnetic configuration under the same conditions, the wide spacer layer will make it very difficult for transmission to occur in either spin channel.

### 3.6 Resonant tunneling in a double barrier

Given the results we have obtained for the collinear trilayer, we will now look at a final collinear tunneling problem based on the trilayer junction but with exact matching between the non-magnetic spacer layer and the left and right semi-infinite leads. In order to achieve this configuration, we adjust the trilayer band schematic (Fig. 3.1) as shown in Fig. 3.7.

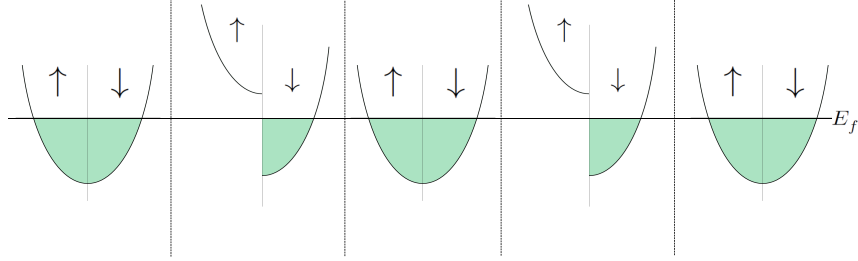


*Fig. 3.7:* Schematic picture showing the  $\uparrow$  and  $\downarrow$  spin bands of the ferromagnetically aligned trilayer with matching across the nonmagnetic spacer and the left and right leads.

This configuration produces a new scattering problem in the  $\uparrow$  spin channel consisting of two separated potential barriers as illustrated in Fig. 3.8.

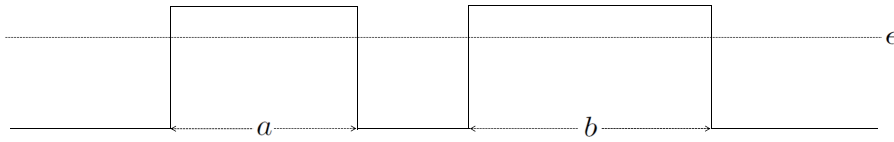


*Fig. 3.8:* Two separated potential barriers.

Studying this general double barrier problem and solving for the total transfer matrix (Eq. 3.11) for a single incident electron travelling with energy  $\epsilon$  from the left, we can immediately determine, as for the general trilayer problem, that the first necessary condition (Eq. 3.14) required for zero reflection reduces to  $\sinh(a - b) = 0$  showing that it is necessary for the barriers to be of equal width in order to support total transmission and so we define

the system as symmetric as illustrated in Fig. 3.9.

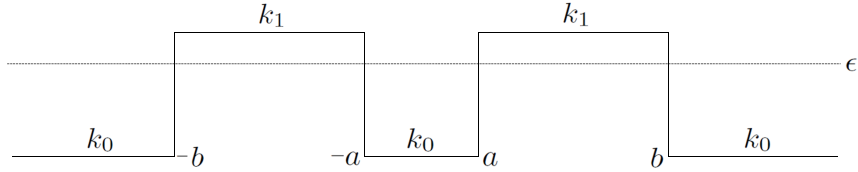


Fig. 3.9: Two separated potential barriers with exact matching providing symmetry.

Here, like with the symmetric trilayer consisting of two matched potential wells separated by a potential barrier, the first condition (Eq. 3.14) is immediately satisfied. The second condition (Eq. 3.15) shows that it is possible to impose zero reflection and hence total transmission for this double barrier configuration by means of satisfying Eq. 3.21

$$\tan 2a|k_0| = \Gamma \quad (3.21)$$

where,

$$\Gamma = \frac{2}{\left(\frac{|k_0|}{k_1} - \frac{k_1}{|k_0|}\right) \tanh(b-a)k_1} \quad (3.22)$$

In this case, the third condition (Eq. 3.16) is automatically satisfied by Eq. 3.21 and so, this is in fact a sufficient condition that directly implies full

transmission. This condition seems surprisingly easy to satisfy since  $\Gamma$  can be any non-zero constant  $\Gamma_0$  and  $\tan 2a|k_0|$  can be any value between  $-\infty$  and  $+\infty$  as illustrated in Fig. 3.10.

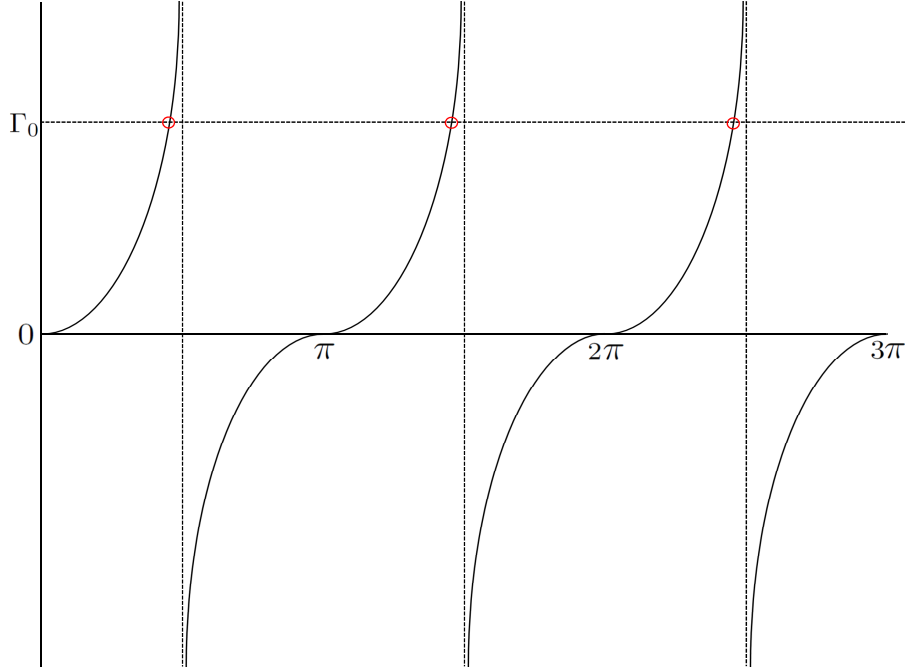


Fig. 3.10: Schematic plot of Eq. 3.21 showing solutions at intersections with constant  $\Gamma_0$ .

In conclusion, we have seen that for a magnetic multilayer junction with a collinear configuration and with matching across the layers such that an incident electron propagating from the left will see a single potential barrier in its path, the rate of transmission reduces as the width of the potential barrier increases. More surprisingly, when introducing a second potential barrier, we can achieve full transmission if the two potential barriers are identical and we can fit an integer number of half wavelengths plus a constant across the spacer separating them.

## 4. SPIN CURRENT COMPONENTS IN A FIVE LAYER JUNCTION

### 4.1 Spin band configuration of a simple five layer junction

In Chapter 3 we looked at the tunneling effects in a ferromagnetic and anti-ferromagnetic trilayer junction contained between left and right leads. In fact, the theoretical approach to the trilayer typically consists of a nonmagnetic spacer layer sandwiched between two semi-infinite ferromagnets, i.e. there are no left and right leads. We will see in Chapter 5 why this approach would not be entirely suitable when using our Landaur formalism but first we will define a simple five layer junction analogous to our trilayer that includes the left and right leads but with the magnetization in the left polarizing magnet rotated by angle  $\theta$  where  $\theta \neq n\pi$  as shown in Fig. 4.1.

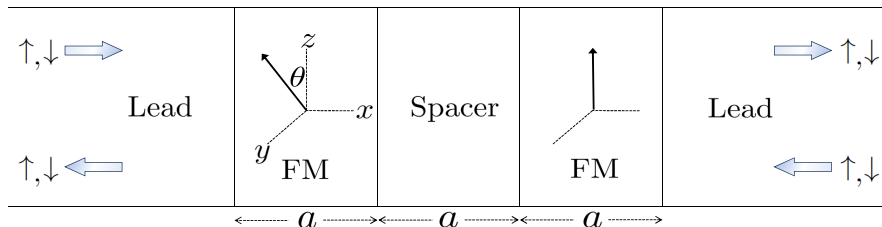


Fig. 4.1: Schematic picture of a simple five layer junction.

---

The left polarizing magnet has its magnetization rotated by angle  $\theta$  in the  $yz$  - plane and the right magnet or switching magnet has its magnetization fixed parallel to the spin quantization axis ( $z$  - axis). For simplicity, the two magnets and the nonmagnetic spacer are all of fixed width  $a$ .

The large arrows represent the  $\uparrow$  and  $\downarrow$  spin incident electrons we will be sending along the  $x$  - axis from the left and right with spin angular momenta parallel ( $\uparrow$ ) and anti-parallel ( $\downarrow$ ) to the net magnetization of the right switching magnet (parallel/anti-parallel to the  $z$  - axis).

In Sec. 2.4 we discussed that in order to calculate the local spin current in a realistic system consisting of ferromagnets with a finite exchange splitting, it is necessary to specify appropriate boundary conditions in the left and right leads such that we can correctly match the wave functions across all interfaces. As a result we have matched both the  $\uparrow$  and  $\downarrow$  spin bands in the left and right leads with zero exchange splitting in each in order to create a realistic physical picture whereby the left and right leads simulate left and right reservoirs, this is shown schematically in Fig. 4.2.

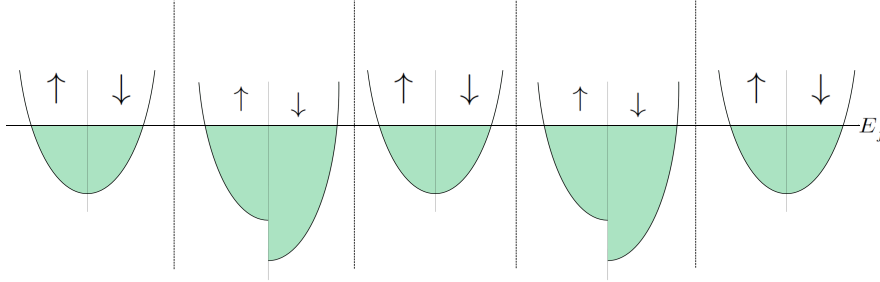


Fig. 4.2: Schematic picture showing the  $\uparrow$  and  $\downarrow$  spin bands of a simple five layer junction.

Using the general solution (Eq. 2.18) to the wave equation  $\psi_i$ , we are able to construct the wave functions in each layer of the five layer junction in terms of the perpendicular components ( $k_{\perp}$ ) of the wave vectors  $k_i^{\downarrow}$  and  $k_i^{\uparrow}$  and solve for the coefficients in each using the general transfer matrix (Eq. 2.22). The wave functions and their coefficients can then be used to calculate the local in- and out-of-plane spin current components for a single propagating wave for each spin orientation in either direction using the expression for  $J$  (Eq. 2.41). Finally, the total spin current components can be calculated using our Landauer formalism (Eq. 2.45) to include all contributions from all electrons incident on the entire system.

## 4.2 Spin current components and destructive interference

We will first calculate the in- and out-of-plane spin current components for a single propagating wave ( $k_{\perp}$ ) and then for the sum over all  $k_{\parallel}$  throughout the five layer junction defined in Sec. 4.1 whereby the ferromagnets are represented as two potential wells and the left and right lead potentials are the

same as that of the nonmagnetic spacer layer as illustrated in Fig. 4.3.

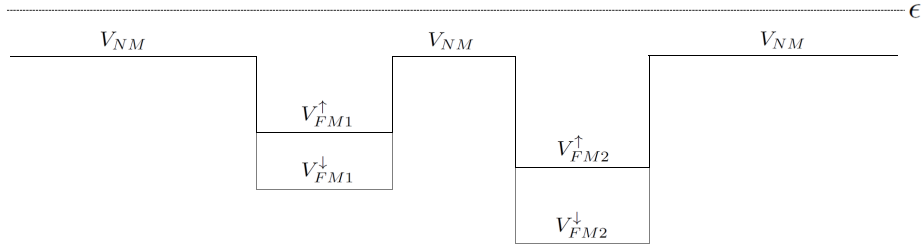


Fig. 4.3: Five layer junction represented by two potential wells.

We have fixed the angle of rotated magnetization in the left polarizing magnet to  $\theta = 1.5$ , the width of the two ferromagnets and the spacer separating them is given by  $a = 18$  and the energy of our incident electron is given by  $\epsilon = 0.5$ . The potentials in each layer are given by  $V_{NM} = -1.0$ ,  $V_{FM1}^{\uparrow} = -1.8$ ,  $V_{FM1}^{\downarrow} = -2.5$ ,  $V_{FM2}^{\uparrow} = -1.5$  and  $V_{FM2}^{\downarrow} = -2.6$ . The asymmetry is introduced by not matching the potentials in either spin band between the two ferromagnets.

The numerical results for the total in-plane spin current component ( $J_{\parallel}^T$ ) calculated for a single  $k_{\perp}$  are illustrated in Fig. 4.4.

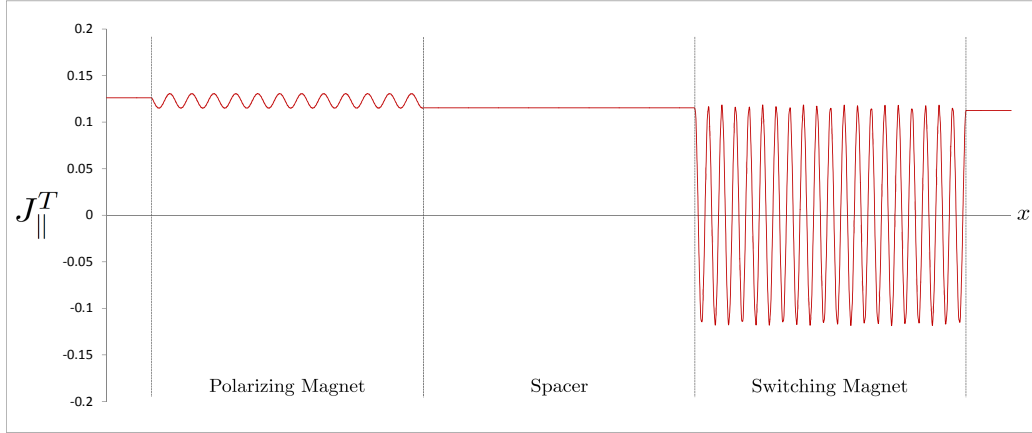


Fig. 4.4:  $J_{\parallel}^T$ , the total in-plane spin current component for incident electrons from the left and right (single  $k_{\perp}$ ) as a function of  $x$ , the position in the junction.

From Fig. 4.4, we see that the total in-plane spin current component in the nonmagnetic leads and spacer layer are constant and join continuously into the magnetic layers. The spin current is continuous at each interface because of the continuity of the wave functions and their derivatives. In the magnetic layers we see oscillations due to the precession of the electron spin in the effective molecular field produced by the magnetization of the magnet (analogous to the precessions in a conventional magnetic field). In the switching magnet (right), these precessions are oscillating about the spin quantization axis whilst in the polarizing magnet (left), we see them offset due to the rotated magnetization in the  $yz - plane$ . The two periods observed in the magnetic layers are brought about by functions of the sum and difference of the wave vectors for each spin band, i.e. The short period is given by a function of  $k^{\uparrow} + k^{\downarrow}$  and the long period is given by a function of  $k^{\uparrow} - k^{\downarrow}$ .

The total spin current is given by the difference between the contributions from either side and our Landauer formalism allows us to calculate these contributions separately. The total in-plane spin current contribution due to incident electrons from the left reservoir ( $J_{\parallel}^L$ ) calculated for a single  $k_{\perp}$  and the total in-plane spin current contribution from the right are illustrated in Fig. 4.5 and Fig. 4.6 respectively.

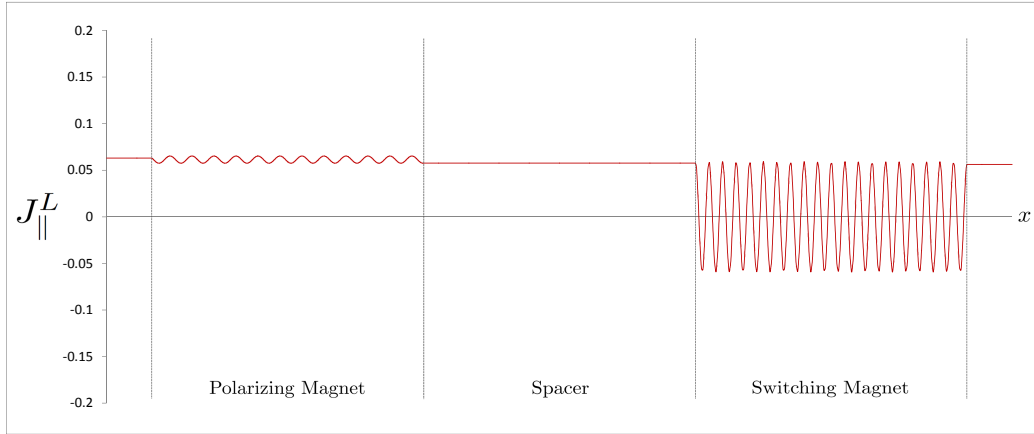


Fig. 4.5:  $J_{\parallel}^L$ , the in-plane spin current component for incident electrons from the left (single  $k_{\perp}$ ) as a function of  $x$ , the position in the junction.

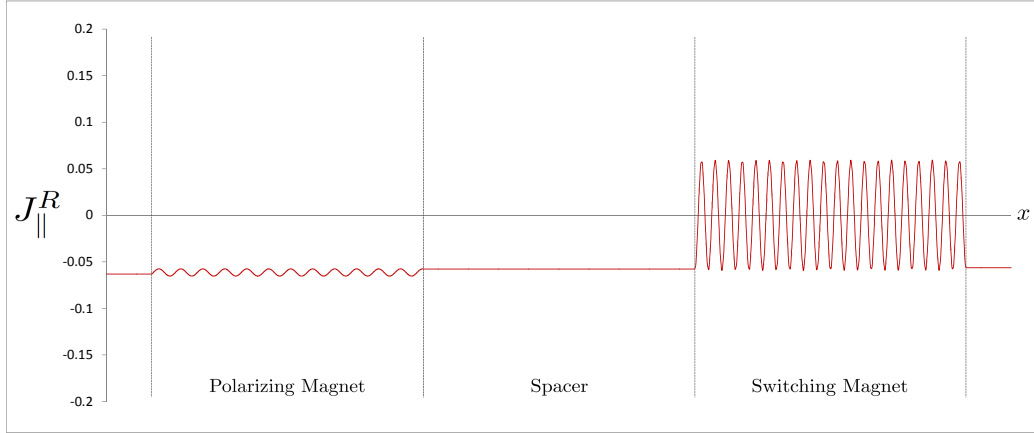


Fig. 4.6:  $J_{\parallel}^R$ , the in-plane spin current component for incident electrons from the right (single  $k_{\perp}$ ) as a function of  $x$ , the position in the junction.

Fig. 4.5 and Fig. 4.6 show that the in-plane contribution from the left is equal in magnitude but opposite sign to the contribution from the right throughout the junction, i.e.  $J_{\parallel}^L = -J_{\parallel}^R$ .

The numerical results for the total in-plane spin current component ( $J_{\parallel}^T$ ) summed over all  $k_{\parallel}$  are illustrated in Fig. 4.7.

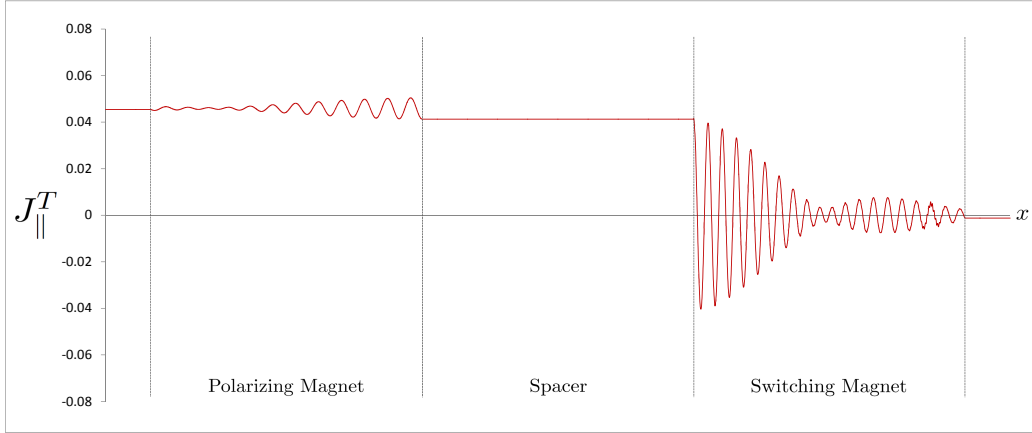


Fig. 4.7:  $J_{\parallel}^T$ , the total in-plane spin current component for incident electrons from the left and right (sum over  $k_{\parallel}$ ) as a function of  $x$ , the position in the junction.

From Fig. 4.7, we see that the in-plane spin current in the magnetic layers decays as a function of the position in the magnet when summing over all  $k_{\parallel}$  as opposed to the constant amplitude of the oscillations seen for a single propagating wave ( $k_{\perp}$ ) shown in Fig. 4.4. This decay is due to the destructive interference of oscillations with different  $k_{\perp}$ . Since  $k_{\parallel}^2 + k_{\perp}^2 = \frac{2m}{\hbar} E_F$ , we have that  $k_{\perp}$  is a rapidly varying function of  $k_{\parallel}$  and for all  $k_{\parallel} \approx 0$ ,  $k_{\perp}$  varies slowly such that the contribution survives as opposed to producing a cancelling effect.

The total in-plane spin current contribution due to incident electrons from the left reservoir ( $J_{\parallel}^L$ ) summed over all  $k_{\parallel}$  and the total in-plane spin current contribution from the right are illustrated in Fig. 4.8 and Fig. 4.9 respectively.

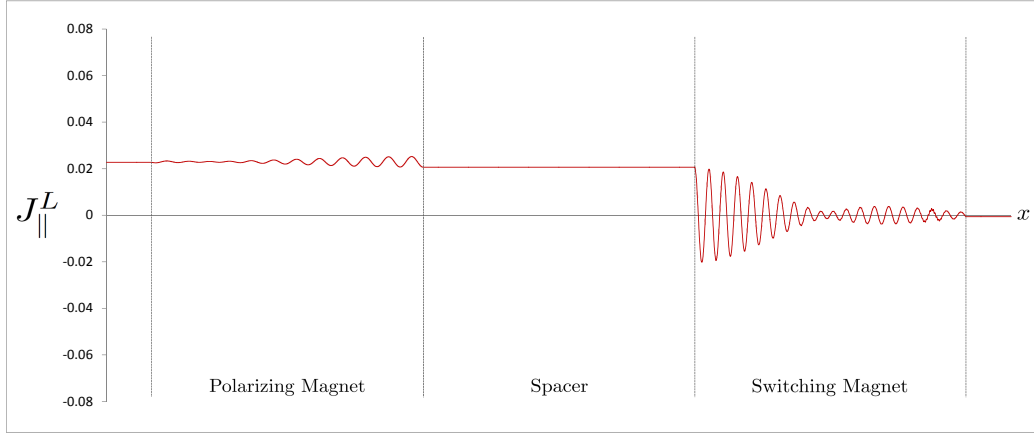


Fig. 4.8:  $J_{\parallel}^L$ , the in-plane spin current component for incident electrons from the left (sum over  $k_{\parallel}$ ) as a function of  $x$ , the position in the junction.

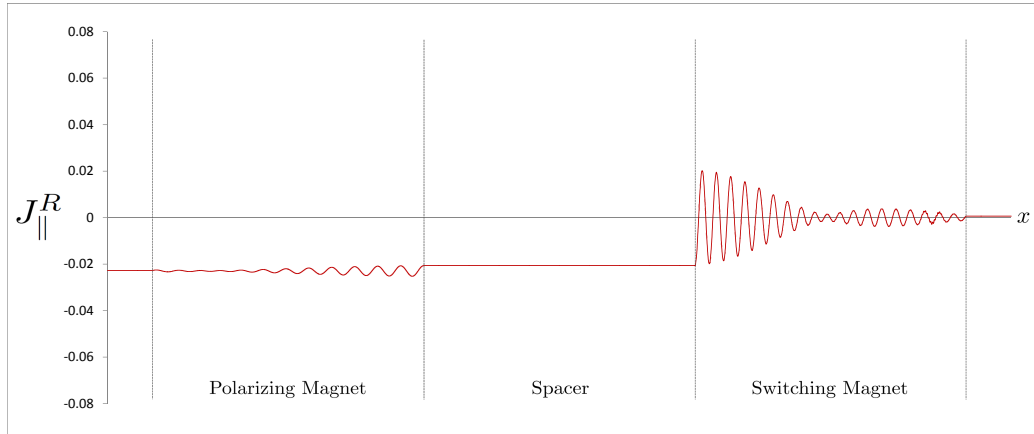


Fig. 4.9:  $J_{\parallel}^R$ , the in-plane spin current component for incident electrons from the right (sum over  $k_{\parallel}$ ) as a function of  $x$ , the position in the junction.

Fig. 4.8 and Fig. 4.9 show that, as observed previously for a single  $k_{\perp}$ , the in-plane contribution from the left is equal in magnitude but opposite sign to the contribution from the right throughout the junction after summing over all  $k_{\parallel}$ .

The numerical results for the total out-of-plane spin current component ( $J_{\perp}^T$ ) calculated for a single  $k_{\perp}$  are illustrated in Fig. 4.10.

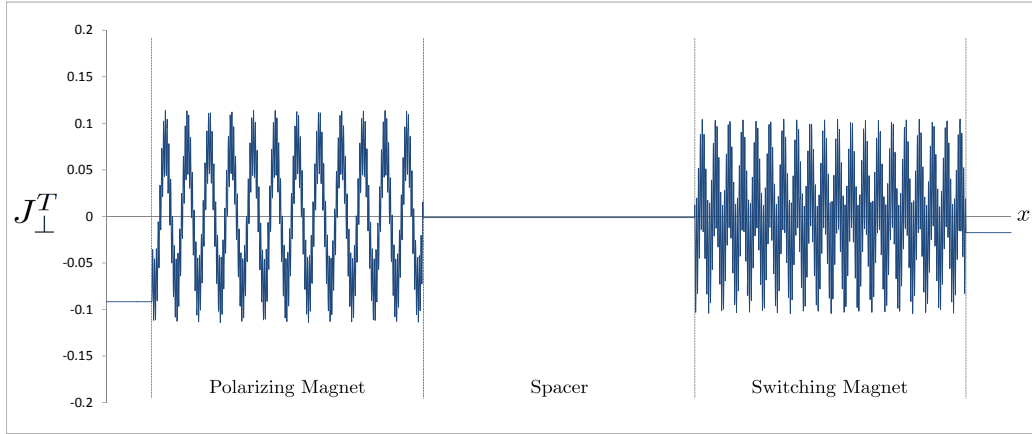


Fig. 4.10:  $J_{\perp}^T$ , the total out-of-plane spin current component for incident electrons from the left and right (single  $k_{\perp}$ ) as a function of  $x$ , the position in the junction.

From Fig. 4.10, we see that similarly to the in-plane spin current, the total out-of-plane spin current component in the nonmagnetic leads and spacer layer are constant and join continuously into the magnetic layers where we see oscillations due to the precession of the electron spin in the effective molecular field. This spin precession in the left and right ferromagnets results in a non-zero out-of-plane spin current component in the nonmagnetic spacer as shown in Fig. 4.11.

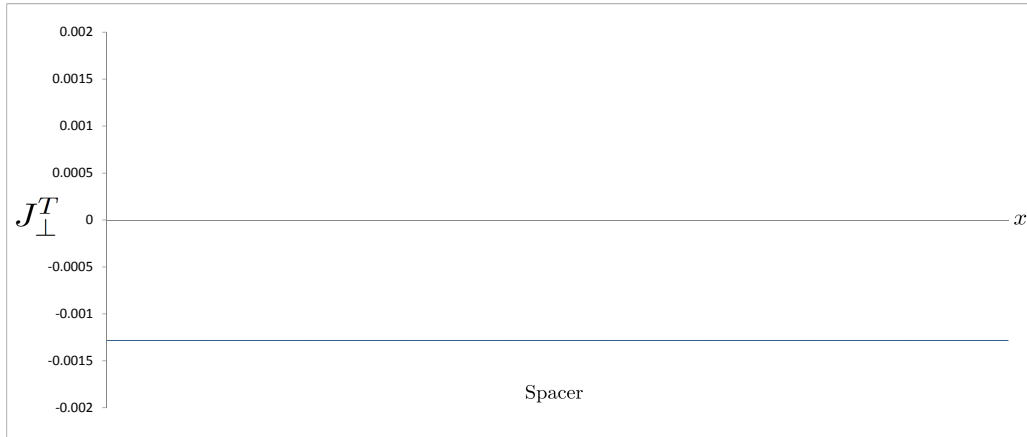


Fig. 4.11:  $J_{\perp}^T$ , the constant non-zero out-of-plane spin current component for incident electrons from the left and right (single  $k_{\perp}$ ) as a function of  $x$ , the position in the nonmagnetic spacer.

The total out-of-plane spin current contribution due to incident electrons from the left reservoir ( $J_{\perp}^L$ ) calculated for a single  $k_{\perp}$  and the total out-of-plane spin current contribution from the right are illustrated in Fig. 4.12 and Fig. 4.13 respectively.

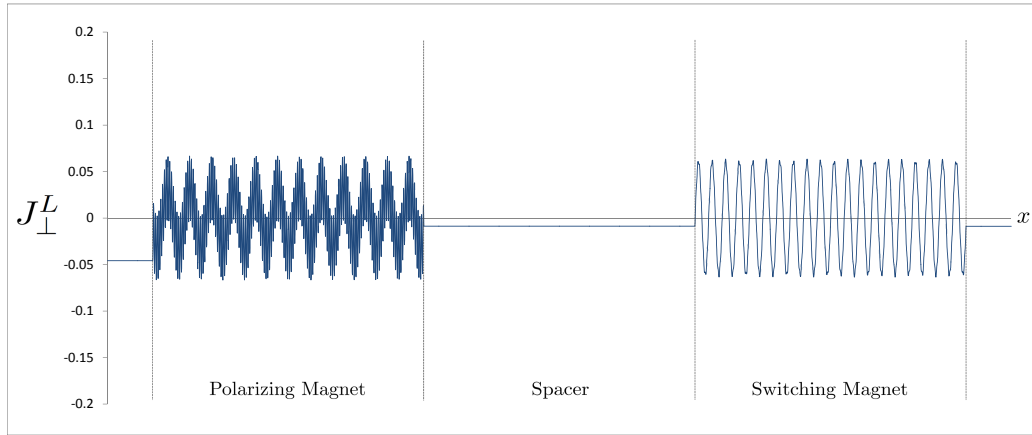


Fig. 4.12:  $J_{\perp}^L$ , the out-of-plane spin current component for incident electrons from the left (single  $k_{\perp}$ ) as a function of  $x$ , the position in the junction.

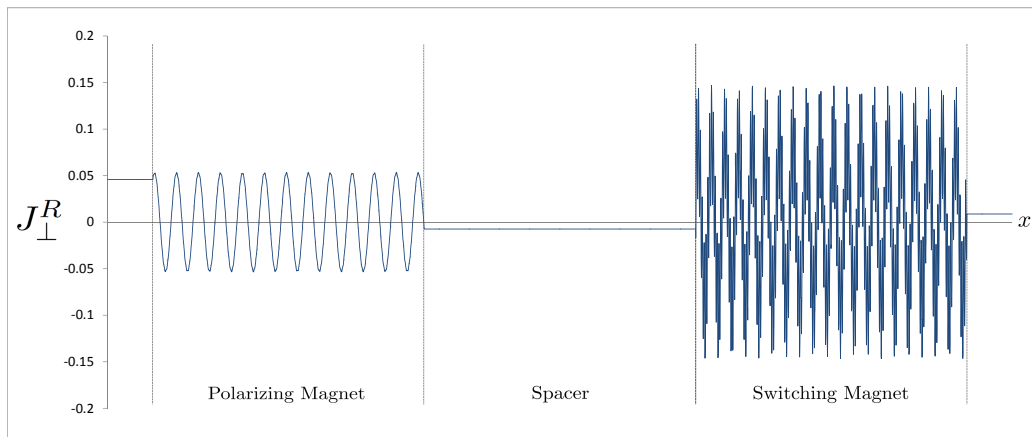


Fig. 4.13:  $J_{\perp}^R$ , the out-of-plane spin current component for incident electrons from the right (single  $k_{\perp}$ ) as a function of  $x$ , the position in the junction.

Fig. 4.12 and Fig. 4.13 show that the out-of-plane contribution from the left is equal in magnitude but opposite sign to the contribution from the right in the nonmagnetic semi-infinite leads.

The numerical results for the total out-of-plane spin current component ( $J_{\perp}^T$ ) summed over all  $k_{\parallel}$  are illustrated in Fig. 4.14.

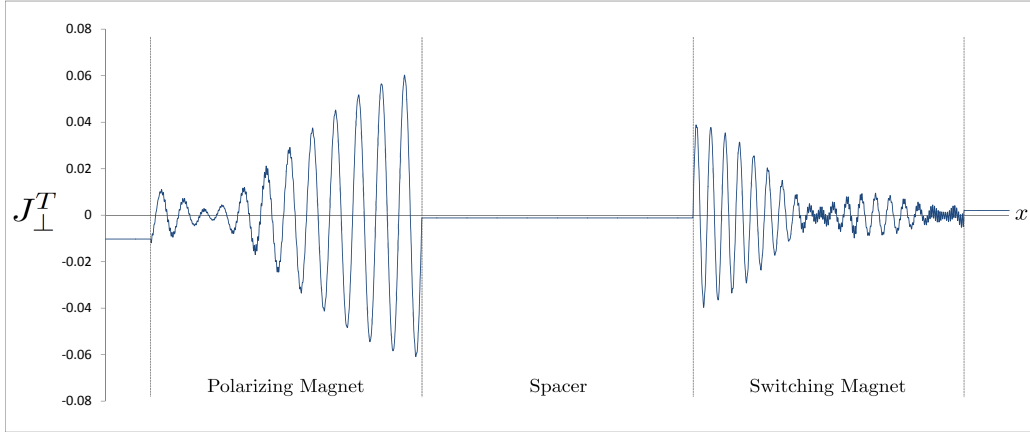


Fig. 4.14:  $J_{\perp}^T$ , the total out-of-plane spin current component for incident electrons from the left and right (sum over  $k_{\parallel}$ ) as a function of  $x$ , the position in the junction.

From Fig. 4.14, we see that the out-of-plane spin current in the magnetic layers decays as a function of the position in the magnet when summing over all  $k_{\perp}$  as opposed to the constant amplitude of the oscillations seen for a single propagating wave ( $k_{\perp}$ ) shown in Fig. 4.10. Similarly to the in-plane spin current, this decay is due to the destructive interference of oscillations with different  $k_{\perp}$ .

More surprisingly, we see that even after summing over all  $k_{\parallel}$ , a non-zero out-of-plane spin current component in the nonmagnetic spacer remains as shown in Fig. 4.15.



Fig. 4.15:  $J_{\perp}^T$ , the constant non-zero out-of-plane spin current component for incident electrons from the left and right (sum over  $k_{\parallel}$ ) as a function of  $x$ , the position in the nonmagnetic spacer.

The total out-of-plane spin current contribution due to incident electrons from the left reservoir ( $J_{\perp}^L$ ) summed over all  $k_{\parallel}$  and the total out-of-plane spin current contribution from the right are illustrated in Fig. 4.16 and Fig. 4.17 respectively.

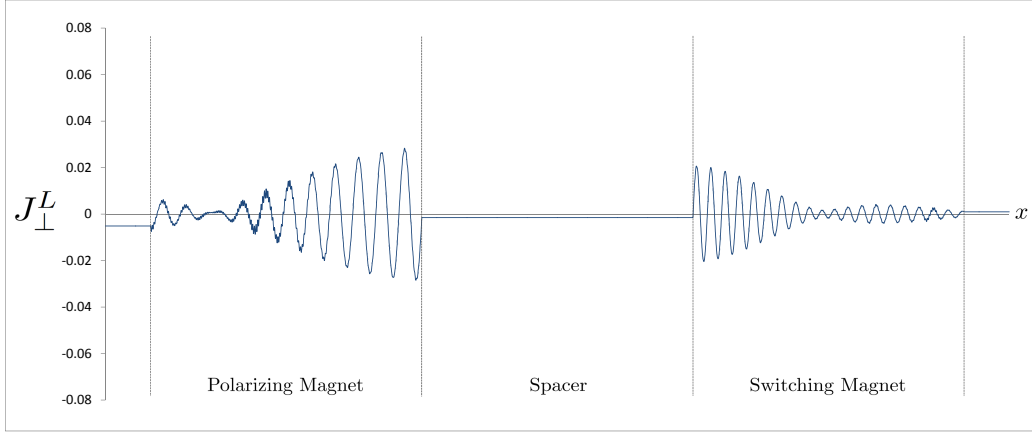


Fig. 4.16:  $J_{\perp}^L$ , the out-of-plane spin current component for incident electrons from the left (sum over  $k_{\parallel}$ ) as a function of  $x$ , the position in the junction.

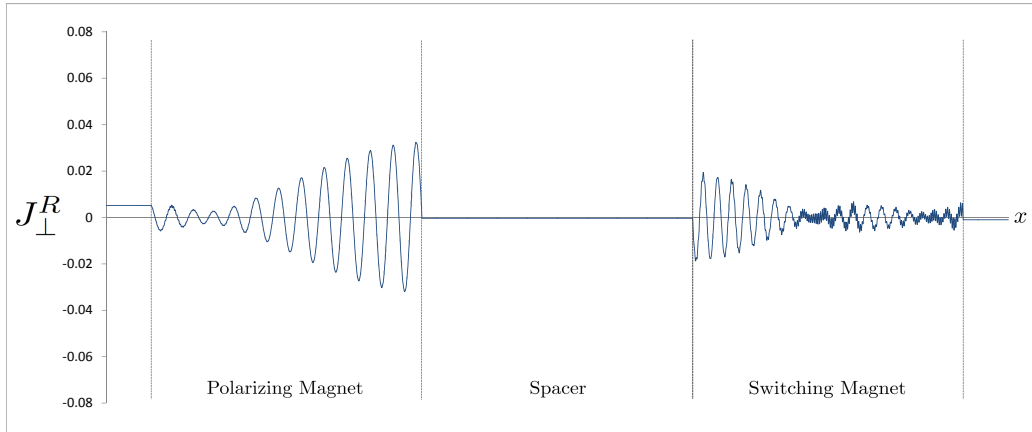


Fig. 4.17:  $J_{\perp}^R$ , the out-of-plane spin current component for incident electrons from the right (sum over  $k_{\parallel}$ ) as a function of  $x$ , the position in the junction.

Fig. 4.16 and Fig. 4.17 show that, as observed previously for a single  $k_{\perp}$ , the out-of-plane contribution from the left is equal in magnitude but opposite sign to the contribution from the right in the nonmagnetic semi-infinite leads.

We have seen that the in-plane spin current contribution from the left is equal in magnitude but opposite sign to the contribution from the right throughout the junction. As a result, the sum of the left and right in-plane spin current component is exactly zero ( $J_{\parallel}^L + J_{\parallel}^R = 0$ ). The sum of the left and right out-of-plane spin current component summed over all  $k_{\parallel}$  is illustrated in Fig. 4.18.

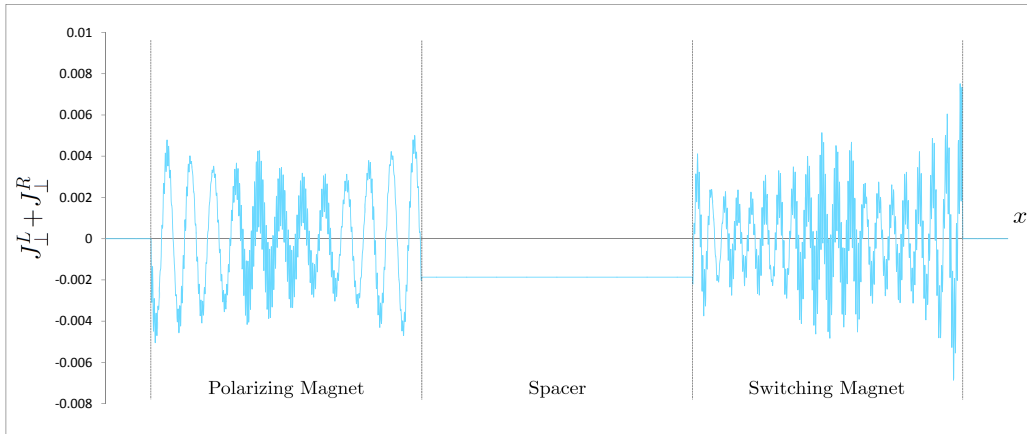


Fig. 4.18:  $J_{\perp}^L + J_{\perp}^R$ . The sum of the total out-of-plane spin current contributions from the left and right as a function of  $x$ , the position in the junction.

Fig. 4.18 shows that the sum of the left and right out-of-plane spin current in the left and right leads is exactly zero as expected however there is a constant non-zero out-of-plane measure in the nonmagnetic spacer. In fact, this is directly proportional to the interlayer exchange coupling found in the spacer layer sandwiched between the two ferromagnets.

### 4.3 Spin current with exact matching in the two ferromagnets

Here we introduce symmetry to the simple five layer junction defined in Sec. 4.1 by matching the potentials in the  $\uparrow$  and  $\downarrow$  spin bands in the left and right ferromagnets as illustrated in Fig. 4.19.

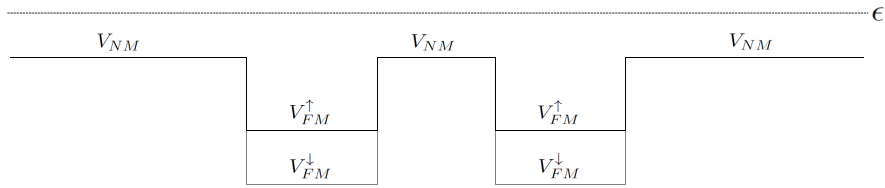


Fig. 4.19: Symmetric five layer junction represented by two matched potential wells.

We have fixed the angle of rotated magnetization in the left polarizing magnet to  $\theta = 1.5$ , the width of the two ferromagnets and the spacer separating them is given by  $a = 18$  and the energy of our incident electron is given by  $\epsilon = 0.5$ . The potentials in each layer are given by  $V_{NM} = -1.0$ ,  $V_{FM}^{\uparrow} = -1.5$  and  $V_{FM}^{\downarrow} = -2.5$ .

The numerical results for the total in-plane spin current component ( $J_{\parallel}^T$ ) summed over all  $k_{\parallel}$  are illustrated in Fig. 4.20.

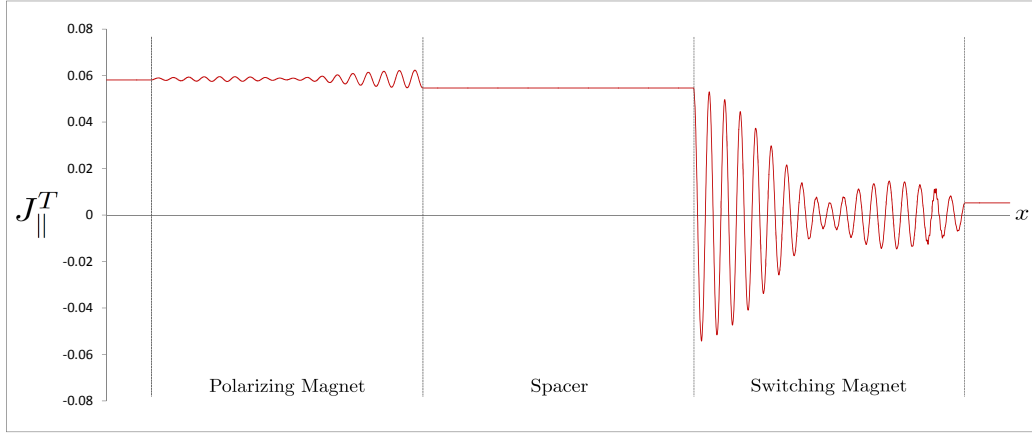


Fig. 4.20:  $J_{\parallel}^T$ , the total in-plane spin current component for incident electrons from the left and right (sum over  $k_{\parallel}$ ) as a function of  $x$ , the position in the symmetric junction.

The total in-plane spin current contribution due to incident electrons from the left reservoir ( $J_{\parallel}^L$ ) summed over all  $k_{\parallel}$  and the total in-plane spin current contribution from the right are illustrated in Fig. 4.21 and Fig. 4.22 respectively.

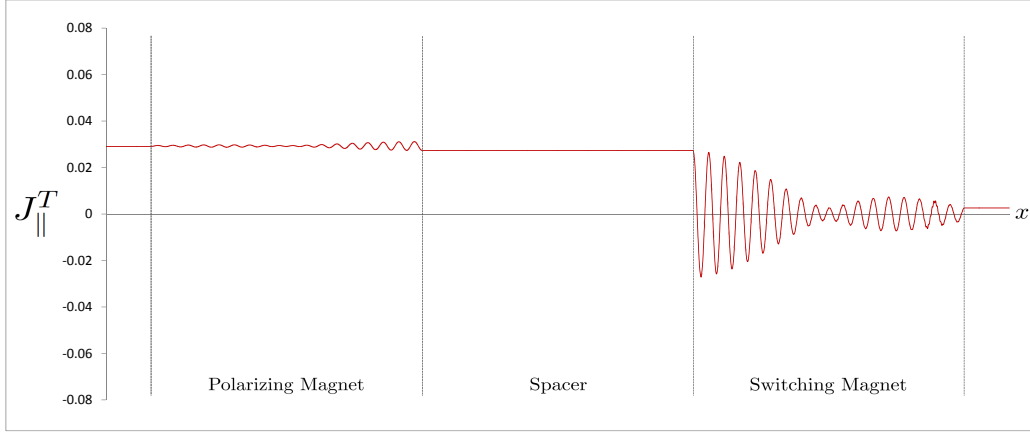


Fig. 4.21:  $J_{\parallel}^L$ , the in-plane spin current component for incident electrons from the left (sum over  $k_{\parallel}$ ) as a function of  $x$ , the position in the symmetric junction.

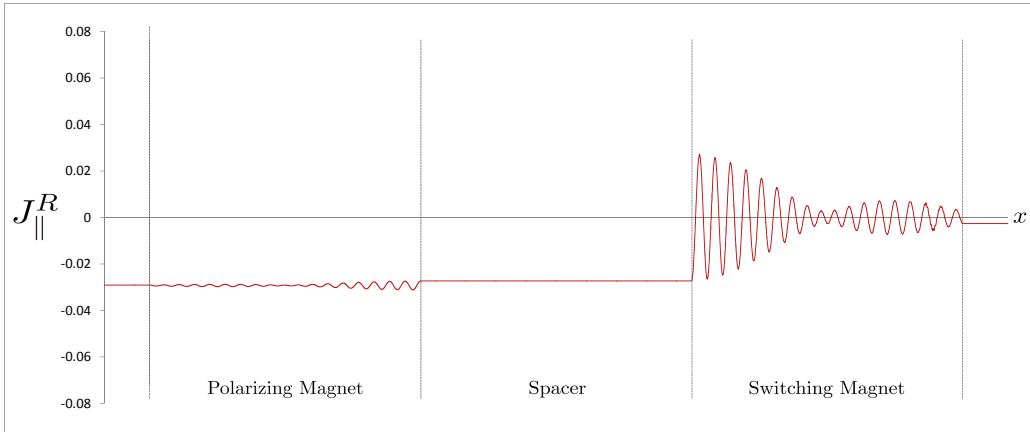


Fig. 4.22:  $J_{\parallel}^R$ , the in-plane spin current component for incident electrons from the right (sum over  $k_{\parallel}$ ) as a function of  $x$ , the position in the symmetric junction.

Fig. 4.20, Fig. 4.21 and Fig. 4.22 shows very similar results for the in-plane spin current component in the symmetric five layer junction to those seen in the asymmetric system in Sec. 4.2.

The numerical results for the total out-of-plane spin current component ( $J_{\perp}^T$ ) summed over all  $k_{\parallel}$  are illustrated in Fig. 4.23.

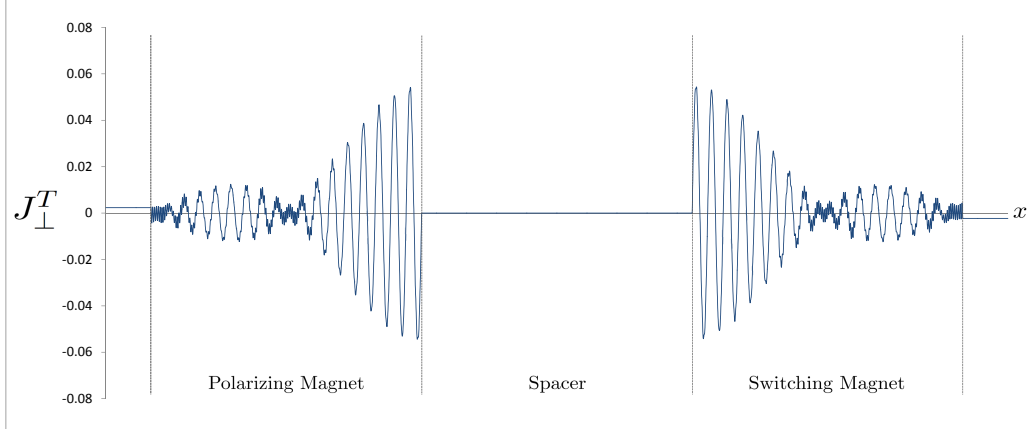


Fig. 4.23:  $J_{\perp}^T$ , the total out-of-plane spin current component for incident electrons from the left and right (sum over  $k_{\parallel}$ ) as a function of  $x$ , the position in the symmetric junction.

The total out-of-plane spin current contribution due to incident electrons from the left reservoir ( $J_{\perp}^L$ ) summed over all  $k_{\parallel}$  and the total out-of-plane spin current contribution from the right are illustrated in Fig. 4.24 and Fig. 4.25 respectively.

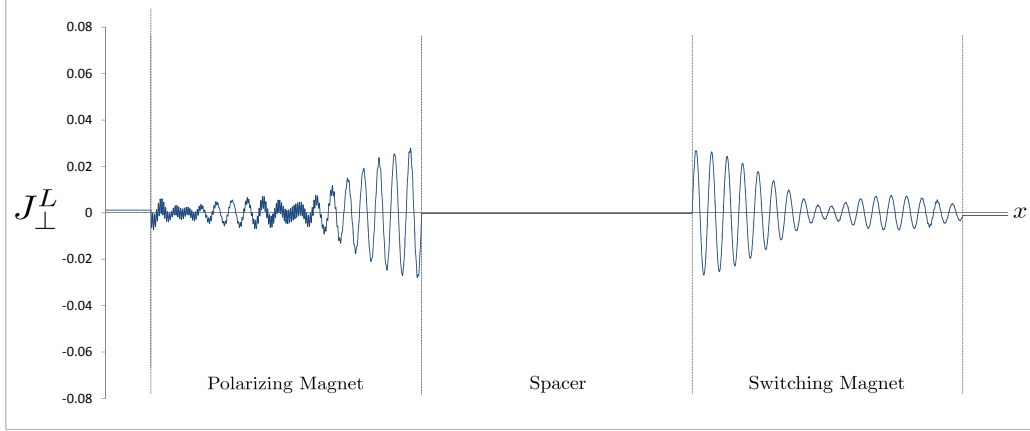


Fig. 4.24:  $J_{\perp}^L$ , the out-of-plane spin current component for incident electrons from the left (sum over  $k_{\parallel}$ ) as a function of  $x$ , the position in the symmetric junction.

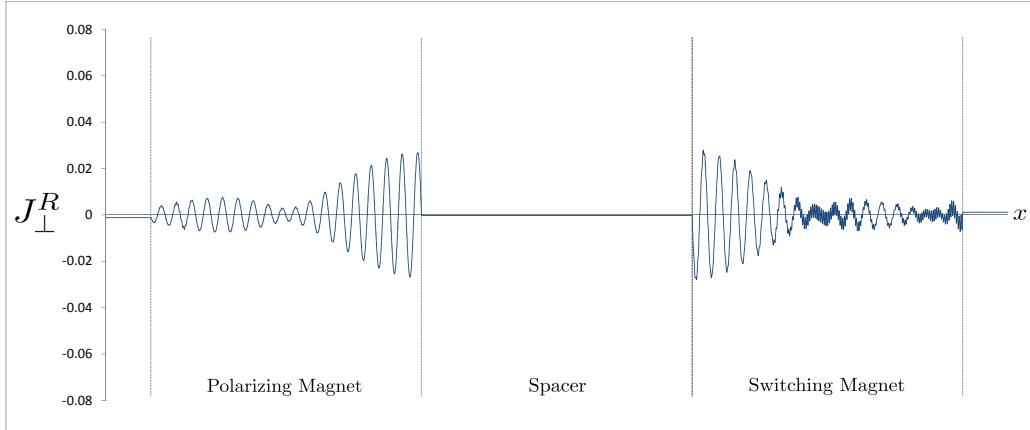


Fig. 4.25:  $J_{\perp}^R$ , the out-of-plane spin current component for incident electrons from the right (sum over  $k_{\parallel}$ ) as a function of  $x$ , the position in the symmetric junction.

In contrast to the out-of-plane spin current seen in the asymmetric system in Sec. 4.2, Fig. 4.23 shows a surprising antisymmetry in the two ferromagnets created when matching the potentials in both spin bands of the left and

right ferromagnets and completing the symmetry of the five layer junction. The total out-of-plane spin current in the right switching magnet is an exact mirror image of that in the left polarizing magnet resulting in exactly zero out-of-plane spin current in the spacer layer because the out-of-plane spin current emerging in the spacer from the left cancels exactly the contribution from the right.

This can be seen by the left and right contributions in Fig. 4.24 and Fig. 4.25 and a closer look at the contribution to the out-of-plane spin current in the spacer due to electrons incident from the left and right reservoirs, as shown in Fig. 4.26 and Fig. 4.27 respectively.

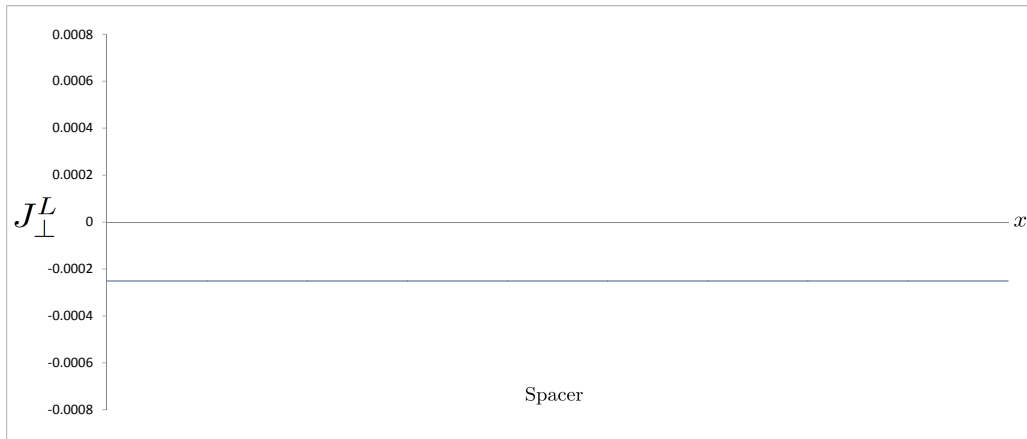


Fig. 4.26:  $J_{\perp}^L$ , the constant non-zero out-of-plane spin current component for incident electrons from the left (sum over  $k_{\parallel}$ ) as a function of  $x$ , the position in the nonmagnetic spacer of the symmetric junction.

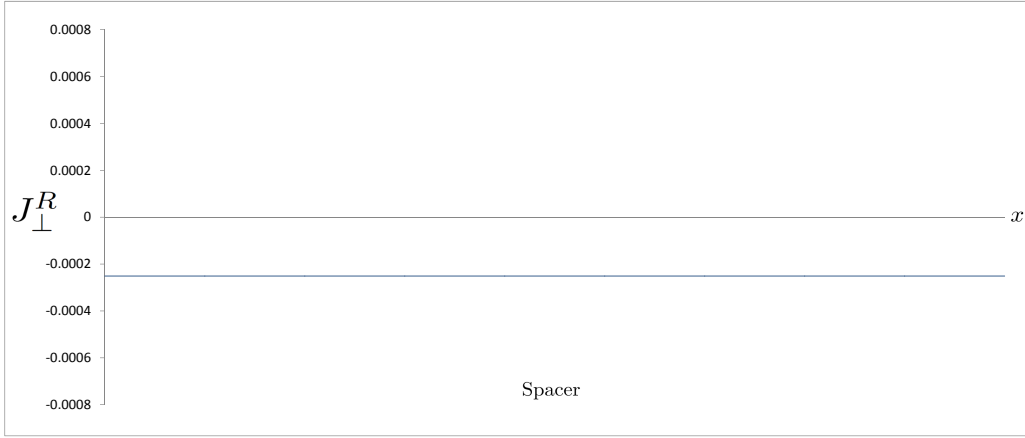


Fig. 4.27:  $J_{\perp}^R$ , the constant non-zero out-of-plane spin current component for incident electrons from the right (sum over  $k_{\parallel}$ ) as a function of  $x$ , the position in the nonmagnetic spacer of the symmetric junction.

The non-zero contribution from the left is exactly equal to the contribution from the right and so the total out-of-plane spin current in the spacer of the symmetric five layer junction, given by  $J_{\perp}^T = J_{\perp}^L - J_{\perp}^R$ , is exactly zero.

Finally, the sum of the left and right in-plane spin current component is exactly zero ( $J_{\parallel}^L + J_{\parallel}^R = 0$ ) throughout the junction as expected. The sum of the left and right out-of-plane spin current component summed over all  $k_{\parallel}$  is illustrated in Fig. 4.28.

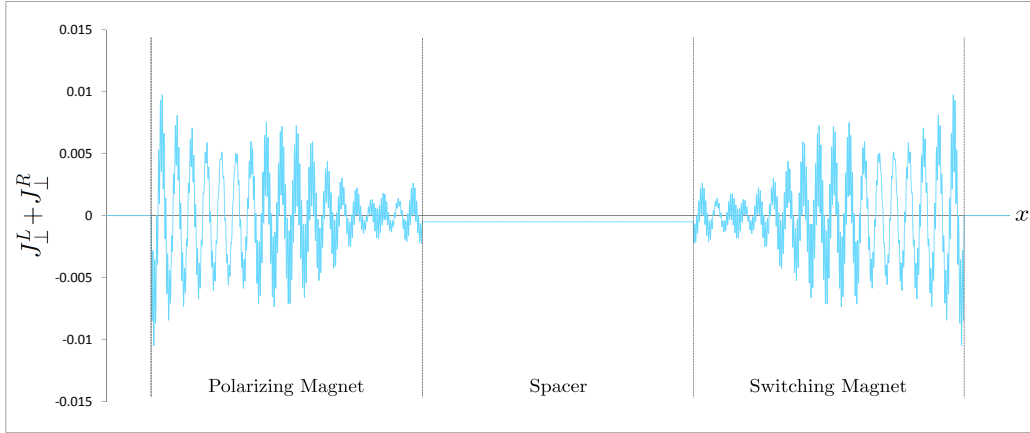


Fig. 4.28:  $J_{\perp}^L + J_{\perp}^R$ . The sum of the total out-of-plane spin current contributions from the left and right as a function of  $x$ , the position in the symmetric junction.

Fig. 4.28 shows that the antisymmetry of the out-of-plane component introduced by the matching of potentials in the ferromagnets means that the contribution from the left (right) in the spacer layer is simply doubled and hence there cannot be zero interlayer exchange coupling in the spacer unless there is zero out-of-plane spin current contribution from the left (right).

#### 4.4 Spin transport properties and interlayer exchange coupling in the nonmagnetic spacer

From the numerical results discussed in Sec. 4.2 and Sec. 4.3, we have been able to confirm the following properties in the left and right nonmagnetic leads of a simple five layer junction (Fig. 4.1).

$$J_{\parallel}^L + J_{\parallel}^R = 0 \quad (4.1)$$

$$J_{\perp}^L + J_{\perp}^R = 0 \quad (4.2)$$

In fact, the sum of the left and right spin current contributions is directly proportional to the interlayer exchange coupling in the nonmagnetic spacer sandwiched between the left and right ferromagnets and so it would be expected that these properties are true for both the in- and out-of-plane components in the semi-infinite leads where there is no interlayer coupling. We can also note that Property 4.1 has been observed to be true throughout the five layer junction.

Using our general solution for the wave function  $\psi_i$  (Eq. 2.18) to construct the wave functions in the left semi-infinite lead with propagating wave  $k_{\perp}$  given by  $k^{\uparrow} = k^{\downarrow} = i|k|$ , we can solve for the expression for the in- and out-of-plane spin current components (Eq. 2.41) in the left lead at  $x = 0$  to give

$$J_{Lead} = i2\frac{\hbar}{m}|k|(A^{\uparrow}A^{\downarrow*} - B^{\uparrow}B^{\downarrow*}) \quad (4.3)$$

where  $A^{\uparrow,\downarrow}$  denote the transmission coefficients and  $B^{\uparrow,\downarrow}$  the reflection coefficients in the left lead.

The total spin current from the left for incident electrons with spin orientation  $\sigma_L \in (\uparrow, \downarrow)$  is therefore given by

$$J_{Lead}^L = i2 \frac{\hbar}{m} |k| \sum_{\sigma_L} (A^\uparrow A^{\downarrow*} - B^\uparrow B^{\downarrow*}) \quad (4.4)$$

When sending an  $\uparrow$  spin electron from the left ( $\sigma_L = \uparrow$ ) we have that the transmission coefficients are given by  $A^\uparrow = 1$  and  $A^\downarrow = 0$ , similarly, when sending a  $\downarrow$  spin electron from the left ( $\sigma_L = \downarrow$ ) we have that the transmission coefficients are given by  $A^\uparrow = 0$  and  $A^\downarrow = 1$ . Therefore, the total spin current from the left for incident electrons with spin orientation  $\sigma_L \in (\uparrow, \downarrow)$  is given in terms of the reflection coefficients alone (Eq. 4.5).

$$J_{Lead}^L = -i2 \frac{\hbar}{m} |k| \sum_{\sigma_L} B^\uparrow B^{\downarrow*} \quad (4.5)$$

Similarly, when sending incident electrons from the right with spin orientation  $\sigma_R \in (\uparrow, \downarrow)$ , we have that the amplitude of the transmission coefficients in the left lead are both zero and so the total spin current in the left lead (from the right) for incident electrons with spin orientation  $\sigma_R \in (\uparrow, \downarrow)$  is also given in terms of the reflection coefficients alone (Eq. 4.6).

$$J_{Lead}^R = -i2 \frac{\hbar}{m} |k| \sum_{\sigma_R} B^\uparrow B^{\downarrow*} \quad (4.6)$$

Furthermore, our numerical properties in the leads (Eq. 4.1 and Eq. 4.2) imply that

$$J_{Lead}^L + J_{Lead}^R = 0 \quad (4.7)$$

More specifically, from Eq. 4.5 and Eq. 4.5, we see that

$$\sum_{\sigma_L} B^\dagger B^{\downarrow*} = - \sum_{\sigma_R} B^\dagger B^{\downarrow*} \quad (4.8)$$

The total spin current in the left lead,  $J_{Lead}^T = J_{Lead}^L - J_{Lead}^R$ , is therefore given by twice the contribution from the left (Eq. 4.9).

$$J_{Lead}^T = -i4 \frac{\hbar}{m} |k| \sum_{\sigma_L} B^\dagger B^{\downarrow*} \quad (4.9)$$

In fact, it is easy to show that the total local spin current in any layer is given by twice the contribution from the left less the sum of the left and right contributions (Eq. 4.10).

$$J^T = J^L - J^R = 2J^L - (J^L + J^R) \quad (4.10)$$

Since the sum of the left and right spin current ( $J^L + J^R$ ) is directly proportional to the interlayer exchange coupling in the nonmagnetic spacer layer, we can introduce  $v = J^L + J^R$  such that

$$J^L + J^R = v \propto \text{Interlayer exchange coupling in the spacer} \quad (4.11)$$

$$J^T = 2J^L - v \propto \text{Spin transport effects} \quad (4.12)$$

We can note here that these properties (Eq. 4.11 and Eq. 4.12) are true in the leads where there is no interlayer coupling ( $v = 0$ ) and the total spin current has been shown to be exactly twice the contribution from the left (Eq. 4.9). They also appear true in the nonmagnetic spacer where we have observed a non-zero interlayer exchange coupling. In fact, from our numeric results, we have been able to confirm the following properties in the nonmagnetic spacer layer of the simple five layer junction.

$$J_{\parallel}^L + J_{\parallel}^R = 0 \quad (4.13)$$

$$J_{\perp}^L + J_{\perp}^R \neq 0 \quad (4.14)$$

We also have the following observation.

$$\frac{J_{\perp}^L}{J_{\perp}^R} \geq 0 \quad (4.15)$$

Property 4.13 is analogous to Property 4.1 in the leads in that this is in fact true throughout the five layer junction. Property 4.14 and Observation 4.15 go hand in hand since Observation 4.15 implies that the out-of-plane spin current contribution from the left has the same sign as the contribution from the right and so there will be a non-zero interlayer exchange coupling in the spacer if there is a non-zero contribution from either side. Furthermore, we saw in Sec. 4.3 that by completing the symmetry by matching the potentials in both spin bands in the left and right ferromagnets, these left and right

contributions are the same and hence the total out-of-plane spin current component in the nonmagnetic spacer layer is reduced to zero. As a result, we can conclude that in order to see a non-zero out-of-plane spin current in the nonmagnetic spacer of a five layer junction, we need to remove symmetry by ensuring that the potentials in the two ferromagnets are not matched in at least one spin band.

#### 4.5 Angular dependence of spin current in the nonmagnetic leads

We have seen previously in Section 4.4 that the in- and out-of-plane spin current components in the leads of a five layer junction can be obtained by calculating the spin current for incident electrons from one side of the junction since  $J_{\perp}^L + J_{\perp}^R = 0$  and  $J_{\parallel}^L + J_{\parallel}^R = 0$ . We also saw that by introducing symmetry by matching the potentials in the left and right ferromagnets, the out-of-plane spin current in the nonmagnetic spacer would reduce to zero however a non-zero measure would remain in the left and right leads.

We will now investigate the origin of the non-zero spin current components in the left and right leads of the symmetric five layer junction (Fig. 4.1) with matching in the left and right ferromagnets (Fig. 4.19) by calculating the individual contributions of  $\uparrow$  and  $\downarrow$  spin electrons sent from either side of the junction for a single propagating wave ( $k_{\perp}$ ). We will do this by looking at the effect of the rotated magnetization in the polarizing magnet on the left lead by varying the angle  $\theta$  between 0 and  $\pi$  and calculating the spin current

contributions for individual electrons with spin orientation parallel ( $J^\uparrow$ ) and anti-parallel ( $J^\downarrow$ ) to the net magnetization of the switching magnet ( $z$ -axis).

The numerical results for the in-plane spin current in the left lead due to individual electrons of either spin orientation incident from the left for  $0 < \theta < \pi$  are illustrated in Fig. 4.29.

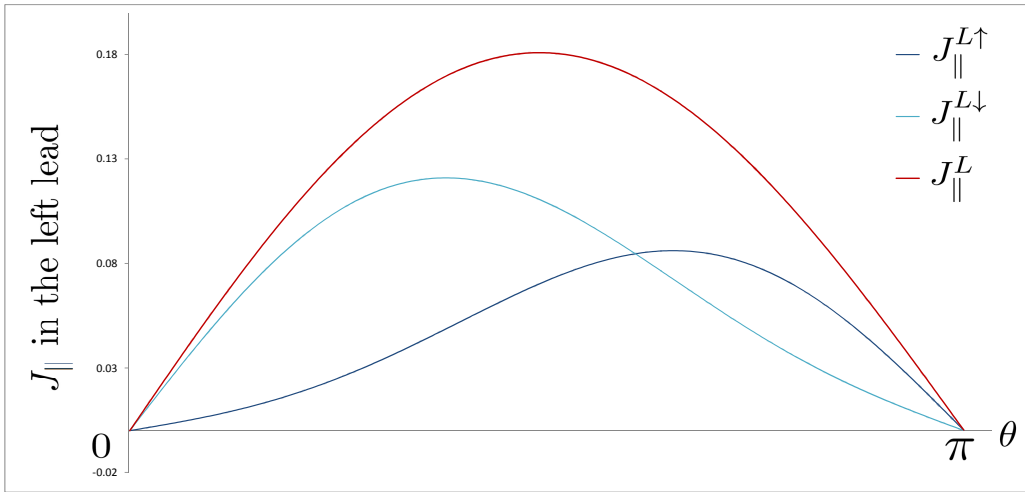


Fig. 4.29:  $J_{\parallel}^{L\uparrow}$ ,  $J_{\parallel}^{L\downarrow}$  and  $J_{\parallel}^L$ . The in-plane spin current in the left lead for  $\uparrow$  and  $\downarrow$  spin electrons incident from the left as a function of  $\theta \in [0, \pi]$ .

Fig. 4.29 shows that the contribution to the in-plane spin current in the left lead due to an  $\uparrow$  spin electron incident from the left ( $J_{\parallel}^{L\uparrow}$ ) is exactly zero for  $\theta = 0$  since the rotated magnetization of the polarizing magnet is aligned with that of the electron spin ( $z$ -axis) and the effect grows gradually as  $\theta$  increases to  $\frac{\pi}{2}$  and is felt more strongly for  $\theta > \frac{\pi}{2}$  before converging rapidly to zero as the anti-parallel configuration is achieved ( $\theta = \pi$ ). Conversely, the contribution to the in-plane spin current in the left lead due to a  $\downarrow$  spin

electron incident from the left ( $J_{\parallel}^{L\downarrow}$ ) has a strong effect when  $\theta < \frac{\pi}{2}$  and weaker effect for  $\theta > \frac{\pi}{2}$ . The magnitude of the  $\uparrow$  spin electron contribution is less than that of the  $\downarrow$  spin electron since the ferromagnetic potentials are lower in the  $\downarrow$  spin band. Finally, we can note that both contributions are of the same sign and the sum of these contributions gives the total in-plane spin current contribution from the left for a single  $k_{\perp}$  given by  $J_{\parallel}^L$ .

The numerical results for the in-plane spin current in the left lead due to individual electrons of either spin orientation incident from the right for  $0 < \theta < \pi$  are illustrated in Fig. 4.30.

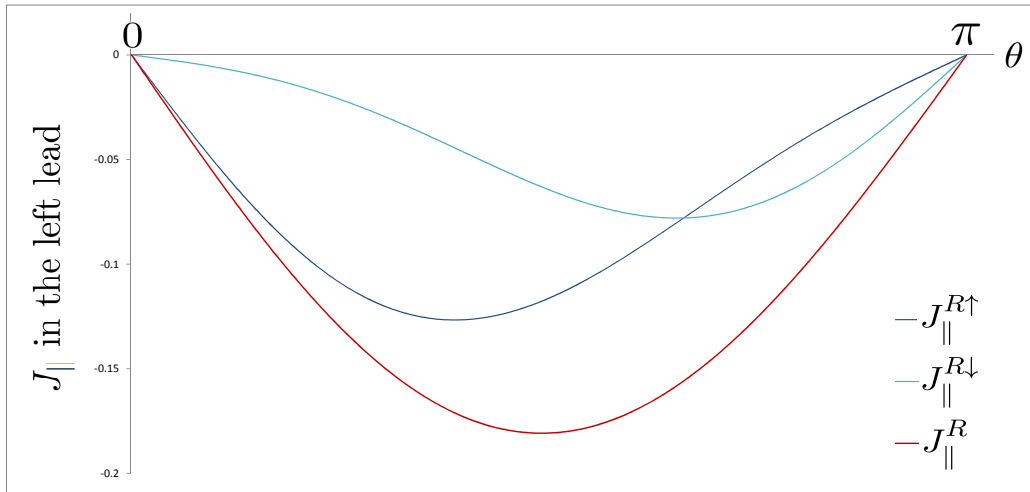


Fig. 4.30:  $J_{\parallel}^{R\uparrow}$ ,  $J_{\parallel}^{R\downarrow}$  and  $J_{\parallel}^R$ . The in-plane spin current in the left lead for  $\uparrow$  and  $\downarrow$  spin electrons incident from the right as a function of  $\theta \in [0, \pi]$ .

Fig. 4.30 shows that the total in-plane spin current contribution from the right for a single  $k_{\perp}$  given by  $J_{\parallel}^R$  is equal but opposite sign to the total contribution from the left as expected. Furthermore, we see that the contribution

due to an  $\uparrow$  spin electron incident from the right is equal but opposite sign to the contribution of a  $\downarrow$  spin electron incident from the left (and similarly for a  $\downarrow$  spin electron from the left and  $\uparrow$  spin electron from the right).

The numerical results for the out-of-plane spin current in the left lead due to individual electrons of either spin orientation incident from the left for  $0 < \theta < \pi$  are illustrated in Fig. 4.31.

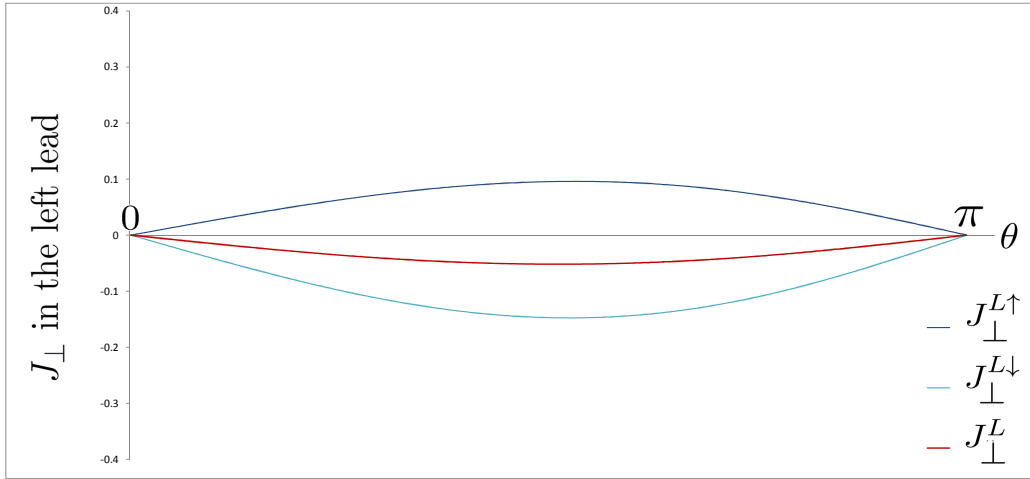


Fig. 4.31:  $J_{\perp}^{L\uparrow}$ ,  $J_{\perp}^{L\downarrow}$  and  $J_{\perp}^L$ . The out-of-plane spin current components in the left lead for  $\uparrow$  and  $\downarrow$  spin electrons incident from the left as a function of  $\theta \in [0, \pi]$ .

Fig. 4.31 shows that unlike the in-plane spin current, the out-of-plane spin current contributions in the left lead due to an  $\uparrow$  spin incident electron is the opposite sign to the contribution due to a  $\downarrow$  spin incident electron however the sum is non-zero and so there is a non-zero out-of-plane spin current contribution from the left for a single  $k_{\perp}$  given by  $J_{\perp}^L$ .

The numerical results for the out-of-plane spin current in the left lead due to individual electrons of either spin orientation incident from the right for  $0 < \theta < \pi$  are illustrated in Fig. 4.32.

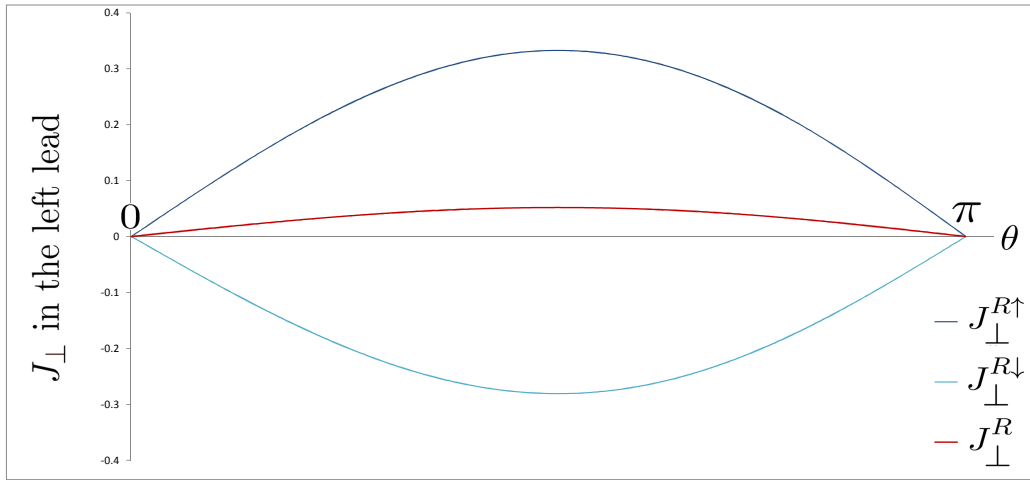


Fig. 4.32:  $J_{\perp}^{R\uparrow}$ ,  $J_{\perp}^{R\downarrow}$  and  $J_{\perp}^R$ . The out-of-plane spin current components in the left lead for  $\uparrow$  and  $\downarrow$  electrons incident from the right as a function of  $\theta \in [0, \pi]$ .

Fig. 4.32 shows that unlike the in-plane spin current, the out-of-plane spin current contributions in the left lead due to  $\uparrow$  and  $\downarrow$  spin incident electrons from either side are all different in magnitude however, the sum of the contributions from either side are equal but opposite sign as expected.

The numerical results for the in-plane spin current in the right lead due to individual electrons of either spin orientation incident from the left for  $0 < \theta < \pi$  are illustrated in Fig. 4.33.

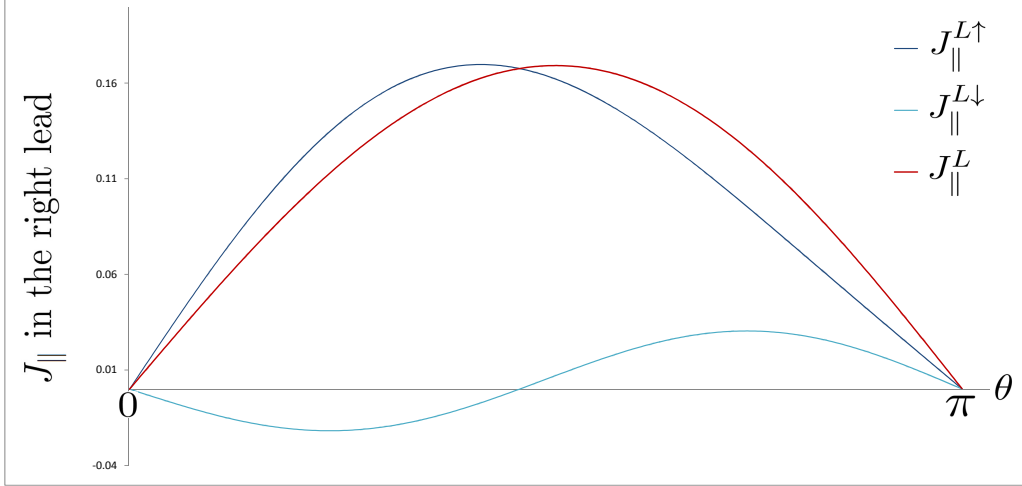


Fig. 4.33:  $J_{\parallel}^{L\uparrow}$ ,  $J_{\parallel}^{L\downarrow}$  and  $J_{\parallel}^L$ . The in-plane spin current in the right lead for  $\uparrow$  and  $\downarrow$  spin electrons incident from the left as a function of  $\theta \in [0, \pi]$ .

Fig. 4.33 shows that the contribution to the in-plane spin current in the right lead due to an  $\uparrow$  spin electron incident from the left ( $J_{\parallel}^{L\uparrow}$ ) is stronger than the contribution due to a  $\downarrow$  spin incident electron from the left due to the magnetization of the right switching magnet fixed parallel to the spin quantization axis ( $z$  - axis).

The numerical results for the in-plane spin current in the right lead due to individual electrons of either spin orientation incident from the right for  $0 < \theta < \pi$  are illustrated in Fig. 4.34.

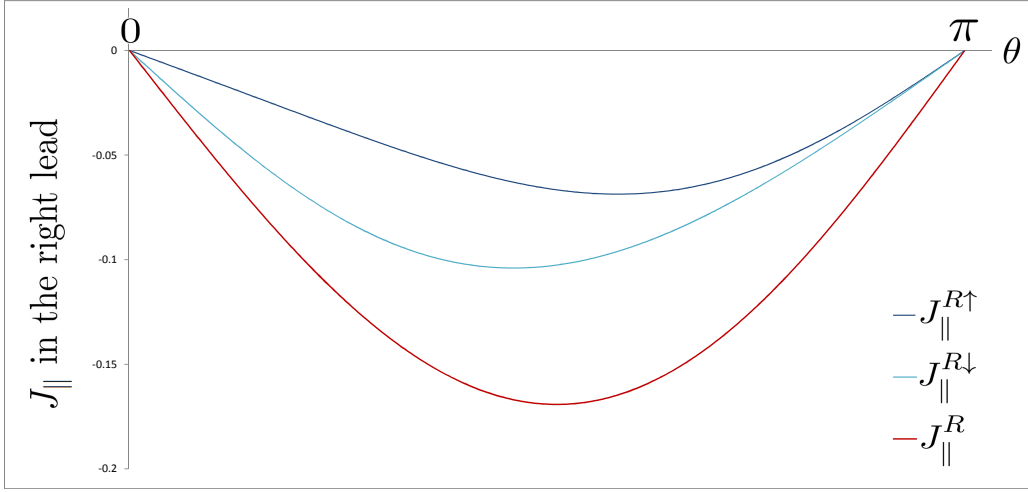


Fig. 4.34:  $J_{\parallel}^{R\uparrow}$ ,  $J_{\parallel}^{R\downarrow}$  and  $J_{\parallel}^R$ . The in-plane spin current in the right lead for  $\uparrow$  and  $\downarrow$  spin electrons incident from the right as a function of  $\theta \in [0, \pi]$ .

Fig. 4.34 shows that the total in-plane spin current contribution from the right for a single  $k_{\perp}$  given by  $J_{\parallel}^R$  is equal but opposite sign to the total contribution from the left as expected however, the individual contributions are more evenly distributed.

The numerical results for the out-of-plane spin current in the right lead due to individual electrons of either spin orientation incident from the left for  $0 < \theta < \pi$  are illustrated in Fig. 4.35.

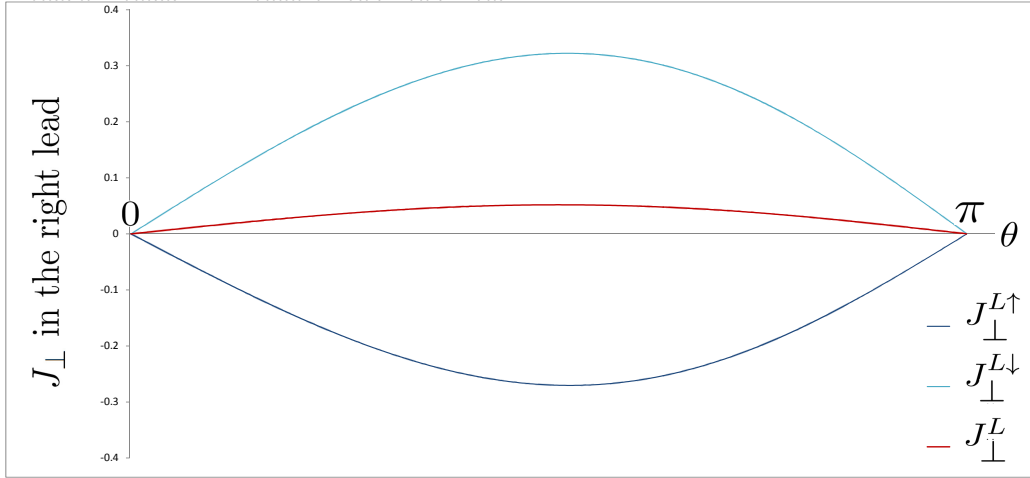


Fig. 4.35:  $J_{\perp}^{L\uparrow}$ ,  $J_{\perp}^{L\downarrow}$  and  $J_{\perp}^L$ . The out-of-plane spin current components in the right lead for  $\uparrow$  and  $\downarrow$  spin electrons incident from the left as a function of  $\theta \in [0, \pi]$ .

Fig. 4.35 shows strong out-of-plane spin current contributions in the spacer due to  $\uparrow$  and  $\downarrow$  spin incident electrons from the left due to the spin transport effects caused by the spin precession at the interfaces of the two ferromagnets however these individual contributions are opposite in sign and so the overall contribution from the left ( $J_{\perp}^L$ ) for a single  $k_{\perp}$  is reduced.

The numerical results for the out-of-plane spin current in the right lead due to individual electrons of either spin orientation incident from the right for  $0 < \theta < \pi$  are illustrated in Fig. 4.36.

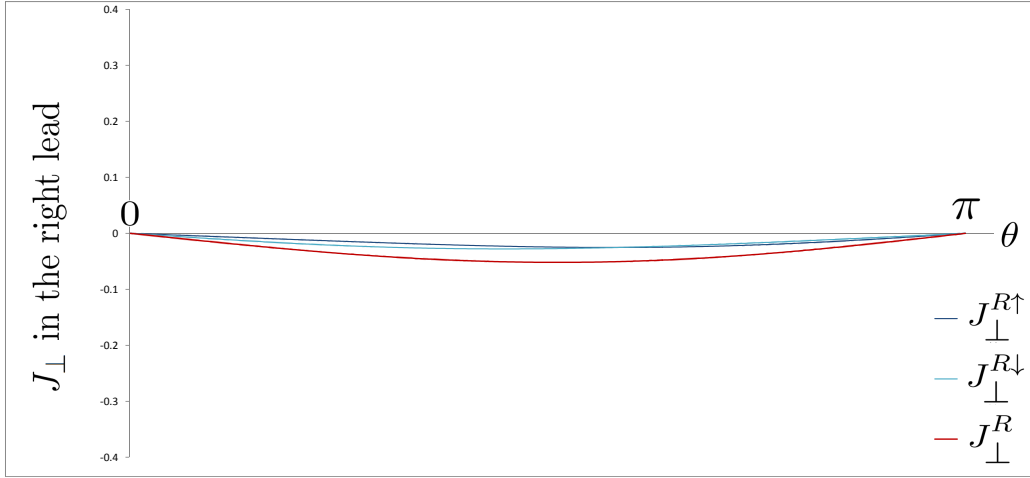


Fig. 4.36:  $J_{\perp}^{R\uparrow}$ ,  $J_{\perp}^{R\downarrow}$  and  $J_{\perp}^R$ . The out-of-plane spin current components in the right lead for  $\uparrow$  and  $\downarrow$  electrons incident from the right as a function of  $\theta \in [0, \pi]$ .

Fig. 4.36 shows much weaker contributions to the out-of-plane spin current in the right lead for individual electrons in either spin band however these contributions are of the same sign such that the sum  $J_{\perp}^R = J_{\perp}^{R\uparrow} + J_{\perp}^{R\downarrow}$  is equal but opposite sign to the out-of-plane contribution from the left,  $J_{\perp}^R = -J_{\perp}^L$ , as expected.

We conclude that the out-of-plane spin current seen in the left and right leads of the five layer junction originates from the individual spin precessions in the left and right ferromagnets. These precessions result in oscillations in the spin current components in the ferromagnets that therefore emerge in general in the leads as non-zero.

#### 4.6 Angular dependence of spin current in the nonmagnetic spacer

We have seen that the spin precession in the left and right ferromagnets of a symmetric five layer junction give rise to non-zero spin current components in the left and right leads and how the individual contributions of  $\uparrow$  and  $\downarrow$  spin electrons incident from the left and right reservoirs differ depending on the magnetic configuration of the two ferromagnets in the junction.

We will now investigate the spin current components in the nonmagnetic spacer of the symmetric five layer junction (Fig. 4.1) with matching in the left and right ferromagnets (Fig. 4.19) by calculating the individual contributions of  $\uparrow$  and  $\downarrow$  spin electrons sent from either side of the junction for a single propagating wave ( $k_{\perp}$ ). We will do this by looking at the effect of the rotated magnetization in the polarizing magnet on the left lead by varying the angle  $\theta$  between 0 and  $\pi$  and calculating the spin current contributions for individual electrons with spin orientation parallel ( $J^{\uparrow}$ ) and anti-parallel ( $J^{\downarrow}$ ) to the net magnetization of the switching magnet ( $z$  - axis).

The numerical results for the in-plane spin current in the spacer due to individual electrons of either spin orientation incident from the left for  $0 < \theta < \pi$  are illustrated in Fig. 4.37.

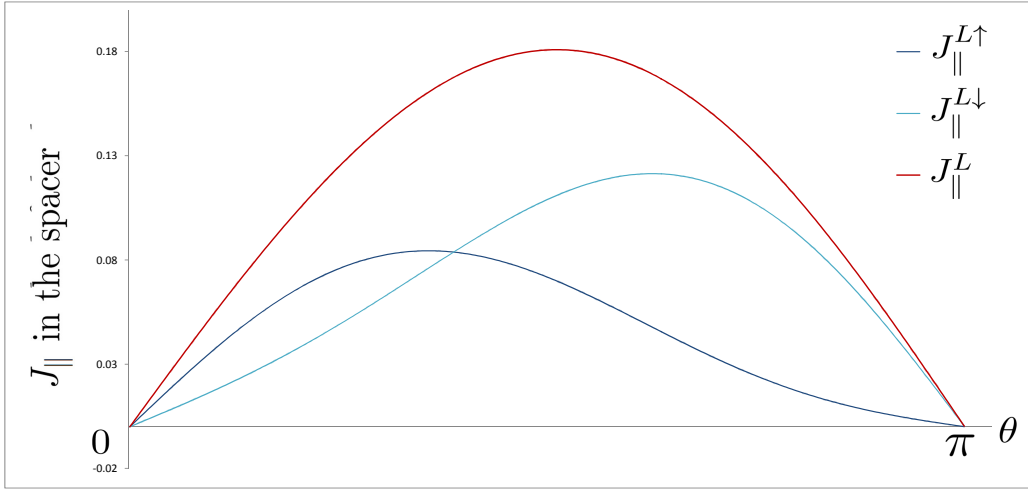


Fig. 4.37:  $J_{\parallel}^{L\uparrow}$ ,  $J_{\parallel}^{L\downarrow}$  and  $J_{\parallel}^L$ . The in-plane spin current in the spacer for  $\uparrow$  and  $\downarrow$  spin electrons incident from the left as a function of  $\theta \in [0, \pi]$ .

Fig. 4.37 shows that the contribution to the in-plane spin current in the spacer due to an  $\uparrow$  spin electron incident from the left ( $J_{\parallel}^{L\uparrow}$ ) is exactly zero for  $\theta = 0$  since the rotated magnetization of the polarizing magnet is aligned with that of the electron spin ( $z$ -axis) and the effect is strongest when  $\theta < \frac{\pi}{2}$ . Similarly, the contribution to the in-plane spin current in the spacer due to a  $\downarrow$  spin electron incident from the left ( $J_{\parallel}^{L\downarrow}$ ) has a stronger effect when  $\theta > \frac{\pi}{2}$ . The magnitude of the  $\uparrow$  spin electron contribution is less than that of the  $\downarrow$  spin electron since the ferromagnetic potentials are lower in the  $\downarrow$  spin band. Finally, we can note that both contributions are of the same sign and the sum of these contributions gives the total in-plane spin current contribution from the left for a single  $k_{\perp}$  given by  $J_{\parallel}^L$ .

The numerical results for the in-plane spin current in the spacer due to individual electrons of either spin orientation incident from the right for

$0 < \theta < \pi$  are illustrated in Fig. 4.38.

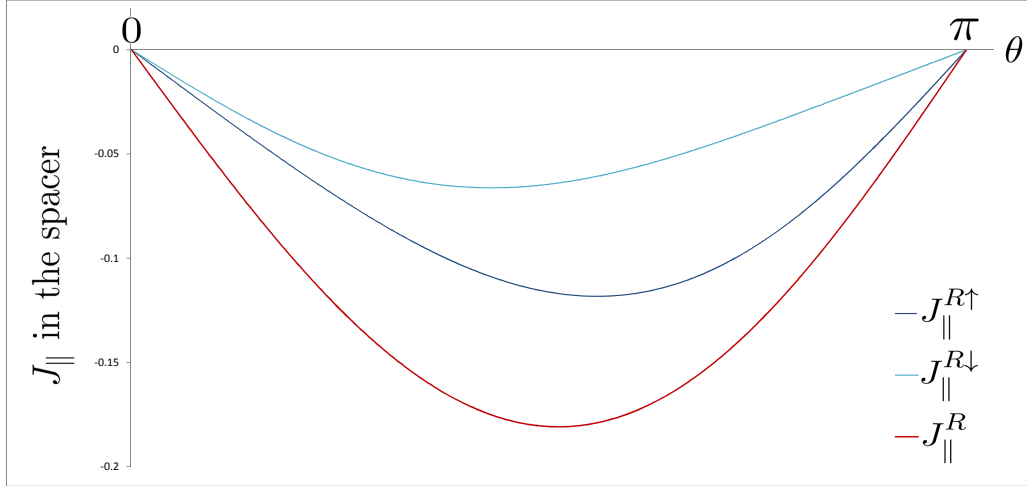


Fig. 4.38:  $J_{\parallel}^{R\uparrow}$ ,  $J_{\parallel}^{R\downarrow}$  and  $J_{\parallel}^R$ . The in-plane spin current in the spacer for  $\uparrow$  and  $\downarrow$  spin electrons incident from the right as a function of  $\theta \in [0, \pi]$ .

Fig. 4.38 shows that the total in-plane spin current contribution from the right for a single  $k_{\perp}$  given by  $J_{\parallel}^R$  is equal but opposite sign to the total contribution from the left as expected. However, we see that the individual contributions due to  $\uparrow$  and  $\downarrow$  spin electrons incident from the right differ from those individual contributions from the left.

The numerical results for the out-of-plane spin current in the spacer due to individual electrons of either spin orientation incident from the left for  $0 < \theta < \pi$  are illustrated in Fig. 4.39.

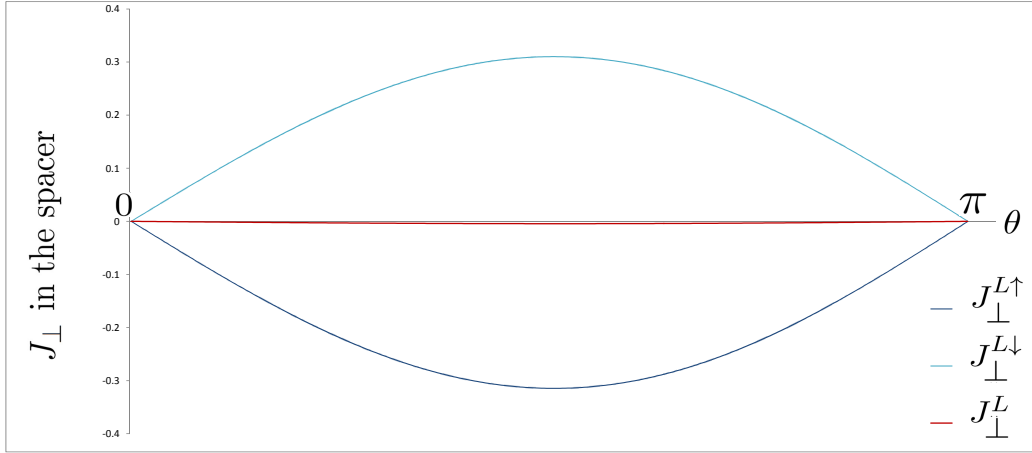


Fig. 4.39:  $J_{\perp}^{L\uparrow}$ ,  $J_{\perp}^{L\downarrow}$  and  $J_{\perp}^L$ . The out-of-plane spin current components in the spacer for  $\uparrow$  and  $\downarrow$  spin electrons incident from the left as a function of  $\theta \in [0, \pi]$ .

Fig. 4.39 shows strong out-of-plane spin current contributions in the right lead due to  $\uparrow$  and  $\downarrow$  spin incident electrons from the left due to the spin transport effects caused by the spin precession at the interfaces of the two ferromagnets however these individual contributions are opposite in sign and so the overall contribution from the left ( $J_{\perp}^L$ ) for a single  $k_{\perp}$  is reduced.

The numerical results for the out-of-plane spin current in the spacer due to individual electrons of either spin orientation incident from the right for  $0 < \theta < \pi$  are illustrated in Fig. 4.40.

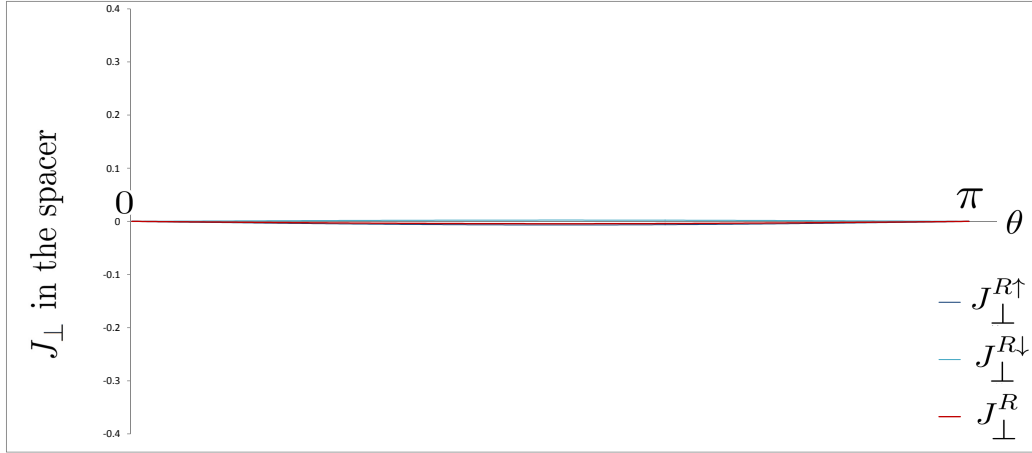


Fig. 4.40:  $J_{\perp}^{R\uparrow}$ ,  $J_{\perp}^{R\downarrow}$  and  $J_{\perp}^R$ . The out-of-plane spin current components in the spacer for  $\uparrow$  and  $\downarrow$  electrons incident from the right as a function of  $\theta \in [0, \pi]$ .

Fig. 4.40 shows much weaker contributions to the out-of-plane spin current in the spacer for individual electrons in either spin band incident from the right however these contributions are of the same sign such that the sum  $J_{\perp}^R = J_{\perp}^{R\uparrow} + J_{\perp}^{R\downarrow}$  is proportional to the out-of-plane contribution from the left and so the total out-of-plane spin current in the spacer for a single  $k_{\perp}$  is approximately zero and we have already seen that the sum over all  $k_{\parallel}$  will be exactly zero given the symmetry of the junction.

We conclude that the out-of-plane spin current seen in the nonmagnetic spacer of the five layer junction originates from the individual spin precessions in the left and right ferromagnets emerging in the spacer however, the contribution of  $\uparrow$  spin electrons strongly oppose the contributions of  $\downarrow$  spin electrons. We will later investigate more closely this cancelling effect in the nonmagnetic spacer.

#### 4.7 Spin current at the interfaces of the polarizing magnet as a function of polarizing magnet width

Here we investigate the effect on the spin current at the interface of the left lead and the left ferromagnet (polarizing magnet) when varying the width  $\omega a$  of the polarizing magnet and compare it with the spin current found inside the polarizing magnet for a fixed width  $\omega_n a$ . We will also run the same comparison at the interface of the polarizing magnet and the nonmagnetic spacer layer.

We first redefine the five layer junction as a dimensionless system consisting of a semi-infinite left lead up to  $x_0 = L$  (a large starting value on the  $x - axis$ ). A finite ferromagnet of thickness  $\omega a$  between  $x_0 = L$  and  $x_1 = L + \omega a$ , a spacer of width  $t a$  located between  $x_1 = L + \omega a$  and  $x_2 = L + (\omega + t)a$  and the switching magnet of width  $a$  between  $x_2 = L + (\omega + t)a$  and  $x_3 = L + (\omega + t + 1)a$  as illustrated in Fig. 4.41.

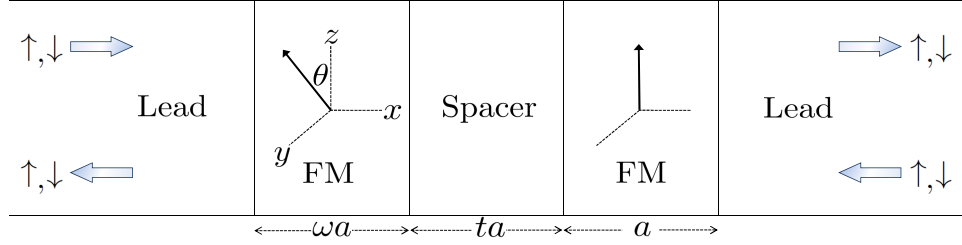


Fig. 4.41: Schematic picture of a simple five layer junction with  $\uparrow$  and  $\downarrow$  spin electrons incident from the left and right semi-infinite leads.

The idea is that  $a$  is the fundamental length scale in the problem and by varying  $t$  and/or  $\omega$ , we can vary spacer thickness and polarizing magnet thickness. As before, the exchange potential of the left (polarizing) magnet is rotated by angle  $\theta$  in the  $yz$  – plane whilst that of the right (switching) magnet is always in the direction of the  $z$  – axis. We will match the potentials in the  $\uparrow$  and  $\downarrow$  spin bands of the two ferromagnets (Fig. 4.42) however we can note that the symmetry will be broken for all  $\omega \neq 1$ .

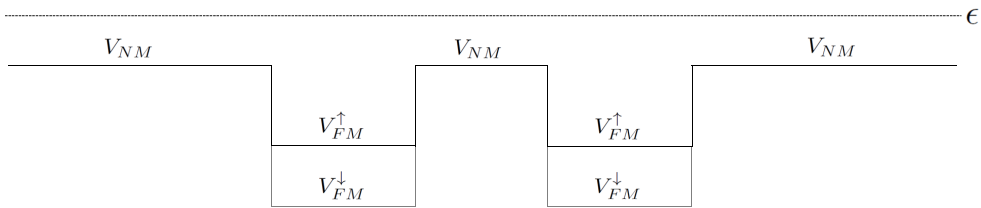


Fig. 4.42: Five layer junction represented by two matched potential wells.

The numerical results for the total in-plane spin current component due to incident electrons from the left and right for all  $k_{\parallel}$  calculated in the left

lead at  $x_0 = L$  as a function of  $\omega \in [\omega_0, \omega_n]$ , the varying width of the polarizing magnet, are illustrated in Fig. 4.43.

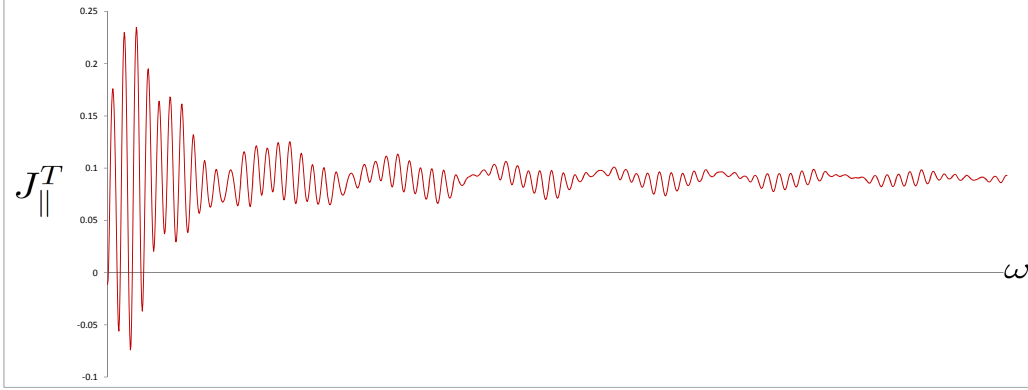


Fig. 4.43:  $J_{\parallel}^T$ , the total in-plane spin current component for incident electrons from the left and right (sum over  $k_{\parallel}$ ), calculated in the left lead as a function of the width  $\omega a$  of the polarizing magnet.

Fig. 4.43 further illustrates the two periods observed previously in the magnetic layers brought about by functions of the sum and difference of the wave vectors for each spin band, i.e. The short period is given by a function of  $k^{\uparrow} + k^{\downarrow}$  and the long period is given by a function of  $k^{\uparrow} - k^{\downarrow}$ . We also see large oscillations for a thin polarizing magnet however as the thickness of the magnet increases, these oscillations reduce and the in-plane spin current converges to a constant value. This is expected since the contributions due to the many reflections in all layers will be high for a thin polarizing magnet however for a large polarizing magnet, there will be little contribution from the right and we have already shown that the spin current components in the left lead arise from the reflection coefficients in that layer.

The numerical results for the total in-plane spin current component due to incident electrons from the left and right for all  $k_{\parallel}$  calculated in the polarizing magnet as a function of  $x \in [L, L + \omega_n a]$ , the position in the polarizing magnet of fixed width  $\omega_n a$ , are illustrated in Fig. 4.44.

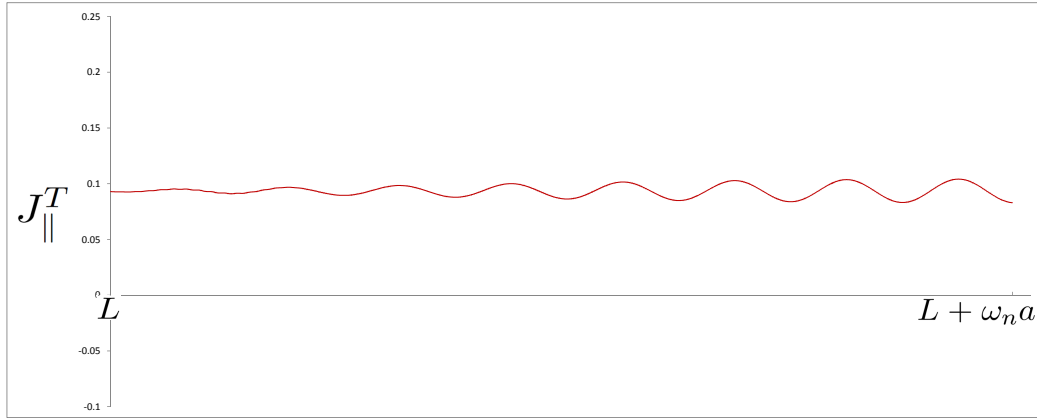


Fig. 4.44:  $J_{\parallel}^T$ , the total in-plane spin current component for incident electrons from the left and right (sum over  $k_{\parallel}$ ), calculated throughout the polarizing magnet of fixed width  $\omega_n a$ .

Fig. 4.44 does not show many oscillations throughout the polarizing magnet since the magnet is fixed at a large width given by  $\omega_n a$  and so there is little contribution from the many transmissions/reflections throughout the junction as expected. This is comparable to Fig. 4.43 whereby the short period vanishes as we approach a thick polarizing magnet.

The numerical results for the total out-of-plane spin current component due to incident electrons from the left and right for all  $k_{\parallel}$  calculated in the left lead at  $x_0 = L$  as a function of  $\omega \in [\omega_0, \omega_n]$ , the varying width of the

polarizing magnet, are illustrated in Fig. 4.45.

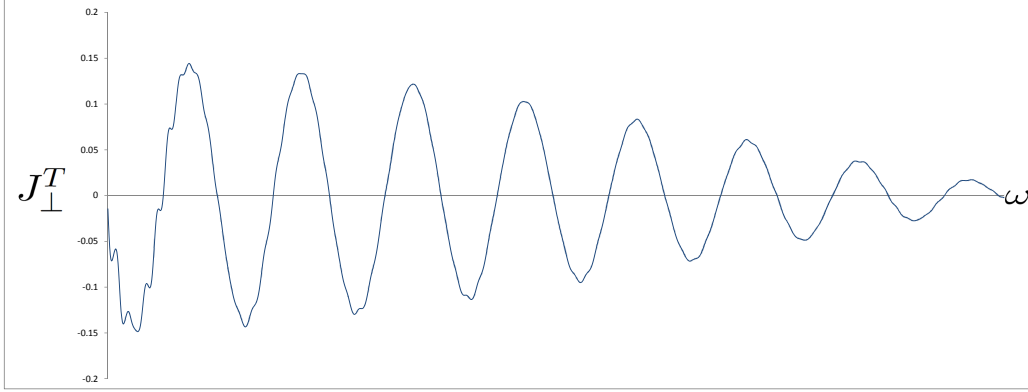


Fig. 4.45:  $J_{\perp}^T$ , the total out-of-plane spin current component for incident electrons from the left and right (sum over  $k_{\parallel}$ ), calculated in the left lead as a function of the width  $\omega a$  of the polarizing magnet.

Fig. 4.45 shows an out-of-plane spin current in the left lead resulting from the oscillations due to the spin precessions in the polarizing magnet however as the thickness of the magnet increases, the out-of-plane spin current converges to zero. This is expected since the contributions due to the many reflections in all layers will be high for a thin polarizing magnet however for a large polarizing magnet, there will be little contribution from the right.

The numerical results for the total out-of-plane spin current component due to incident electrons from the left and right for all  $k_{\parallel}$  calculated in the polarizing magnet as a function of  $x \in [L, L + \omega_n a]$ , the position in the polarizing magnet of fixed width  $\omega_n a$ , are illustrated in Fig. 4.46.

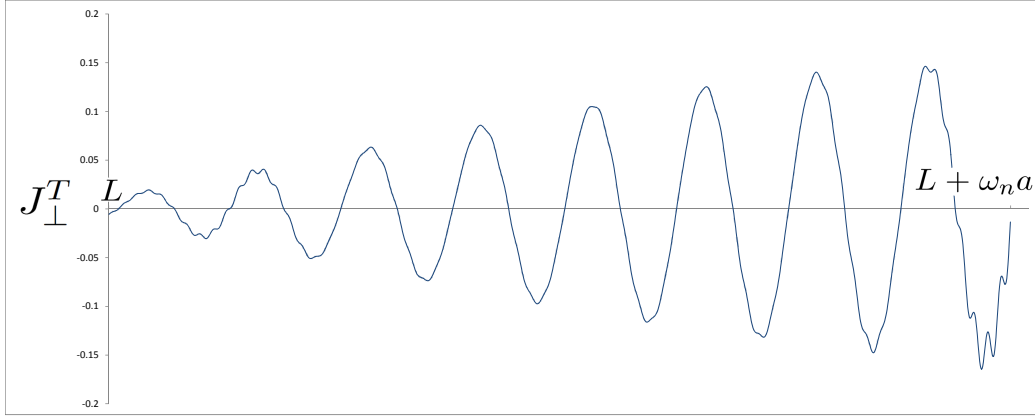


Fig. 4.46:  $J_{\perp}^T$ , the total out-of-plane spin current component for incident electrons from the left and right (sum over  $k_{\parallel}$ ), calculated throughout the polarizing magnet of fixed width  $\omega_n a$ .

Fig. 4.46 shows some interference near the left and right interfaces of the polarizing magnet since the magnet is fixed at a large width given by  $\omega_n a$  and so the interference is reduced within the magnet. We can also note that the amplitude of the oscillations of the out-of-plane spin current in the polarizing magnet increases along the  $x$  – axis as we approach the interface with the nonmagnetic spacer due to the contributions of the many reflections in the layers to the right of the thick polarizing magnet. These oscillations give rise to a non-zero measure of out-of-plane spin current in the nonmagnetic spacer (right interface).

We will investigate the origin of out-of-plane spin current in the nonmagnetic spacer in Chapter 6 by looking specifically at an interface between a semi-infinite magnet and a semi-infinite nonmagnet and obtaining qualitative insight into the out-of-plane spin current found in a non-magnetic spacer

sandwiched between two finite ferromagnets. First, we will define appropriate boundary conditions that will further clarify the interference observed at these interfaces.

## 5. LANDAUER BOUNDARY CONDITIONS

### 5.1 *Limit of a semi-infinite potential step*

We mentioned in Chapter 4 that our Landauer formalism may not be entirely appropriate when studying the typical trilayer junction whereby the nonmagnetic spacer layer is sandwiched between two semi-infinite ferromagnets. The reasoning being that without the left and right leads, we may not be able to set appropriate boundary conditions that simulate the Landauer reservoirs. Furthermore, the results for a single propagating wave ( $k_{\perp}$ ) in the limit of a finite ferromagnet would never approach those of a semi-infinite ferromagnet. To illustrate this, we will look at a single interface representing a semi-infinite potential step as shown schematically in Fig. 5.1.

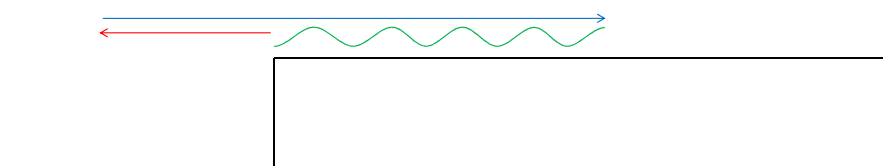


*Fig. 5.1:* Schematic picture of a single semi-infinite potential step.

The incident electrons travelling above the potential step from the left will be partially reflected and the wave functions in the semi-infinite step

would oscillate with a constant amplitude resulting from the interference at the interface. In the case of a dual interface system consisting of a finite potential step of width  $a$ , the interference in the potential step would arise from both interfaces and since the amplitude is constant, this would not disappear in the limit  $a \rightarrow \infty$  as shown schematically in Fig. 5.2.

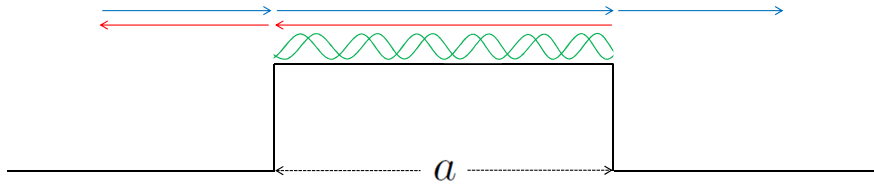
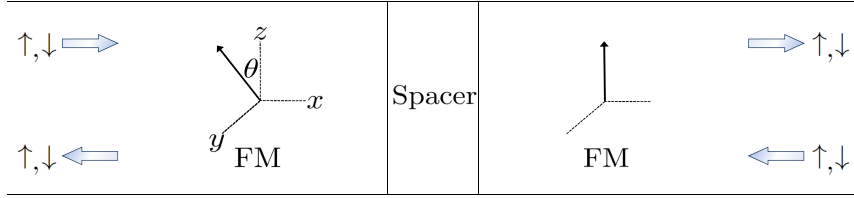


Fig. 5.2: Schematic picture of a single finite potential step in the limit  $a \rightarrow \infty$ .

The sum over all  $k_{\parallel}$  would remove this due to the destructive interference which would destroy the interactions between the two interfaces.

## 5.2 Five layer junction approximation to the classical trilayer with semi-infinite ferromagnets

Here we look at the classical trilayer junction consisting of two semi-infinite ferromagnets separated by a nonmagnetic spacer layer as shown schematically in Fig. 5.3.



*Fig. 5.3:* Schematic picture of the classical theoretical trilayer junction (two semi-infinite magnets separated by a nonmagnetic spacer).

We shall consider the situation where the left and right semi-infinite ferromagnets are treated as potential wells with exact matching in the  $\uparrow$  and  $\downarrow$  spin bands such that the system is completely symmetric as illustrated in Fig. 5.4 below.

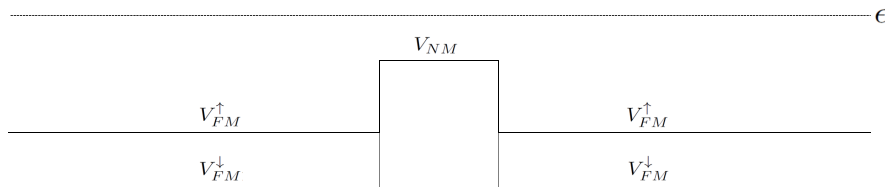


*Fig. 5.4:* Classical trilayer represented by two semi-infinite potential wells with exact matching in both spin bands.

It is assumed in this case that this provides a more physical representation of the left and right identical Landauer reservoirs.

We will calculate the spin current components throughout the trilayer

and compare these to an approximation of the trilayer using the five layer model whereby the width  $L$  of both ferromagnets are large ( $L \rightarrow \infty$ ) however the left and right leads are maintained as shown schematically in Fig. 5.5.

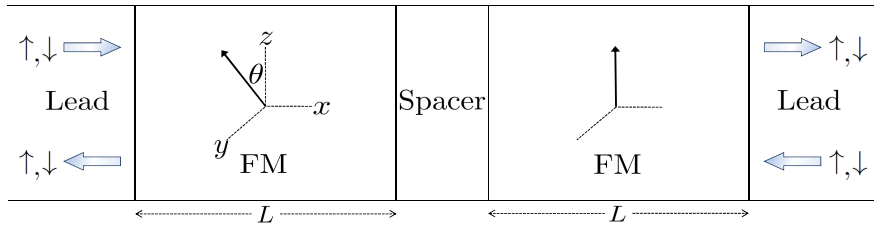


Fig. 5.5: Schematic picture of two semi-infinite magnets separated by a nonmagnetic spacer with left and right leads.

We will choose our parameters in line with the classical trilayer such that the potentials are matched accordingly as illustrated in Fig. 5.6 below.

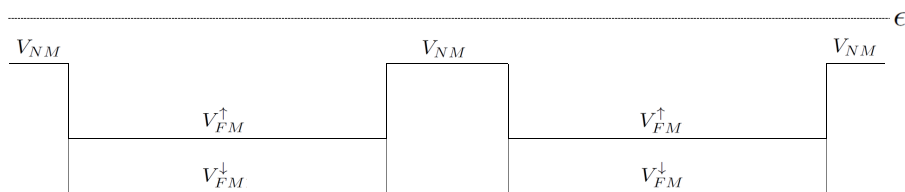


Fig. 5.6: Five layer approximation to the classical trilayer represented by two large potential wells with exact matching in both spin bands.

We have seen in Sec. 5.1 that it is necessary to look at the total sum over all  $k_{\parallel}$  since for a single propagating wave, the finite ferromagnets in the five

---

layer junction can never be equivalent to the semi-infinite ferromagnets of the classical trilayer junction since electrons travelling above the potential of the spacer layer will always experience interference from the left and right interfaces and this will never disappear no matter how wide we make the finite ferromagnets. We will therefore calculate the sum over all  $k_{\parallel}$  such that the destructive interference causes the interactions of the two interfaces to decay in the limit of the large ferromagnets.

Finally, since we are calculating the spin current components seen in perfectly symmetric junctions, it is sufficient to simply calculate the contributions from the right of the junction by sending electrons along the  $x$ -axis from the right with spin angular momenta parallel ( $\uparrow$ ) and anti-parallel ( $\downarrow$ ) to the net magnetization of the right switching magnet (parallel/anti-parallel to the  $z$ -axis) in order to obtain a complete picture of the total spin current components as shown in our earlier results for a symmetric five layer junction (Sec. 4.3).

Fig. 5.7 shows the numerical results for the total in-plane spin current summed over all  $k_{\parallel}$  as a function of  $x$ , the position in a central region of the infinite classical trilayer junction with exact matching of the left and right semi-infinite ferromagnets. It also shows the comparative results in the same region of the symmetric five layer junction.

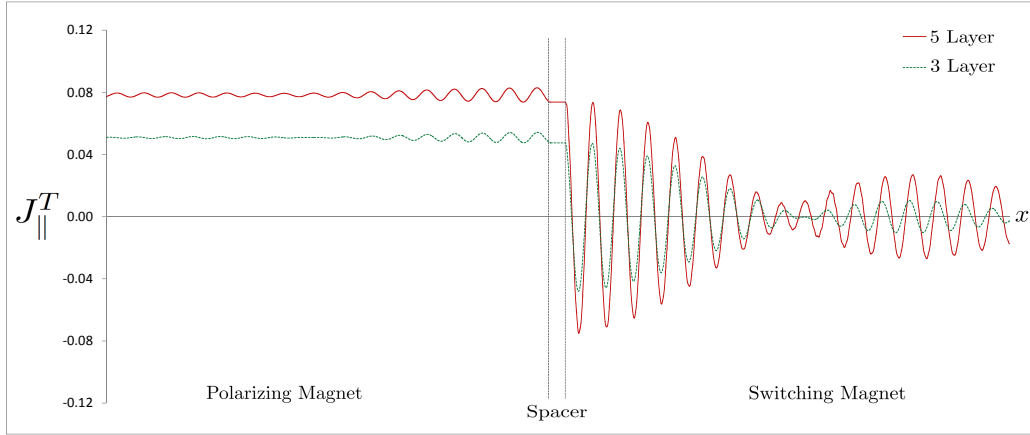


Fig. 5.7: The total in-plane spin current ( $J_{\parallel}^T$ ) as a function of  $x$ , the position spanning the interfaces of the spacer in the classical trilayer junction (3 Layer) as well as the comparative results for the five layer approximation (5 Layer).

Similarly, Fig. 5.8 shows the numerical results for the total out-of-plane spin current summed over all  $k_{\parallel}$  as a function of  $x$ , the position in a central region of the infinite classical trilayer junction with exact matching of the left and right semi-infinite ferromagnets. It also shows the comparative results in the same region of the symmetric five layer junction.

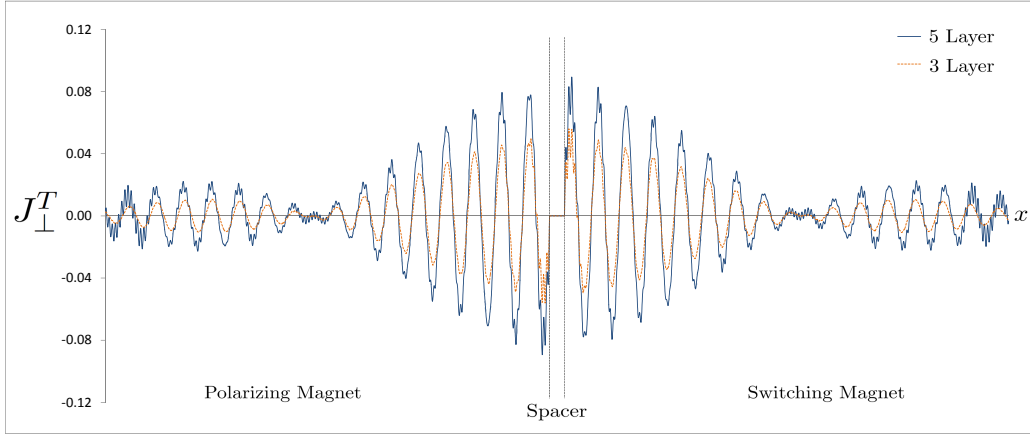


Fig. 5.8: The total out-of-plane spin current ( $J_{\perp}^T$ ) as a function of  $x$ , the position spanning the interfaces of the spacer in the classical trilayer junction (3 Layer) as well as the comparative results for the five layer approximation (5 Layer).

The results illustrated in Fig. 5.7 and Fig. 5.8 show that using the Landauer formalism to study the five layer junction with large ferromagnets provides a good approximation to the classical trilayer junction with semi-infinite ferromagnets and no leads when the two Landauer reservoirs are identical and we calculate the total spin current components (sum over  $k_{\parallel}$ ) in order to minimise the differences created by the additional interfaces introduced by the five layer junction. However, it should be noted that at individual  $k$ -points the trilayer with semi-infinite magnets can give physically incorrect results. The origin of this is due to the fact that Landauer boundary conditions are incompatible with magnetic leads [29]. Nevertheless when integrated over  $k_{\parallel}$  the results for a trilayer seem to be physically reasonable.

## 6. OUT-OF-PLANE SPIN CURRENT IN THE NONMAGNETIC SPACER

### 6.1 Origin of out-of-plane spin current

The results on spin current presented in Chapter 4 clearly demonstrate that an “anomalous” out-of-plane spin current exists in a magnetic configuration in which the magnetizations of the polarizing and switching magnets both lie in the  $y, z - plane$  (Fig. 6.1). In this situation one might naively expect that the spin current is also polarized in the  $y, z - plane$  and there cannot be an out-of-plane component  $J_{\perp}$ .

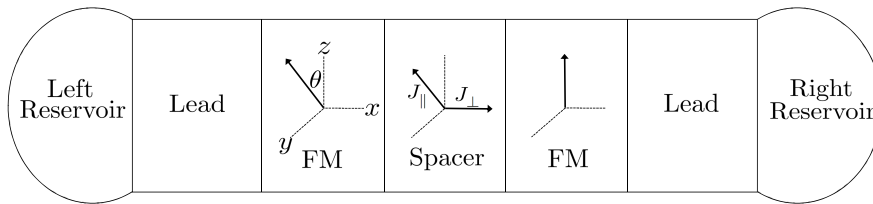


*Fig. 6.1:* Magnetic nanostructure showing the magnetizations of the polarizing and switching magnets and the resulting in- and out-of-plane spin current components in the nonmagnetic spacer.

The existence of the out-of-plane spin current component has, therefore,

---

been questioned, in particular, since it did not seem to appear in some early calculations [8]. These early calculations were for junctions with identical polarizing and switching magnets, in which case we have already shown that it is simply the symmetry of the junction which prevents a non-zero out-of-plane spin current to appear in the nonmagnetic spacer layer. When the symmetry of the junction is broken, the out-of-plane spin current in the nonmagnetic spacer layer is always non-zero. Given this somewhat controversial nature of the out-of-plane spin current, it is important to investigate how it may arise.

The Landauer formalism we have developed is the only approach that allows us to investigate the physical origin of the out-of-plane spin current and clarify its properties. The Landauer calculation of the spin current has at least two great advantages over the Keldysh formalism [24] used previously. First of all, one can separate explicitly within the Landauer approach the components of the spin current incident on and reflected from a magnet. Moreover, the contributions to the total spin current of the  $\uparrow$  and  $\downarrow$  spin electrons emitted from the left and right reservoirs can be determined separately. Finally, in some simple cases the spin current can be calculated analytically so that one can see explicitly how an out-of-plane spin current component can arise.

We shall, therefore, begin with the simplest case of an interface between a semi-infinite magnet and a semi-infinite nonmagnet which can be solved analytically.

## 6.2 Interface between a semi-infinite magnet and a semi-infinite nonmagnet

Here we consider a single interface at  $x_0 = 0$  with a semi-infinite switching magnet on the left with its magnetization rotated by angle  $\theta$  in the  $y, z$ -plane and a semi-infinite nonmagnet to the right as shown schematically in Fig. 6.2.

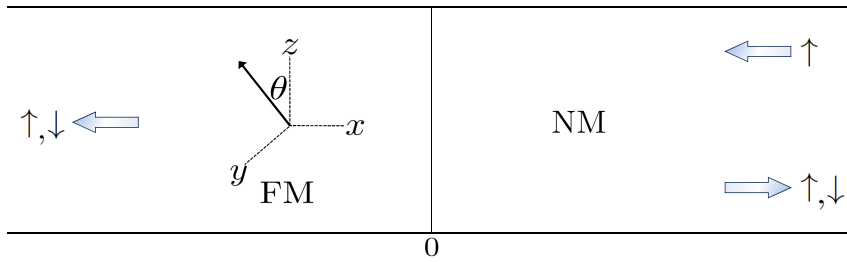


Fig. 6.2: Schematic picture of a single interface between a semi-infinite magnet and a semi-infinite nonmagnet.

Initially, we will send  $\uparrow$  spin electrons only from the right and nothing from the left resulting in  $\uparrow$  and  $\downarrow$  spin electrons being transmitted across the interface into the switching magnet and both  $\uparrow$  and  $\downarrow$  spin electrons being reflected back into the nonmagnet. It should be noted that by sending  $\uparrow$  spin electrons only from the nonmagnet into the magnet we assume implicitly that the electron beam in the nonmagnet is spin-polarized in the “up” direction ( $z$ -axis). We shall first investigate the consequences of such a configuration and discuss later how it is related to our Landauer formulation for a general

magnetic multilayer.

Using our definition of a column vector of coefficients  $\vec{A}_i$  (Eq. 2.20) and the transfer matrix  $M_i^T$  (Eq. 2.22) such that  $\vec{A}_i = M_i^T \vec{A}_{i-1}$ , we have for our single interface problem that  $\vec{A}_1 = M^T \vec{A}_0$ .

If we write the transfer matrix  $M^T$  as a 4x4 matrix with elements  $m_{ij}$  then we have

$$\begin{pmatrix} A_1^\uparrow \\ 1 \\ A_1^\downarrow \\ 0 \end{pmatrix} = \begin{pmatrix} m_{11} & m_{12} & m_{13} & m_{14} \\ m_{21} & m_{22} & m_{23} & m_{24} \\ m_{31} & m_{32} & m_{33} & m_{34} \\ m_{41} & m_{42} & m_{43} & m_{44} \end{pmatrix} \begin{pmatrix} 0 \\ B_0^\uparrow \\ 0 \\ B_0^\downarrow \end{pmatrix} \quad (6.1)$$

giving us four simultaneous equations with four unknowns

$$A_1^\uparrow = m_{12}B_0^\uparrow + m_{14}B_0^\downarrow \quad (6.2a)$$

$$1 = m_{22}B_0^\uparrow + m_{24}B_0^\downarrow \quad (6.2b)$$

$$A_1^\downarrow = m_{32}B_0^\uparrow + m_{34}B_0^\downarrow \quad (6.2c)$$

$$0 = m_{42}B_0^\uparrow + m_{44}B_0^\downarrow \quad (6.2d)$$

Thus allowing us to solve for all unknown coefficients in terms of the  $ij^{th}$

elements of the transfer matrix

$$A_1^\uparrow = \frac{m_{12}m_{44} - m_{14}m_{42}}{m_{22}m_{44} - m_{24}m_{42}} \quad (6.3)$$

$$A_1^\downarrow = \frac{m_{32}m_{44} - m_{34}m_{42}}{m_{22}m_{44} - m_{24}m_{42}} \quad (6.4)$$

$$B_0^\uparrow = \frac{m_{44}}{m_{22}m_{44} - m_{24}m_{42}} \quad (6.5)$$

$$B_0^\downarrow = \frac{-m_{42}}{m_{22}m_{44} - m_{24}m_{42}} \quad (6.6)$$

Substituting for  $k_i^\uparrow, k_i^\downarrow$  in our transfer matrix (Eq. 2.22) where  $k_1^\uparrow = k_1^\downarrow = k_1$ , we can deduce analytical expressions for the coefficients in both layers.

$$A_1^\uparrow = \left( \frac{k_1 - k_0^\uparrow}{k_1 + k_0^\uparrow} \right) \cos^2 \frac{\theta}{2} + \left( \frac{k_1 - k_0^\downarrow}{k_1 + k_0^\downarrow} \right) \sin^2 \frac{\theta}{2} \quad (6.7)$$

$$A_1^\downarrow = \left( \frac{k_1 - k_0^\uparrow}{k_1 + k_0^\uparrow} - \frac{k_1 - k_0^\downarrow}{k_1 + k_0^\downarrow} \right) \sin \frac{\theta}{2} \cos \frac{\theta}{2} \quad (6.8)$$

$$B_0^\uparrow = \frac{2k_1 \cos \frac{\theta}{2}}{k_1 + k_0^\uparrow} \quad (6.9)$$

$$B_0^\downarrow = \frac{-2k_1 \sin \frac{\theta}{2}}{k_1 + k_0^\downarrow} \quad (6.10)$$

The expressions for the amplitude of the reflection coefficients in the non-magnet (Eq. 6.7) and (Eq. 6.8) and transmission coefficients in the magnet

(Eq. 6.9) and (Eq. 6.10) show immediately that when all wave functions are propagating waves, we have that all  $k_i^{\uparrow,\downarrow}$  are imaginary resulting in entirely real coefficients.

The next step is to calculate the spin current components in the nonmagnet by substituting these coefficients into our general solution for the wave functions  $\psi_{i=1}^{\uparrow,\downarrow}$  (Eq. 2.18). Since the spin current is constant throughout the nonmagnet we can calculate the spin current components in the nonmagnet resulting from a single  $\uparrow$  spin electron incident from the right ( $J_R^\uparrow$ ) by solving for  $J$  (Eq. 2.41) at  $x = 0$  to give

$$J_R^\uparrow = \frac{\hbar}{m} \{A_1^\uparrow A_1^{\downarrow*} (k_1 - k_1^*) - A_1^{\downarrow*} (k_1 + k_1^*)\} \quad (6.11)$$

From Eq. 6.11 we can see that for all  $k$  propagating we have  $k_1 = i|k_1|$  and  $A_1^\uparrow = \pm |A_1^\uparrow|$ ,  $A_1^\downarrow = \pm |A_1^\downarrow|$ , i.e. real constants, and the above expression for  $J_R^\uparrow$  reduces to

$$J_R^\uparrow = \pm i 2 \frac{\hbar}{m} |k_1 A_1^\uparrow A_1^\downarrow| \quad (6.12)$$

The real part of Eq. 6.12 is zero and since the out-of-plane spin current component is given by  $J_\perp = \Re\{J\}$  (Eq. 2.41b), there will be zero out-of-plane spin current. If however, there is at least one wave function that is completely reflected, the out-of-plane spin current in the nonmagnet will be non-zero.

We can also note that by setting  $\theta = 0, \pi$ , we have  $A_1^\downarrow = 0 \Rightarrow J_R^\uparrow = 0$  and hence there is zero in- and out-of-plane spin current in the nonmagnet as expected.

Another observation can be made with regard to the potentials in the magnet and nonmagnet. If we match the potential in the nonmagnet with the potential of either spin band in the magnet, say  $k_1 = k_0^\uparrow$ , we have

$$\begin{aligned} J_R^\uparrow &= \frac{\hbar}{m} \{A_1^\uparrow A_1^{\downarrow*} (k_1 - k_1^*) - A_1^{\downarrow*} (k_1 + k_1^*)\} \\ &= -i2 \frac{\hbar}{m} |k_1| \left| \frac{k_1 - k_0^\downarrow}{k_1 + k_0^\downarrow} \right|^2 \sin^3 \frac{\theta}{2} \cos \frac{\theta}{2} \end{aligned} \quad (6.13)$$

Eq. 6.13 shows that the out-of-plane spin current vanishes regardless of whether the wave functions of the other spin band ( $k_0^\downarrow$ ) are propagating or not.

It is now necessary to give the correct physical interpretation of our results obtained for a single interface between a semi-infinite magnet and a semi-infinite nonmagnet. First of all we need to comment on our use of the terms “in-plane” and “out-of-plane” spin current components. For these terms to be meaningful, the plane in the spin space we refer to needs to be defined such that the spin current at any point in a plane in the spin space flows with components parallel (“in-plane”) and perpendicular (“out-of-plane”) to the plane. For this we need to specify two vectors in the spin space which are non-collinear. The first one is clearly in the direction of the magnetization of the semi-infinite magnet. The only other vector in the spin space available is

---

in the direction of the spin-polarized current of electrons in the nonmagnet, i.e. the positive direction of the  $z - axis$  in our case. This implies that, in reality, our “nonmagnet” plays the role analogous to that of a second magnet or half-magnet whereby all  $\downarrow$  electrons have been filtered out. It follows that to be able to talk about an out-of-plane spin current we always need to have two magnets with non-collinear magnetizations in our system.

Our results that an out-of-plane spin current reflected from a magnet is non-zero, provided there is total reflection in at least one spin channel at the interface, are only valid for a spin-polarized beam of electrons incident on the magnet. It is, therefore, essential to investigate what happens when we have a true nonmagnet with an equal probability of electrons having spin polarization  $\uparrow$  and  $\downarrow$ . This is precisely the situation assumed in the Landauer reservoirs. It is therefore necessary to repeat the calculation described above for electrons incident from a nonmagnet with an opposite spin polarization. We could do this using the transfer matrix formalism described above but we can also use another method which allows us to alter very simply the direction of the spin polarization of the electrons incident on the magnet. That is we can send from the nonmagnet (right), a beam of electrons with spin polarization in an arbitrary direction and keep the direction of the magnetization of the magnet fixed in the positive direction of the  $z - axis$ .

We first need to find the spin wave function of an electron with spin orientation in an arbitrary direction characterized by the polar angles  $\theta$  and  $\phi$ .

### 6.3 Electrons with arbitrary spin polarization incident on a magnet with fixed magnetization

Here we consider again a single interface at  $x_0 = 0$  with a semi-infinite magnet on the left and a semi-infinite nonmagnet on the right. This time we will send from the nonmagnet (right), a beam of electrons with spin polarization in an arbitrary direction allowing us to keep the direction of the magnetization of the magnet fixed in the positive direction of the  $z$ -axis whilst the electrons incident from the right nonmagnet have their spin polarization in an arbitrary direction characterized by the polar angles  $\theta$  in the  $yz$ -plane and  $\phi$  in the  $xz$ -plane as illustrated in Fig. 6.3.

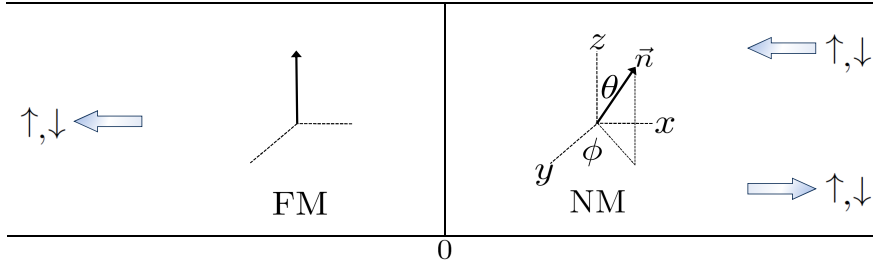


Fig. 6.3: Schematic picture of a single interface between a semi-infinite magnet and a semi-infinite nonmagnet with arbitrary spin polarization.

We will need to calculate the spin wave function in the nonmagnet by first solving an eigenvalue problem given by

$$(\vec{\sigma} \cdot \vec{n}) \chi = 1 \chi \quad (6.14)$$

where 1 is the eigenvalue of a state with a spin quantization axis in the direction of the unit vector  $\vec{n}$  given by

$$\vec{n} \equiv (\sin \theta \cos \phi, \sin \theta \sin \phi, \cos \theta) \quad (6.15)$$

and  $\vec{\sigma}$  denotes the spin operators for each component  $\sigma_x, \sigma_y$  and  $\sigma_z$  given by

$$\sigma_x = \begin{pmatrix} 0 & 1 \\ 1 & 0 \end{pmatrix}, \sigma_y = \begin{pmatrix} 0 & -i \\ i & 0 \end{pmatrix}, \sigma_z = \begin{pmatrix} 1 & 0 \\ 0 & -1 \end{pmatrix} \quad (6.16)$$

Therefore he have from Eq. 6.15 and Eq. 6.16 that

$$\vec{\sigma} \cdot \vec{n} = \sin \theta \cos \phi \begin{pmatrix} 0 & 1 \\ 1 & 0 \end{pmatrix} + \sin \theta \sin \phi \begin{pmatrix} 0 & -i \\ i & 0 \end{pmatrix} + \cos \theta \begin{pmatrix} 1 & 0 \\ 0 & -1 \end{pmatrix} \quad (6.17)$$

By letting  $\chi = \begin{pmatrix} \alpha \\ \beta \end{pmatrix}$ , we have from Eq. 6.14 and Eq. 6.17

$$\sin \theta \cos \phi \begin{pmatrix} \beta \\ \alpha \end{pmatrix} + i \sin \theta \sin \phi \begin{pmatrix} -\beta \\ \alpha \end{pmatrix} + \cos \theta \begin{pmatrix} \alpha \\ -\beta \end{pmatrix} = \begin{pmatrix} \alpha \\ \beta \end{pmatrix} \quad (6.18)$$

This gives two simultaneous equations

$$\alpha (\cos \theta - 1) + \beta (\sin \theta \cos \phi - i \sin \theta \sin \phi) = 0 \quad (6.19a)$$

$$\alpha (\sin \theta \cos \phi + i \sin \theta \sin \phi) - \beta (\cos \theta + 1) = 0 \quad (6.19b)$$

Furthermore, since the determinant is zero for all  $\theta$  and  $\phi$ , we can solve for the ratio  $\frac{\alpha}{\beta}$  to give

$$\frac{\alpha}{\beta} = \frac{\sin \theta (\cos \phi - i \sin \phi)}{1 - \cos \theta} = \frac{\cos \frac{\theta}{2} e^{-i\frac{\phi}{2}}}{\sin \frac{\theta}{2} e^{i\frac{\phi}{2}}} \quad (6.20)$$

Therefore we can choose

$$\chi = \begin{pmatrix} \alpha \\ \beta \end{pmatrix} = \begin{pmatrix} \cos \frac{\theta}{2} e^{-i\frac{\phi}{2}} \\ \sin \frac{\theta}{2} e^{i\frac{\phi}{2}} \end{pmatrix} \quad (6.21)$$

Here we can note that for  $\theta = \phi = 0$  we have

$$\begin{pmatrix} \alpha \\ \beta \end{pmatrix} = \begin{pmatrix} 1 \\ 0 \end{pmatrix} \quad (6.22)$$

which is correct since the spin is in the direction of the  $z$ -axis.

We now need to solve for the wave function  $\psi_1^{\uparrow,\downarrow}$  in the nonmagnet with  $k_1$  propagating implying  $k_1 = i|k_1|$  giving

$$\psi_1^\uparrow = \alpha e^{-i|k_1|x} \quad (6.23a)$$

$$\psi_1^\downarrow = \beta e^{-i|k_1|x} \quad (6.23b)$$

Since the spin current is constant throughout the nonmagnet we can calculate the spin current components in the nonmagnet resulting from a single  $\uparrow$  spin electron incident from the right ( $J_R^\uparrow$ ) by solving for  $J$  (Eq. 2.41a) at  $x = 0$  to give

$$J_R^\uparrow = -i \frac{\hbar}{m} |k_1| \sin \theta (\cos \phi - i \sin \phi) \quad (6.24)$$

Therefore, since the in- and out-of-plane spin current components are given by  $J_\parallel = \Im\{J\}$  and  $J_\perp = \Re\{J\}$  respectively (Eq. 2.41b), we have

$$J_\parallel = -\frac{\hbar}{m} |k_1| \sin \theta \cos \phi \quad (6.25a)$$

$$J_\perp = -\frac{\hbar}{m} |k_1| \sin \theta \sin \phi \quad (6.25b)$$

We will look at a comparative configuration whereby the incident spin current is in the  $yz$  - plane implying  $\phi = 0$  giving zero out-of-plane spin current as

shown below

$$J_{\parallel} = -\frac{\hbar}{m} |k_1| \sin \theta \quad (6.26a)$$

$$J_{\perp} = 0 \quad (6.26b)$$

We can also note that for  $\theta = \frac{\pi}{2}$  and  $\phi = \frac{\pi}{2}$ , the spin current is in the direction of the  $x$  - *axis* and

$$J_{\parallel} = 0 \quad (6.27a)$$

$$J_{\perp} = -\frac{\hbar}{m} |k_1| \quad (6.27b)$$

The next step is to match the wave functions at the interface directly. We are not sending any electrons from the left and as we are interested in the out-of-plane spin current in the nonmagnet, we will be looking at the case of total reflection in both spin channels in the magnet giving  $k_0^{\uparrow} = |k_0^{\uparrow}|$  and  $k_0^{\downarrow} = |k_0^{\downarrow}|$ . Therefore, the wave equations in the left magnet are given by

$$\psi_0^{\uparrow} = B_0^{\uparrow} e^{|k_0^{\uparrow}|x} \quad (6.28a)$$

$$\psi_0^{\downarrow} = B_0^{\downarrow} e^{|k_0^{\downarrow}|x} \quad (6.28b)$$

We will have  $\alpha, \beta$  providing the incident wave from the right giving the

following wave equations in the right nonmagnet

$$\psi_1^\uparrow = A_1^\uparrow e^{i|k_1|x} + \alpha e^{-i|k_1|x} \quad (6.29a)$$

$$\psi_1^\downarrow = A_1^\downarrow e^{i|k_1|x} + \beta e^{-i|k_1|x} \quad (6.29b)$$

Here we note that  $B_0^\uparrow, B_0^\downarrow$  are exponentially decaying waves in the magnet where  $x < 0$  implying that  $|k_0^\uparrow|, |k_0^\downarrow| > 0$  such that  $e^{|k_0^\uparrow|x}, e^{|k_0^\downarrow|x}$  are decaying in the left magnet. And so matching these wave functions and their derivatives at  $x = 0$  we have four simultaneous equations

$$B_0^\uparrow = A_1^\uparrow + \alpha \quad (6.30a)$$

$$B_0^\downarrow = A_1^\downarrow + \beta \quad (6.30b)$$

$$|k_0^\uparrow|B_0^\uparrow = i|k_1|(A_1^\uparrow - \alpha) \quad (6.30c)$$

$$|k_0^\downarrow|B_0^\downarrow = i|k_1|(A_1^\downarrow - \beta) \quad (6.30d)$$

Solving for the amplitude of the reflection coefficients in the nonmagnet we have

$$A_1^\uparrow = \frac{\alpha(i|k_1| + |k_0^\uparrow|)}{i|k_1| - |k_0^\uparrow|} \quad (6.31)$$

$$A_1^\downarrow = \frac{\beta(i|k_1| + |k_0^\downarrow|)}{i|k_1| - |k_0^\downarrow|} \quad (6.32)$$

Substituting into our expression for the spin current  $J$  (Eq. 2.41), we have for a single  $\uparrow$  spin electron incident from the right,  $(J_R^\uparrow)$  given by

$$J_R^\uparrow = \frac{-4\frac{\hbar}{m}|k_1|^2\alpha\beta^*(|k_0^\uparrow| - |k_0^\downarrow|)}{(i|k_1| - |k_0^\uparrow|)(i|k_1| + |k_0^\downarrow|)} \quad (6.33)$$

We are interested in the spin current resulting from incident waves in the  $yz$  - plane implying  $\phi = 0$  which reduces  $\alpha\beta^*$  to  $\sin\frac{\theta}{2}\cos\frac{\theta}{2}$  giving

$$J_R^\uparrow = \frac{-2\frac{\hbar}{m}|k_1|^2\sin\theta(|k_0^\uparrow| - |k_0^\downarrow|)}{(i|k_1| - |k_0^\uparrow|)(i|k_1| + |k_0^\downarrow|)} \quad (6.34)$$

Since we have total reflection in both spin channels and zero incident spin current, Eq. 6.34 is an expression for the reflected spin current in the nonmagnet and we can see immediately that the reflected spin current components for electrons incident with spin orientations  $\theta$  and  $(\theta + \pi)$  have opposite signs. Therefore, the unpolarized electrons incident from the Landauer reservoir imply that for each electron with spin polarization  $\theta$  there is also an electron with spin in the opposite direction  $(\theta + \pi)$ . It follows that there is no reflected in- or out-of-plane spin current flowing back to the reservoir. However, we can now use our single interface results to discuss qualitatively what happens at the interface between a nonmagnetic spacer and the second (switching) magnet. In that case, electrons incident from the spacer on the switching

magnet are spin polarized and we may assume, for simplicity, that the incident electrons are fully polarized in the  $\theta$  direction in the  $yz$ -plane. We can therefore use the result for the reflected spin current given above (Eq. 6.34). We first consider the reflected in-plane spin current  $J_{\parallel}^{ref} = \Im\{J_R^{\uparrow}\}$ .

$$J_{\parallel}^{ref} = \frac{-2\frac{\hbar}{m}|k_1|^3 \sin\theta(|k_0^{\uparrow}| - |k_0^{\downarrow}|)^2}{(|k_1|^2 + |k_0^{\uparrow}|^2)(|k_1|^2 + |k_0^{\downarrow}|^2)} \quad (6.35)$$

Eq. 6.35 shows that the sign of  $J_{\parallel}^{ref}$  is proportional to  $-2\frac{\hbar}{m}|k_1|^3 \sin\theta$ . That is to say the reflected in-plane spin current for electrons incident with spin orientations  $\theta$  and  $(\theta + \pi)$  have opposite signs and tend to cancel. Furthermore, in the limit of a strongly reflecting interface, we have  $|k_0^{\uparrow}| \gg |k_1|$  and  $|k_0^{\downarrow}| \gg |k_1|$ . In that case it is clear from Eq. 6.34 that the reflected in-plane spin current contribution is reduced.

We now consider the reflected out-of-plane spin current  $J_{\perp}^{ref} = \Re\{J_R^{\uparrow}\}$  given by the real part of Eq. 6.34.

$$J_{\perp}^{ref} = \frac{-2\frac{\hbar}{m}|k_1|^2 \sin\theta(|k_0^{\uparrow}| - |k_0^{\downarrow}|)(|k_1|^2 + |k_0^{\uparrow}k_0^{\downarrow}|)}{(|k_1|^2 + |k_0^{\uparrow}|^2)(|k_1|^2 + |k_0^{\downarrow}|^2)} \quad (6.36)$$

Since the incident spin current is entirely polarized in the  $yz$ -plane there is no incident out-of-plane spin current component and there is therefore no compensation for the reflected out-of-plane spin current component given by Eq. 6.36. It follows from this that  $J_{\perp}$  is always non-zero but can have either positive or negative sign depending on the relative magnitudes of  $|k_0^{\uparrow}|$  and

$|k_0^\downarrow|$ . Furthermore, in the limit of a strongly reflecting interface, we do not see the same reduction of out-of-plane spin current as seen for the in-plane spin current.

In conclusion, these results for the single interface will be useful for understanding the behaviour of a general junction containing both polarizing and switching magnets. However, we need to bear in mind that in such a system there are multiple reflections from multiple interfaces. Since the out-of-plane spin current component may be generated as a result of these multiple reflections, the results seen for a single interface should only be used as a qualitative guide.

#### *6.4 Incident and reflected spin currents in a junction with an insulating switching magnet*

We have seen in Chapter 4 and indeed throughout this thesis a number of interesting results when studying the spin current components in each layer of a magnetic multi-layered junction consisting of a nonmagnetic spacer layer with a finite polarizing magnet on the left and a finite switching magnet on the right, all of which contained within left and right leads (Fig. 2.2).

For simplicity, these results have been demonstrated where possible using a consistent configuration whereby the two ferromagnets have been treated as potential wells in both the  $\uparrow$  and  $\downarrow$  spin bands (Fig. 4.2).

---

There are of course many possible configurations to which our Landauer formalism can be applied, each providing a new insight into the spin transport effects seen throughout such junctions. When investigating the five layer junction configured such that the finite ferromagnets are represented as potential barriers, it can be observed that by varying the potentials in the switching magnet, the in-plane spin current in the spacer decreases rapidly when the potentials in the switching magnet are high. On the other hand, the out-of-plane spin current did not seem to depend strongly on the heights of this potential barrier representation of the switching magnet. This has prompted me to investigate the situation when the potentials of both the  $\uparrow$  and  $\downarrow$  spin electrons in the switching magnet are so high that they represent potential barriers through which electrons must tunnel into the right lead, thus acting as an insulating switching magnet.

A simple way to demonstrate this result would be to redefine our five layer junction (Fig. 4.41) such that the width  $p$  of the switching magnet can be modified and the  $\uparrow$  and  $\downarrow$  spin potentials can remain fixed as illustrated in Fig. 6.4.

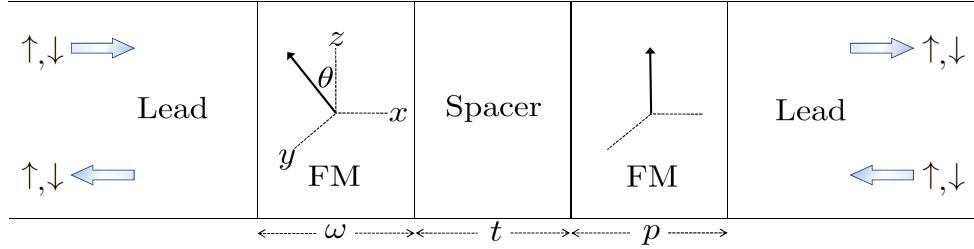


Fig. 6.4: Schematic picture of a simple five layer junction with  $\uparrow$  and  $\downarrow$  spin electrons incident from the left and right semi-infinite leads.

We have removed the fundamental length scale,  $a$ , in the problem however, as before, the exchange potential of the left (polarizing) magnet is rotated by angle  $\theta$  in the  $yz$ –plane whilst that of the right (switching) magnet is always in the direction of the  $z$ –axis. We will match the potentials in the  $\uparrow$  and  $\downarrow$  spin bands of the two ferromagnets (Fig. 6.5) however they are now represented as two potential barriers as shown schematically in Fig. 6.5. We can also note that the symmetry will be broken for all  $p \neq \omega$ .

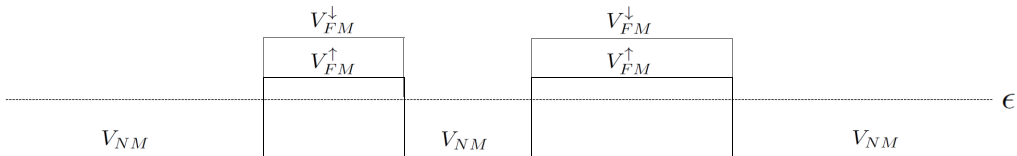


Fig. 6.5: Five layer junction represented by two matched potential barriers.

We have fixed the angle of rotated magnetization in the left polarizing magnet to  $\theta = 1.5$ , the width of the polarizing magnet and spacer is given

by  $\omega = t = 1$  and the potentials in each layer are given by  $V_{NM} = -1.0$ ,  $V_{FM}^\uparrow = 1.5$  and  $V_{FM}^\downarrow = 2.5$ .

The numerical results for the total in-plane ( $J_\parallel^T$ ) and out-of-plane ( $J_\perp^T$ ) spin current components summed over all  $k_\parallel$  calculated in the spacer at  $x_0 = L + \omega$  as a function of  $p \in [p_0, p_n]$ , the varying width of the switching magnet with the width of the polarizing magnet and spacer fixed such that  $p_0 = \omega = t$ , are illustrated in Fig. 6.6.

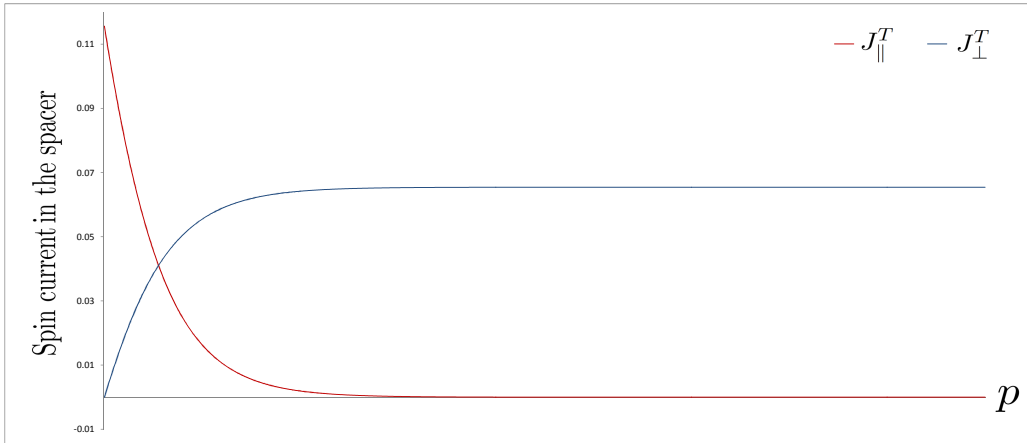


Fig. 6.6:  $J_\parallel^T$  and  $J_\perp^T$ . The total in- and out-of-plane spin current components (sum over  $k_\parallel$ ), calculated in the spacer as a function of the width of the switching magnet,  $p \in [p_0, p_n]$ .

Fig. 6.6 shows exactly zero out-of-plane spin current at  $p_0$  which is expected since  $p_0 = \omega = t$  and hence we have complete symmetry. As the width of the switching magnet increases, the out-of-plane spin current increases and converges to a constant. On the other hand, the in-plane spin current component exists in the completely symmetric configuration however

---

it converges rapidly to zero as the thickness of the switching magnet increases.

It is interesting to analyse this case by examining separately the contributions to the spin current components of electrons incident on and reflected from the switching magnet. We should not confuse this with sending individual electrons from the left (right) reservoir as done previously. In fact, it should be noted that it is sufficient to consider only the electrons emitted from the left reservoir since the electrons emitted from the right reservoirs are almost entirely reflected from the right (switching) magnet back to the right reservoir as the width of the switching magnet approaches  $p_n$ . They, therefore, do not reach the left (polarising) magnet and have thus only a negligible effect on the spin current in the spacer.

We will therefore calculate the total spin current components in the non-magnetic spacer and seek to extract these incident (and reflected) contributions on the switching magnet directly from the wave functions within the spacer.

The wave functions  $\psi^{\uparrow,\downarrow}$  in the spacer are always a linear combination of the waves moving from left to right and those moving from right to left. This is the case even when we are sending electrons only from a single (left/right) reservoir. We can therefore isolate within the Landauer approach the contributions to the spin current components coming from the electrons incident on the switching magnet and those reflected from the switching magnet. This can be seen directly in our original formulation of the general solution for the

wave function  $\psi_i$  (Eq. 2.18) and the expression for the in- and out-of-plane spin current components (Eq. 2.41).

We can construct the wave functions in the spacer layer with propagating waves  $k_\perp$  given by  $k^\uparrow = k^\downarrow = i|k|$  and solve for the expression for the spin current components (Eq. 2.41) in the spacer. Given that the spin current is constant in the spacer, we can choose  $x = 0$  to give

$$J_{Spacer} = i2\frac{\hbar}{m}|k|(A^\uparrow A^{\downarrow*} - B^\uparrow B^{\downarrow*}) \quad (6.37)$$

where  $A^{\uparrow,\downarrow}$  denote the transmission coefficients (incident on the switching magnet) and  $B^{\uparrow,\downarrow}$  the reflection coefficients (reflected from the switching magnet) in the spacer.

The total spin current for all incident electrons with spin orientation  $\sigma \in (\uparrow, \downarrow)$  is therefore given by

$$J_{Spacer}^T = i2\frac{\hbar}{m}|k|\sum_{\sigma}(A^\uparrow A^{\downarrow*} - B^\uparrow B^{\downarrow*}) \quad (6.38)$$

The numerical results for the contributions to the total in-plane spin current component ( $J_{\parallel}^T$ ) summed over all  $k_{\parallel}$  due to the electrons in the spacer that are incident on the switching magnet (given by  $J_{\parallel}^{inc}$ ) and those that are reflected by the switching magnet back into the spacer (given by  $J_{\parallel}^{ref}$ ), calculated in the spacer at  $x_0 = L + \omega$  as a function of  $p \in [p_0, p_n]$ , the varying

width of the switching magnet with the width of the polarizing magnet and spacer fixed such that  $p_0 = \omega = t$ , are illustrated in Fig. 6.7.

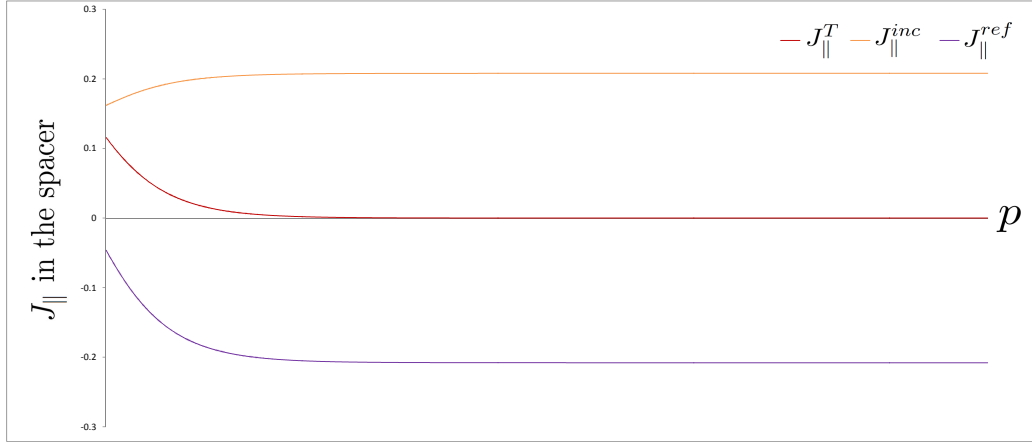


Fig. 6.7:  $J_{\parallel}^{inc}$ ,  $J_{\parallel}^{ref}$  and  $J_{\parallel}^T$ . The total in-plane spin current (sum over  $k_{\parallel}$ ) separated into the contributions due to the incident and reflected electrons within the spacer, calculated in the spacer as a function of the width of the switching magnet,  $p \in [p_0, p_n]$ .

Fig. 6.7 shows that the incident and reflected in-plane spin currents are always of opposite sign. Moreover, as the width  $p$  of the switching magnet (potential barrier) increases, the magnitude of the reflected contribution of the in-plane spin current approaches the magnitude of the incident contribution. It follows that the total in-plane spin current tends to zero as the transparency of the switching magnet potential barrier decreases.

The physical interpretation of these results is that the incident and reflected in-plane spin current contributions interfere destructively. This is analogous to the behaviour of the ordinary charge current. The charge cur-

rent associated with electrons tunneling through a potential barrier decreases exponentially with the barrier height (width). Since the charge current is conserved everywhere, the low value of the charge current on the right of the potential barrier, which must be equal to the total charge current flowing on the left of the barrier, can only be explained by the destructive interference of electron waves incident on and reflected from the barrier. The in-plane spin current thus behaves just like the charge current.

We shall see that the behaviour of the out-of-plane spin current is quite different. The numerical results for the contributions to the total out-of-plane spin current component ( $J_{\perp}^T$ ) summed over all  $k_{\parallel}$  due to the electrons in the spacer that are incident on the switching magnet (given by  $J_{\perp}^{inc}$ ) and those that are reflected by the switching magnet back into the spacer (given by  $J_{\perp}^{ref}$ ), calculated in the spacer at  $x_0 = L + \omega$  as a function of  $p \in [p_0, p_n]$ , the varying width of the switching magnet with the width of the polarizing magnet and spacer fixed such that  $p_0 = \omega = t$ , are illustrated in Fig. 6.8.

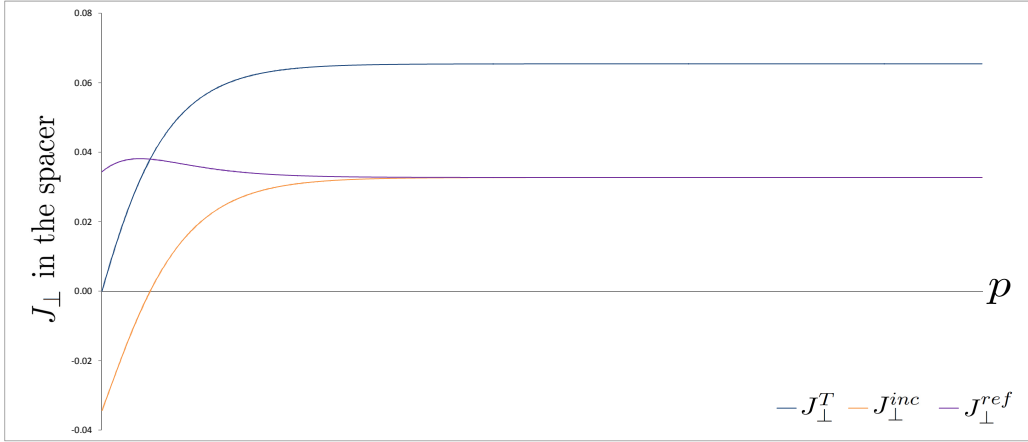


Fig. 6.8:  $J_{\perp}^{inc}$ ,  $J_{\perp}^{ref}$  and  $J_{\perp}^T$ . The total out-of-plane spin current (sum over  $k_{\parallel}$ ) separated into the contributions due to the incident and reflected electrons within the spacer, calculated in the spacer as a function of the width of the switching magnet,  $p \in [p_0, p_n]$ .

Fig. 6.8 shows that, in contrast to the in-plane spin current, the reflected contribution of the out-of-plane spin current does not cancel the incident contribution. It follows that the total out-of-plane spin current in the spacer layer tends to saturate to a finite nonzero value as the switching magnet potential barrier width increases. These results can be understood qualitatively as follows.

When the switching magnet potential barrier is very high (wide), the incident electrons are almost totally reflected. The incident and reflected electron waves thus tend to form standing waves in the nonmagnetic spacer layer. Unlike propagating waves, standing waves have real wave functions. We note that the in-plane spin current is given by the imaginary part of our expression for the spin current components (see Eq. 2.41 of Sec. 2.3) while

---

the out-of-plane spin current is given by the real part of the same expression. It is, therefore, clear that the in-plane spin current vanishes for a high (wide) switching magnet potential barrier but the out-of-plane spin current remains finite.

These results are interesting and potentially important since they show that the out-of-plane spin current can be large even when the charge current and the in-plane spin current are both negligibly small. However, in real systems we cannot manipulate the height (width) of the switching magnet potential barrier since they are given for any specific material combination of the spacer and switching magnet. In fact, the switching magnet potential barrier is not high for fully metallic junctions studied experimentally.

This problem was bypassed by Autes et al. [28] who proposed to include in a metallic magnetic junction an additional insulating layer inserted after the switching magnet. They showed using the Keldysh formalism that even in the presence of a high insulating barrier after the switching magnet, the out-of-plane spin current in the nonmagnetic spacer layer remains finite.

In the next section we shall analyse such a modified six-layer junction using our Landauer formalism. This allows us to explain the results obtained within the Keldysh formalism in terms of the incident and reflected spin currents.

### 6.5 Junction with an insulating barrier

Here we introduce a 6th layer acting as an insulating barrier on the right side of the junction as shown schematically in Fig. 6.9.

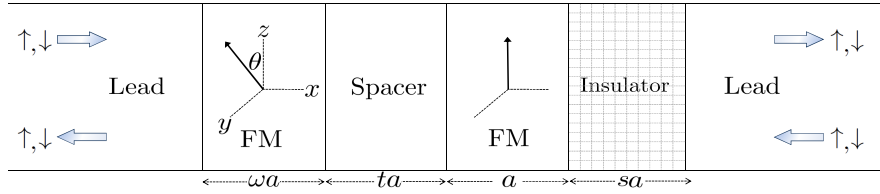
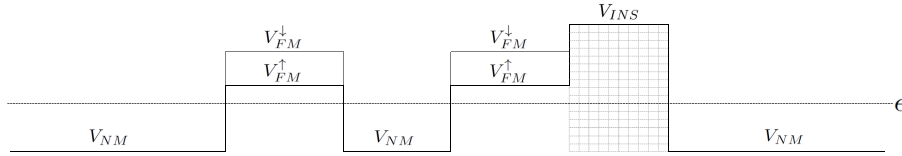


Fig. 6.9: Schematic picture of a six layer junction with  $\uparrow$  and  $\downarrow$  spin electrons incident from the left and right semi-infinite leads.

We now have a dimensionless system consisting of a semi-infinite left lead up to  $x_0 = L$  (a large starting value on the x-axis). A finite ferromagnet of thickness  $\omega a$  between  $x_0 = L$  and  $x_1 = L + \omega a$ , a spacer of width  $ta$  located between  $x_1 = L + \omega a$  and  $x_2 = L + (\omega + t)a$ , the switching magnet of width  $a$  between  $x_2 = L + (\omega + t)a$  and  $x_3 = L + (\omega + t + 1)a$  and the additional non-magnetic metallic insulating barrier of width  $sa$  between  $x_3 = L + (\omega + t + 1)a$  and  $x_4 = L + (\omega + t + 1 + s)a$ .

As before, the exchange potential of the left magnet is rotated by angle  $\theta$  in the  $yz$ -plane whilst that of the right magnet is always in the  $z$ -direction ( $\theta = 0$ ). We will match the potentials in the  $\uparrow$  and  $\downarrow$  spin bands of the two ferromagnets, thus producing two identical potential barriers in each spin channel and include a third, larger potential barrier representing the insula-

tor as shown schematically in Fig. 6.10.



*Fig. 6.10:* Six layer junction represented by two matched potential barriers (magnets) followed by a third potential barrier (insulator).

We will first reproduce the results obtained for a single-orbital tight-binding band using the Keldysh formalism [24]. The dependences of the in-plane, out-of-plane and charge currents on the width of the insulating barrier are shown in Fig. 6.11.

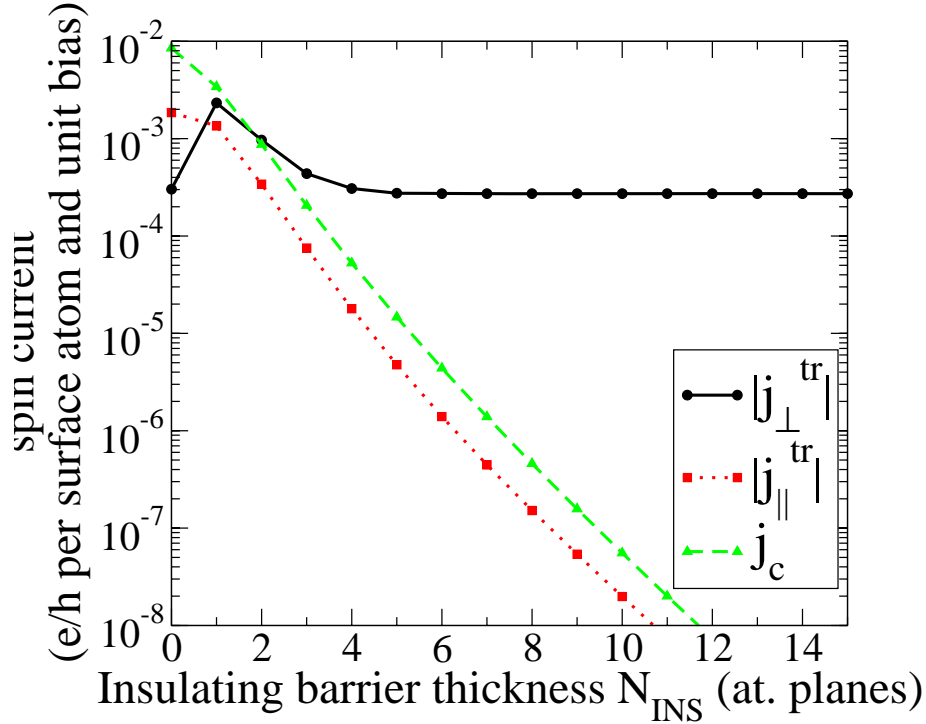


Fig. 6.11: Keldysh spin (charge) current as a function of the width of the insulating barrier (taken from [28]).

It can be seen that the in-plane spin current and charge current decrease exponentially with the barrier width but the out-of-plane spin current saturates to a finite value. This behaviour is reminiscent of the behaviour of the spin current in a junction with an insulating switching magnet discussed in the previous section.

We shall now apply to the six layer junction shown in Fig. 6.9 our Landauer formalism. We have fixed the angle of rotated magnetization in the left polarizing magnet to  $\theta = 1.5$ , the widths of the two ferromagnets and spacer are given by  $a = \omega = t = 1$  and the potentials in each layer are given

by  $V_{NM} = -1.0$ ,  $V_{FM}^\uparrow = 1.0$ ,  $V_{FM}^\downarrow = 2.0$  and  $V_{INS} = 30.0$ .

The dependences of the total in-plane ( $J_{\parallel}^T$ ) and out-of-plane ( $J_{\perp}^T$ ) spin currents on the insulating barrier width ( $sa$ ), together with the corresponding results for the ordinary charge current ( $J_c$ ), are shown in Fig. 6.12.

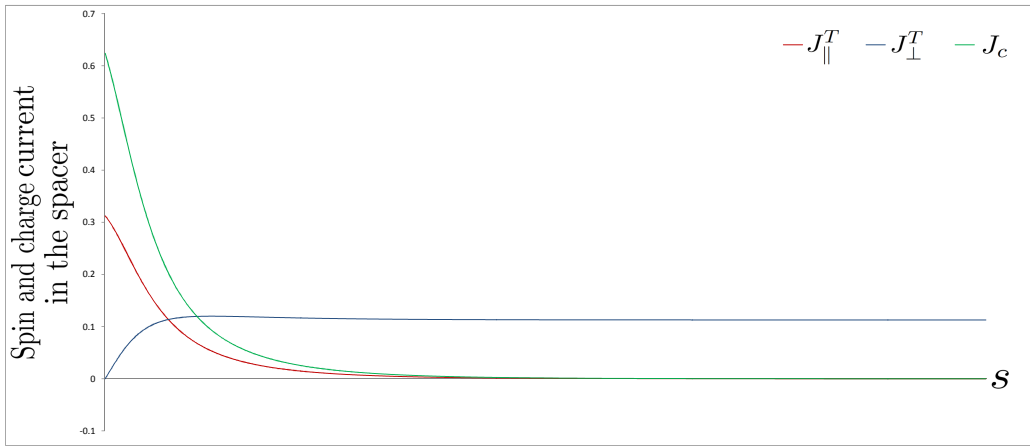


Fig. 6.12:  $J_{\parallel}^T$ ,  $J_{\perp}^T$  and  $J_c$ . The total in- and out-of-plane spin current components (sum over  $k_{\parallel}$ ), calculated in the spacer as a function of the width of the insulating layer,  $s \in [s_0, s_n]$ , along with the corresponding results for the charge current.

Not surprisingly the behaviour of all the currents shown in Fig. 6.12 is qualitatively the same as the corresponding results obtained within the Keldysh formalism. In our case, we have started at  $s_0 = 0$ , such that the insulating layer vanishes and we are left with the completely symmetric five layer junction and so we have exactly zero out-of-plane spin current in the spacer. As the width of the insulating layer increases, we see the same behaviour observed both in our earlier results for the insulating switching mag-

net (Sec. 6.4) and in the Keldysh results for the insulating barrier (Fig. 6.11).

We now examine the behaviour of the spin current contributions incident on and reflected from the switching magnet. As in the previous section, Fig. 6.13 shows the dependence of the incident and reflected in-plane spin currents on the insulating barrier width,  $sa$ .

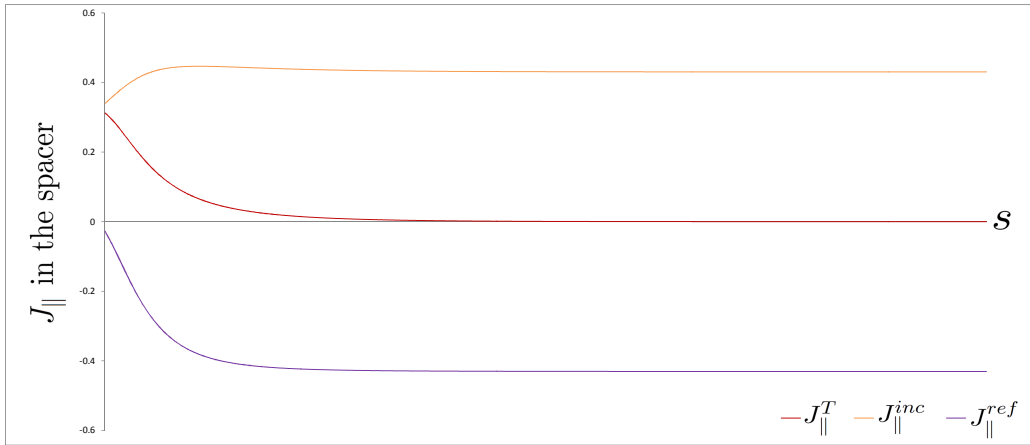


Fig. 6.13:  $J_{\parallel}^{inc}$ ,  $J_{\parallel}^{ref}$  and  $J_{\parallel}^T$ . The total in-plane spin current (sum over  $k_{\parallel}$ ) separated into the contributions due to the incident and reflected electrons within the spacer, calculated in the spacer as a function of the width of the insulating layer,  $s \in [s_0, s_n]$ .

Similarly, Fig. 6.14 shows the dependence of the incident and reflected out-of-plane spin currents on the insulating barrier width,  $sa$ .

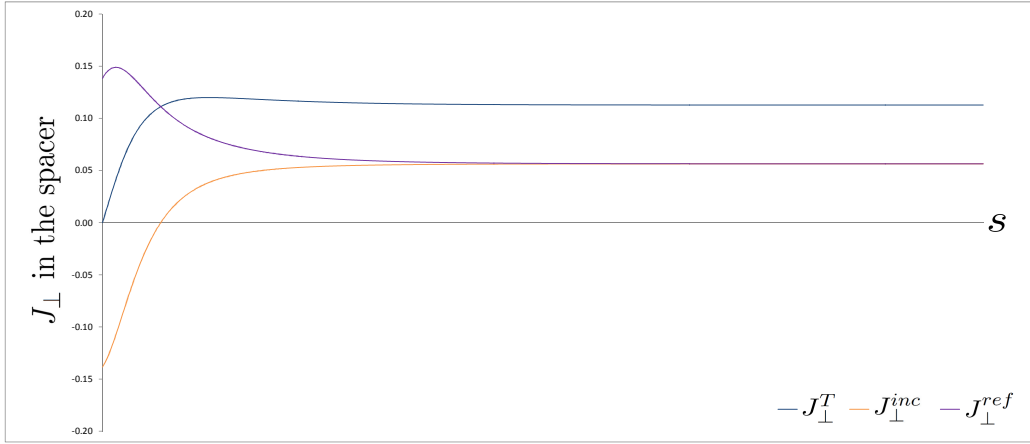


Fig. 6.14:  $J_{\perp}^{inc}$ ,  $J_{\perp}^{ref}$  and  $J_{\perp}^T$ . The total out-of-plane spin current (sum over  $k_{\parallel}$ ) separated into the contributions due to the incident and reflected electrons within the spacer, calculated in the spacer as a function of the width of the insulating layer,  $s \in [s_0, s_n]$ .

We find again that the incident and reflected in-plane spin currents (Fig. 6.13) tend to compensate one another, which results in a vanishing total in-plane spin current. On the other hand, there is no such compensation for the out-of-plane spin current (Fig. 6.14) and that is the reason why it saturates to a finite value with an increasing insulating barrier width. The physical explanation of the behaviour of the in-plane and out-of-plane spin currents in terms of standing waves which form in the nonmagnetic spacer is qualitatively the same as that already given in Sec. 6.4.

We conclude this section by stating that our Landauer formalism provides a solid physical underpinning of the rather surprising and seemingly improbable results obtained by Autes et al. [28] within the rigorous but physically non-transparent Keldysh formalism.

## 7. CONCLUSIONS

In this thesis we formulated a methodology based on Landauer's theory of transport of spin that allowed us to study the spin transport effects found in magnetic multi-layered junctions using a more comprehensive approach than those taken previously. It allowed us to calculate the total spin current throughout the magnetic and non-magnetic metallic layers of various multi-layered junctions in order to verify qualitatively the results found before using the nonequilibrium Keldysh formulation. More importantly, we were able to deconstruct these results into individual scattering problems allowing us to see how the spin current comprises of the many contributions due to incident and reflected electrons moving from left to right and right to left in each layer of the junction and thus providing additional information about the physics of the spin transport that cannot be obtained from Keldysh alone.

We showed that there is zero out-of-plane spin current in the nonmagnetic spacer layer sandwiched between two ferromagnets with a non-zero angle of rotated magnetisation (in-plane) between the two magnets only when perfect symmetry is introduced because the contribution from the left cancels exactly the contribution from the right. As a result, we identified that by not matching the potentials in the left polarizing magnet with those of the right switching magnet in either the  $\uparrow$  or  $\downarrow$  spin band, we would introduce a

---

difference between the contributions from the left and right and hence obtain non-zero out-of-plane spin current in the spacer.

We deduced symmetry properties in the left and right semi-infinite leads of a general multi-layered junction showing that the contribution from the left is equal but opposite in sign to that from the right and concluded that the out-of-plane spin current seen in the left and right leads of the five layer junction originates from the individual spin precessions in the left and right ferromagnets. These precessions result in oscillations in the spin current components in the ferromagnets that therefore emerge in general in the leads as non-zero.

We identified the limits within the Landauer approach when studying theoretical junctions consisting of semi-infinite ferromagnets (classical trilayer). The results for a single propagating wave ( $k_{\perp}$ ) in the limit of a finite ferromagnet would never approach those of a semi-infinite ferromagnet due to the interferences from both interfaces of the finite magnet. We showed that the total spin current given by the sum over all  $k_{\parallel}$  would remove this limitation due to the destructive interference causing the oscillations found in the ferromagnets to decay and thus destroying the interactions between the two interfaces. Using this result we were able to provide a reasonable approximation using our realistic five layer junction with left and right Landauer reservoirs (leads) and finite ferromagnets to the classical trilayer junction in which the left and right ferromagnets are semi-infinite. However, we note that at individual  $k$ -points the trilayer with semi-infinite magnets can give

---

physically incorrect results.

We used the Landauer formalism we had developed to investigate the physical origin of the out-of-plane spin current by calculating analytically the spin current components found in a simple junction consisting of a single interface between a semi-infinite magnet and a semi-infinite nonmagnet. It followed from the two non-collinear vectors defining the spin space given by the direction of the magnetization of the semi-infinite magnet and the direction of the spin-polarized current of electrons in the nonmagnet that the nonmagnet was in fact acting as a second magnet or half-magnet whereby all  $\downarrow$  electrons had been filtered out and thus, we concluded that in order to talk about an out-of-plane spin current we will always need to have two magnets with non-collinear magnetizations in our system. We then introduced an arbitrary spin polarization in the semi-infinite nonmagnet in order to simulate the situation assumed in the Landauer reservoirs and obtained qualitative insight into the existence of out-of-plane spin current in a realistic nonmagnet. This could be extended to the interface between a nonmagnetic spacer and the second (switching) magnet. In that case, electrons incident from the spacer on the switching magnet are spin polarized and so our analytical expressions showed qualitatively that the reflected in-plane spin current tends to cancel the incoming contribution, however, the reflected out-of-plane spin current would not be cancelled in this way since there is no incoming out-of-plane contribution due to the fact that the incident spin current is entirely polarized in-plane. Our calculations clearly demonstrated that one needs a minimum of two interfaces with magnetic layers in order to obtain a non-

---

zero out-of-plane spin current in the nonmagnetic spacer. Hence all theories that do not treat all the interfaces rigorously are fundamentally incapable of describing correctly the out-of-plane spin current.

When investigating a five layer junction whereby the two ferromagnets were represented as potential barriers, we saw that the in-plane spin current in the nonmagnetic spacer would decrease to zero as the potential in the right switching magnet increased. The out-of-plane spin current in the spacer proved to be less dependant on the magnitude of the switching magnet potential step. The results for this situation whereby the right switching magnet was acting as an insulating barrier prompted us to investigate a junction with realistic ferromagnets and an additional nonmagnetic layer on the right acting as the insulating barrier. Our results were qualitatively the same as those obtained previously for a single-orbital tightbinding band using the Keldysh formalism. The in-plane spin current and ordinary charge current in the spacer both converge to zero whilst the out-of-plane spin current converges to a non-zero constant as the potential (width) of the insulating layer increases. Our Landauer formalism allowed us for the first time to separate the contributions to the spin current components in the spacer due to electrons incident on and reflected from the switching magnet. This showed conclusively that the incident and reflected in-plane spin currents are always of opposite sign. Moreover, as the potential of the insulating barrier increases, the magnitude of the reflected contribution of the in-plane spin current approaches the magnitude of the incident contribution producing a cancelling effect. The physical interpretation of these results is based on the

---

destructive interference of the incident and reflected in-plane spin current contributions. This is analogous to the behaviour of the ordinary charge current. The charge current associated with electrons tunneling through a potential barrier decreases exponentially with the barrier height (width). Since the charge current is conserved everywhere, the low value of the charge current on the right of the potential barrier, which must be equal to the total charge current flowing on the left of the barrier, can only be explained by the destructive interference of electron waves incident on and reflected from the barrier. The in-plane spin current thus behaves just like the charge current.

In contrast, when investigating the out-of-plane spin current in the spacer, we found that the incident and reflected contributions are equal and constant once the potential of the insulating barrier increases beyond a potential threshold and thus we do not see a cancelling effect. The physical interpretation in this case is qualitatively the same as in the case of the insulating switching magnet. The incident electrons are almost totally reflected by the switching magnet back into the nonmagnetic spacer and so the incident and reflected electron waves thus tend to form standing waves in the spacer layer. Unlike propagating waves, standing waves have real wave functions. When calculating the spin current, the in- and out-of-plane spin current components are obtained in our formalism by the imaginary and real parts of the same expression respectively and so it is, therefore, clear that the in-plane spin current in the spacer vanishes in the presence of a large switching magnet potential barrier or insulating layer, however, the out-of-plane spin current remains finite. These results are interesting and potentially important since

---

they show that the out-of-plane spin current in the nonmagnetic spacer can be large even when the charge current and the in-plane spin current are both negligibly small.

Future research into the application of this finite out-of-plane spin current in the spacer in the presence of an insulating barrier is pertinent to our result that the in-plane spin current vanishes due to a cancellation between the contributions within the layer that are incident on and reflected from the adjacent interface. Our ability to separate such contributions using our Landauer formalism and indeed the ability to calculate the contributions of individual electrons incident from either side of a junction has afforded us a tool that provides far greater physical insight into the spin transport effects in any magnetic multi-layered junction than those used previously. This tool has led us to the analytical result that the out-of-plane spin current in a semi-infinite non-magnet adjacent to a semi-infinite magnet is non-zero if there is at least one wave function that is completely reflected back into the non-magnet, a result that can potentially be exploited in a number of physical applications that therefore requires further investigation. This also provides motivation to solve analytically a junction consisting of two interfaces to gain more concrete physical insight into the origin of a non-zero out-of-plane spin current in a non-magnetic spacer sandwiched between two semi-infinite ferromagnets to those he have already obtained qualitatively. Furthermore, our formulation is not limited to the five layer junction studied throughout this thesis and can therefore be used to investigate junctions consisting of many layers such as a domain wall.



## BIBLIOGRAPHY

- [1] A modern approach to quantum mechanics, by Townsend, University Science Books (2000), p31 and p80.
- [2] Eisberg, Robert; Resnick, Robert (1985). Quantum Physics of Atoms, Molecules, Solids, Nuclei, and Particles (2nd ed.). pp. 272-3.
- [3] C. Kittel, Introduction to solid state physics, Wiley, New York, 1956.
- [4] M. A. M. Gijs and G. E. W. Bauer, Adv. Phys. 46, 285 (1997).
- [5] A.Fert and I.A. Campbell: J. Phys. F: Metal Physics 6, 849 (1976).
- [6] P. Grünberg, R. Schreiber, Y. Pang, M.B. Brodsky, and H. Sower: Phys. Rev. Lett. 57, 2442 (1986).
- [7] J. S. Moodera, L. R. Kinder, T. M. Wong, and R. Meservey, Phys. Rev. Lett. 74, 3273 (1995).
- [8] J. C. Slonczewski, J. Magn. Magn. Mater. 159, L1 (1996); J. Magn. Magn. Mater. 195, L261 (1999); J. Magn. Magn. Mater. 247, 324 (2002).
- [9] S. S. P. Parkin, Xin Jiang, C. Kaiser, A. Panchula, K. Roche, and M. Samant, Proceedings of the IEEE 91, 661 (2003); W. H. Butler and A. Gupta, Nature Mater. 3, 845-847 (2004); S. S. P. Parkin, C. Kaiser, A.

- 
- Panchula, P. M. Rice, B. Hughes, M. Samant, and SEE-Hun Yang, *Nature Mater.* 3, 862 (2004).
- [10] S.S.P. Parkin, N. More, and K.P. Roche: *Phys. Rev. Lett.* 64, 2304(1990).
- [11] D.M. Edwards and J. Mathon, *Current induced switching of magnetization Nanomagnetism*, ed. by D.L. Mills and J.A.C. Bland, Elsevier (2006), p. 273.
- [12] X. G. Zhang and W. H. Butler, *Phys. Rev. B* 51, 10085 (1995); W. H. Butler, X. G. Zhang, D. M. C. Nicholson, and J. M. MacLaren, *Phys. Rev. B* 52, 13399 (1995); P. Zahn, I. Mertig, M. Richter, and H. Eschrig, *Phys. Rev. Lett.* 75, 2996 (1995).
- [13] S. Zhang and P. M. Levy, *J. Appl. Phys.* 69, 4786 (1991); P. M. Levy, *Solid State Phys.* 47, 367 (1994); P. M. Levy and S. Zhang, *J. Magn. Magn. Mater.* 151, 315 (1995).
- [14] R. Landauer, *IBM J. Res. Dev.* 1, 223 (1957).
- [15] L.V. Keldysh, *Soviet Physics JETP* 20, 1018 (1965).
- [16] C. Caroli, R. Combescot, P. Nozieres, and D. Saint-James, *J. Phys. C* 4, 916 (1971).
- [17] D.M. Edwards in: *Exotic states in quantum nanostructures*, ed. by S. Sarkar, Kluwer Academic Press (2002).
- [18] *Quantum Theory of Spintronics in Magnetic Nanostructures*, J.Mathon, A.Umerski, p50.

- 
- [19] M. Tsoi, A. G. M. Jansen, J. Bass, W. C. Chiang, M. Seck, V. Tsoi, and P. Wyder, *Phys. Rev. Lett.* 80, 4281(1998); M. Tsoi, A. G. M. Jansen, J. Bass, W. C. Chiang, V. Tsoi, and P. Wyder, *Nature (London)* 406, 46 (2000); E. B. Myers, D. C. Ralph, J. A. Katine, R. N. Louie, and R. A. Buhrman, *Science* 285, 867 (1999); J. A. Katine, F. J. Albert, R. A. Buhrman, E. B. Meyers, and D. C. Ralph, *Phys. Rev. Lett.* 84, 3149 (2000); F. J. Albert, J. A. Katine, R. A. Buhrman, and D. C. Ralph, *Appl. Phys. Lett.* 77, 3809 (2000); J. Grollier, V. Cros, A. Hamzic, J. M. George, H. Jaffres, A. Fert, G. Faini, J. Ben Youssef, and H. Legall, *Appl. Phys. Lett.* 78, 3663 (2001).
- [20] J. Grollier, V. Cros, A. Hamzic, J. M. George, H. Jaffres, A. Fert, G. Faini, J. Ben Youssef, and H. Legall, *Appl. Phys. Lett.* 78, 3663 (2001); *Phys. Rev. B* 67, 174402 (2003).
- [21] *Quantum Theory of Spintronics in Magnetic Nanostructures*, J. Mathon, A. Umerski, p15.
- [22] J. Mathon, A. Umerski, and M. Villeret, *Phys. Rev. B* 55, 14378 (1997).
- [23] G.D. Mahan, *Many Particle Physics*, 2nd Ed., Plenum Press, New York (1990).
- [24] D. M. Edwards, F. Federici, J. Mathon, and A. Umerski, *Phys. Rev. B* 71, 134501 (2005).
- [25] *Quantum Mechanics (Non-Relativistic Theory) Volume 3 Third Edition*, L.D. Landau and E.M. Lifshitz

- 
- [26] R.E. Camley and J. Barnas: Phys. Rev. Lett. 63 664 (1989); J. Barnas, A. Fuss, R.E. Camley, P. Grünberg, and W. Zinn: Phys. Rev. B 42, 8110 (1990).
- [27] Introduction To Quantum Mechanics, B. H. Bransden and C. J. Joachain, Longman (0100) (1989), p289
- [28] G. Autes, J. Mathon and A. Umerski, J. Appl. Phys. 111, 053909 (2012).
- [29] A. Umerski, private communication